

**FEASIBILITY STUDY OF SLOT THERMAL MANAGEMENT FOR
HAIRPIN WINDINGS WITH EMBEDDED ULTRATHIN HEAT PIPE IN
TRACTION ELECTRIC MACHINES**

Pouria Farokhi Kojour

Thesis submitted for the degree of
Master of Science by Research and Thesis

Supervisor: Dr Bo Li

**University of
Kent**

School of Engineering, Mechanical Engineering,

University Kent,

Canterbury,

CT2 7NT,

United Kingdom

August 2023

Acknowledgments

I am profoundly grateful to have the opportunity to express my sincere appreciation to all those who have contributed to the successful completion of this Master's by research study.

First and foremost, I extend my heartfelt gratitude to my supervisor Dr Bo Li for their invaluable guidance, unwavering support, and insightful feedback throughout every stage of this research endeavor. Your expertise, dedication, and encouragement have been instrumental in shaping the direction and quality of this thesis.

I am also indebted to the panel of my submission review, Professor John Batchelor for their thoughtful insights and constructive critiques, which greatly enriched the depth and scope of this study.

My sincere appreciation extends to the faculty members and staff at University of Kent for fostering an environment of academic excellence and providing the necessary resources that facilitated my research journey.

I would like to express my gratitude to my wife and friend for their unwavering support, understanding, and encouragement, even during the most demanding phases of this research. Your belief in me was a constant source of motivation.

Lastly, I am thankful to all the participants and individuals who graciously offered their time, insights, and expertise for the purpose of this study. Without their willingness to share their knowledge and experiences, this research would not have been possible.

In conclusion, this work stands as a collective effort, and I am profoundly thankful to each and every individual who played a role, no matter how big or small, in the realization of this Master's by research study.

Abstract

This study investigates a novel cooling technique for hairpin windings in high-speed permanent magnet synchronous motors (PMSMs). The increasing demand for high power density in electric propulsion necessitates addressing the challenge of higher current density in compact electric machines. Consequently, thorough research into thermal management systems becomes imperative to effectively address the escalating cooling requirements. Recent trends have witnessed the swift adoption of hairpin windings in traction motors, driven by their advantages such as reduced manufacturing time, precise conductor placement, decreased AC copper loss, and improved copper fill factor in comparison to traditional random windings. The proposed cooling technique uses ultrathin heat pipes to enhance the cooling of solid copper bar windings placed within the stator slots. Heat pipes are highly efficient heat transfer devices that use the evaporation and condensation of a working fluid to transfer heat over long distances. The ultrathin heat pipes used in this study are specially designed to fit within the narrow stator slots of PMSMs. Numerical simulations were conducted to investigate the performance of the proposed cooling method. The simulations showed that the proposed cooling method can significantly improve heat transfer efficiency within the PMSM stator. Hotspot temperatures near the phase current rating were reduced by 10% to 25%. Additionally, heat dissipation from the stator body increased by up to 40%. The improved heat transfer efficiency and heat dissipation achieved with the proposed cooling method can lead to a number of benefits, including increased power density, extended motor life, and reduced operating costs. The proposed cooling method has the potential to be a promising solution for the thermal management of hairpin windings in PMSMs.

KEY WORDS: Hairpin winding, Heat pipe, Thermal management, AC/DC Losses, Cooling

Contents

Introduction.....	1
1.1 Electrification and Advancements in Traction Motors.....	1
1.2 Permanent Magnet Synchronize Motors.....	2
1.3 Current Technologies.....	3
1.4 Hairpin Windings in EV Technology.....	4
1.5 Importance of Thermal Management Study.....	5
<i>1.5.1 Iron losses.....</i>	<i>6</i>
<i>1.5.2 Copper losses.....</i>	<i>7</i>
<i>1.5.3 Mechanical losses.....</i>	<i>7</i>
<i>1.5.4 Magnet losses.....</i>	<i>7</i>
<i>1.5.5 Stray losses.....</i>	<i>8</i>
1.6 Cooling Strategies.....	8
<i>1.6.1 Air Cooling.....</i>	<i>9</i>
<i>1.6.2 Liquid Cooling.....</i>	<i>9</i>
1.7 Heat pipe.....	10
<i>1.7.1 Operating principles.....</i>	<i>11</i>
<i>1.7.2 Fundamental Limits.....</i>	<i>12</i>
1.8 The aims and objective.....	14
Literature review.....	15
2.1 Thermal Management Strategies for Enhanced Electric Motor Performance in the Electric Vehicle Industry.....	15
2.2 Cooling Approaches in Magnetic Motors.....	16
<i>2.2.2 Liquid Cooling Method.....</i>	<i>20</i>
2.3 Heat Conduction Improvement.....	25
2.4 Innovative Cooling Techniques: Heat Pipes for Enhancing Motor Performance.....	29
2.5 Thermal Modelling in Hairpin Winding with Heat Pipe.....	32
2.6 Research study.....	32
<i>2.6.1 Gaps in recent studies.....</i>	<i>33</i>
<i>2.6.2 Research aims and objectives.....</i>	<i>34</i>
Methodology.....	36
3.1 Geometry.....	36
3.2 Visualization of Hairpin Winding Layout for Electric Motors.....	38
3.2 Assumptions.....	41
3.3 Governing Equations and Boundary Conditions.....	42

3.3.1 Electromagnetic field	42
3.3.2 Energy and Fluid flow.....	44
3.4 Calculations and CFD Simulation Conditions	45
3.5 Grid independence	48
3.6 Validation.....	49
Result and Discussion	51
4.1 Magnetic Flux Distribution	51
4.2 Electromagnetic Volumetric Loss Density	52
4.2 AC/DC Losses in Hairpin Winding Motor.....	53
4.3 Thermal Performance and Temperature Distribution	55
4.4 Thermal Performance Analysis and Heat Pipe Effectiveness	58
4.4.1 Effect of losses and heat pipe on capillary pressure	58
4.4.2 Velocity and Pressure Profiles in the Liquid Region	60
4.4.3 Velocity and Pressure Profiles in the Vapor Region	60
4.4.4 Maximum Temperature in Stator	61
4.4.5 Temperature in Windings.....	62
4.5 Efficiency.....	64
4.6 Heat pipe effects compared to water jacker cooling in hairpin winding	64
Conclusion	66
Future Work and Limitation	71
Simulation Setup	A
A.1 Heat Pipe Model	A
A.2 Hairpin Winding Model.....	B
A.3 Energy Equations in Solid and Fluid Parts	C
A.4 Mathematical Equations and Implementation of current research in COMSOL Physics Design Builder	D
A.4.1 COMSOL Physics Builder Introduction	D
A.4.2 Capillary pressure limitation.....	D
A.4.3 Mathematical Novelty in the Energy Equation.....	E
A.4.4 Dependent Variables Declaration:	G
A.4.5 AC and DC Losses as External Heat Sources in the Energy Equation	H
A.5 Physics Set Up in COMSOL Physics Builder	I
A.5.1 Geometry Type.....	I
A.5.2 Physics Interface Features	I
A.5.3 Customized Physics Interfaces	J

<i>A.5.4 Interactive Programming</i>	J
<i>A.5.5 Eliminating Coding Barriers</i>	J
<i>A.5.6 Tree Structure Representation</i>	J
A.6 COMSOL Physics Builder Settings in Current study	K
<i>A.6.1 Dependent Variables Declaration</i>	K
<i>A.6.2 Programming Governing Equations</i>	M
<i>A.6.3 Coefficient Form Equation:</i>	O
<i>A.6.4 Define Constant Parameters</i>	R
<i>A.6.5 Boundary Condition Domain Feature</i>	T
References	A

List of Figures

Fig 1.1 The information about the highest power output of electric and hybrid vehicle motors currently available and their future plans.....	2
Fig 1.2 Hairpin Winding Design details.....	4
Fig 1.3 Different heat losses in electric motors.....	6
Fig 1.4 Cooling strategies in field of Thermal Management for Hairpin Windings motors.....	9
Fig 1.5 Heat pipe physical structure.....	11
Fig 1.6 Heat transport capacity of HP as a function of temperature along with operational constraints.....	13
Fig 2.1 Schematic of research aims and objectives.....	35
Fig 3.1 Schematic diagram of (a) Stator and rotor body, (b) Stator with heat pipe, (c) 1/8 Stator section, and (d) Flat heat pipe side view.....	37
Fig 3.2 Top view of wiring arrangement of hairpin windings.....	39
Fig 3.3 six-layer winding design for hairpin winding motor with 48 slots, 8 poles, and a maximum of four parallel branches.....	40
Fig 3.4 Boundary conditions in (a) stator and (b) flat heat pipe.....	45
Fig 3.5 Coupling framework in the research study.....	46
Fig 3.6 Generated meshes in the research study.....	49
Fig 3.7 Validated results with experimental research.....	50
Fig 4.1 Magnetic flux distribution in case number 1 with 3000 rpm speed.....	52
Fig 4.2 Electromagnetic volumetric loss contour.....	53
Fig 4.3 Copper loss and iron loss calculated in this study in different phase current and rotational speed.....	54
Fig 4.4 Temperature distribution in the motor for (a) Heat Pipe container, (b) stator with heat pipe, (c) temperature distribution in side section of the motor and temperature distribution in the outer surface of the heat pipe in upside, and (d) pressure distribution in the vapor chamber of heat pipe.....	56
Fig 4.5 Temperature distribution in middle section of the stator.....	58
Fig 4.6 Effect of losses in liquid pressure drop.....	59
Fig 4.7 Velocity and Pressure Profiles in the Liquid Region.....	60
Fig 4.8 Temperature distribution in middle section of the stator.....	61
Fig 4.9 Comparison of the maximum temperature generated in the stator by volumetric heat losses from copper losses and iron losses.....	62
Fig 4.10 Average temperature difference in winding layers for cases with heat pipe and without heat pipe in $I=7$ A.....	63
Fig 4.11 Motor's efficiency in different current and speed conditions.....	64
Fig 4.12 Maximum temperature differences in stator in current study and Zou et al. [91].....	65
Fig 4.13 Temperature differences in winding layers in current study and Zou et al. [91].....	66

List of Tables

Table 2.1 Air cooling strategy as a cooling approach in magnetic motors	18
Table 2.2 Liquid cooling strategy as a cooling approach in magnetic motors	23
Table 2.3 Implementing novel materials as a cooling strategy in magnetic motors	27
Table 2.4 Heat Pipe strategy as a cooling approach in magnetic motors	30
Table 3.1 50 kW Hairpin Winding Main Physical Parameters	38
Table 3.2 Material properties used for simulation study	41
Table 3.3 Simulated cases in the paper	48
Table 3.4 Mesh independence check.....	49

NOMENCLATURE

I	Phase current	[A]	μ	Viscosity	[Pa.s]
I_m	Peak current	[A]	c_p	Specific heat capacity	[J/kg.K]
R_s	Specific gas constant	[J/mol.K]	σ	Surface tension	[N/m]
T	Temperature	[K]	M_n	Molar mass	[kg/mol]
T_{ref}	Reference temperature	[K]	q_{evap}	Heat of evaporation	[W/m ²]
k	Thermal conductivity	[W/m.K]	\dot{m}	Normal mass flux	[]
k_{eff}	effective thermal conductivity	[W/m.K]	λ	Enthalpy of vaporization	[kJ/kg]
h	Heat transfer coefficient	[W/m ² .K]	θ	Rotor angle	[Edeg]
h_{fg}	Latent heat	[kJ/kg]	\emptyset	Phase angle	[Edeg]
ρ	Density	[kg/m ³]	φ	Porosity	[]
ρ_v	Vapor density	[kg/m ³]	κ	Scaling factor	[]
p	Pressure	[Pa]	Q_{int}	Heat source in stator iron region	[W/m ³]
p_{ref}	Reference pressure	[Pa]	Q_{inc}	Heat source in coppers winding	[W/m ³]
Δp_c	Capillary pressure	[Pa]	R_c	Winding resistance	[Ω]
p_{sat}	Saturated pressure	[Pa]			

Subscripts

m	Magnet	ext	External
c	Copper	s	Solid
i	Iron	f	Fluid

Chapter 1

Introduction

1.1 Electrification and Advancements in Traction Motors

The global attention towards technologies that play a pivotal role in realizing a carbon-neutral society has intensified, largely due to the risks posed by climate change and the global warming [1]. In response to that, the transportation sector, known for its substantial energy consumption, is now experiencing a crucial and important shift towards electrification [2,3]. This transformation is not only an essential step in carbon emissions reduction, but also a strategic movement to align with the sustainable energy goals of the world while mitigating the impacts of environmental challenges.

Within the global goal for achieving 'net zero' in response to climate change and emissions reduction requirements, the momentum behind approving electrification within the transportation sector is clear [4,5]. Numerous nations and automobile manufacturers have committed to phasing out traditional vehicle sales within the coming decade [6]. These ambitious pledges translate into substantially elevated performance benchmarks for powertrains in pure/hybrid electric vehicles (EVs) [7], where the central component is the electric machine. The core competitive edge in electric machine advancements lies primarily in their capacity to attain remarkable power density (measured in kW/kg or kW/L) and superior efficiency, all while maintaining a crucial balance with cost-effectiveness (kW).

As shown in Fig 1.1, the USA's Department of Energy and the UK's Advanced Propulsion Centre have outlined a visionary set of motor-level advancements to be accomplished by 2025, propelling far beyond the capabilities of any motor currently in use within commercial EVs [7]. This initiative essentially entails a bold push at the forefront of next-generation traction motor progress, simultaneously elevating torque density and rotational speed [8]. The measure of torque density is fundamentally tied to the motor's magnetic and electric capacities. Leveraging robust permanent magnets (PMs) and ferromagnetic materials to achieve substantial magnetic loading has firmly established the PM motor as the preferred choice for EV traction. However, the adoption of higher current loads often accompanies amplified power losses, presenting intricate thermal

management hurdles. Similarly, increasing rotational speed introduces additional losses and faces constraints rooted in the mechanical integrity of the rotor, in addition to the operational capabilities of power electronic motors.

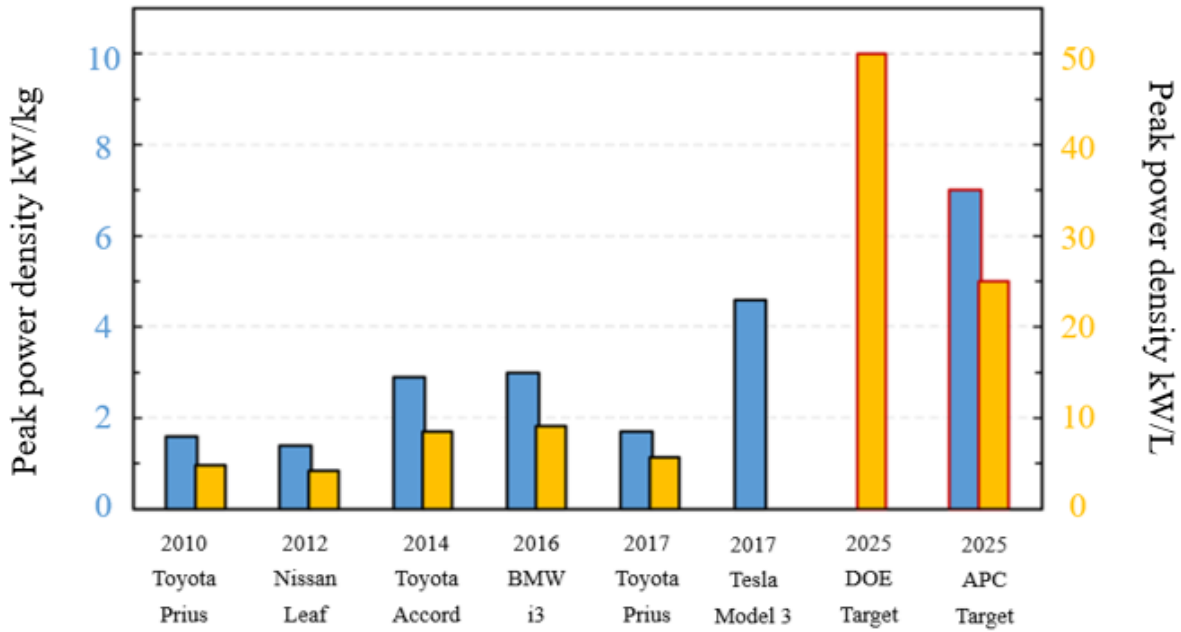


Fig 1.1 The information about the highest power output of electric and hybrid vehicle motors currently available and their future plans [7,8].

1.2 Permanent Magnet Synchronize Motors

The essential core of electromechanical energy conversion lies within the windings accommodated in stators, functioning under inherently elevated temperatures due to copper losses and iron losses from both direct current (DC) and alternating current (AC) sources. These losses play a substantial role in determining the motor's power density. In the initial stages of EV traction motor development, demonstrated by models like the 2010 Toyota Prius and the 2012 Nissan Leaf, stator windings were constructed using stranded round wires [9]. Despite these thin wires exhibiting minimal skin and proximity effects at an individual strand level, their operation at high speeds could result in significantly heightened AC losses on a collective "bundle level," attributed to circulating currents between parallel strands [10].

The escalating demands for higher power density and enhanced efficiency in traction motors have spurred a revolution in winding technologies. Within the EV sector, conventional random windings are gradually being substituted by hairpin windings featuring rectangular conductor bars [11]. One inherent advantage of hairpin windings, when compared to stranded round wires, is their ability to achieve a high slot fill factor, resulting in substantially reduced direct current (DC) resistance and associated losses. Moreover, due to the notable enhancement in the consistency and precision of conductor placement within and outside slots, advanced cooling techniques can be effectively employed to elevate current density and loading, thereby further amplifying power density. This specific winding approach was initially introduced by Cai et al. [12] and further refined by Cai [13]. It involves the arrangement of rectangular-shaped conductor bars in a single array along the depth of the stator slots. Following these innovations, the hairpin winding configuration has been subsequently implemented in well-known hybrid electric vehicles (HEVs) like the Chevrolet Bolt/Volt [14] and Toyota Prius [15].

1.3 Current Technologies

At low frequencies, the current distribution in the armature conductors is uniform. However, at higher frequencies, skin and proximity effects can occur, increasing conductor resistance and losses. Litz wires can be used to mitigate these effects, but they are expensive and complex to manufacture, making them only suitable for high-frequency applications [16]. In transportation applications, such as the automotive sector, random winding is the preferred solution due to its cost-effectiveness. Random winding is flexible and can be used to create a variety of winding configurations, but it has a low fill factor, resulting in a larger and heavier motor with a relatively low power density. Additionally, the random distribution of conductors in the slots can lead to an uneven winding voltage distribution, which can reduce overall reliability [17].

Traction machines can have either form-wound windings or hairpin windings, which are made of flat rectangular conductors [18]. Hairpin windings are widely used in high-power density traction applications and are gaining increasing attention in the research literature [19]. The main advantage of hairpin windings over form-wound windings is the higher slot fill factor, which is the ratio of conductive to insulating materials in the slot. Hairpin windings are also more efficient than form-wound windings because the rectangular wires fit the shape of the slot better, reducing

the length of the end-winding and the DC copper loss [20]. Additionally, the flat and "massive" shape of each hairpin leg reduces the DC copper loss generated by the active parts. Finally, hairpin windings can be produced more quickly and cheaply than form-wound windings, making them suitable for mass production [21]. Hairpin windings have several advantages over form-wound windings, including higher slot fill factor, better thermal slot conductivity, lower DC resistance, better voltage distribution, and automated fabrication process [22]. These advantages make hairpin windings well-suited for the automotive industry, where power density and efficiency are critical. As a result, hairpin windings are becoming increasingly popular in traction applications.

1.4 Hairpin Windings in EV Technology

Fig 1.2 shows the fundamental concept of hairpin windings, which displays a photographic representation of a conductor sample corresponding to the stator prototype introduced within this article. The term 'hairpin' is employed to describe a conductor that is bent into a 'U-shape,' featuring two parallel extending legs that can be axially inserted into stator slots from one end of the motor. Through precise manipulation facilitated by computer numerical control (CNC), the legs of a sequence of hairpin conductors can be positioned at specific locations (across different slots) and radial positions (within distinct layers of a single slot), based on accurately planned winding arrangements. Following insertion, the legs of the hairpin conductors stick out from the opposite stator end and are subsequently twisted in either the same or reverse direction. With an appropriately determined distance, each conductor leg is aligned closely with another. Ultimately, the adjacent conductor legs are paired and welded together to establish interconnection among phase branches.

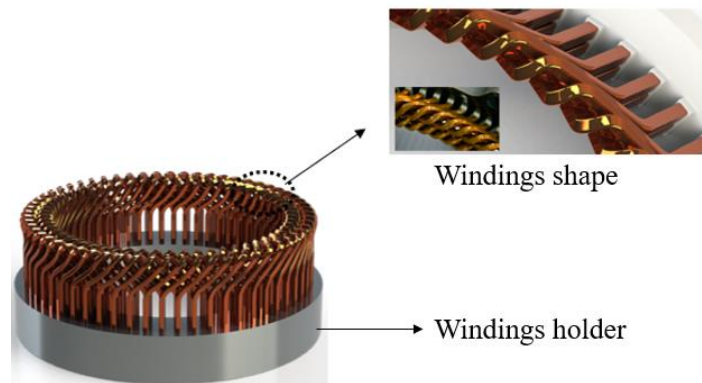


Fig 1.2 Hairpin winding design details.

To enhance the market of electric vehicles, it is essential to improve the performance of electric motors by increasing their power output, power density, torque density, and speed capabilities [23-25]. As motors are designed for higher power densities, they experience a notable increase in energy loss, leading to more complex thermal management challenges. Consequently, effective thermal management techniques have become imperative. The thermal systems of high-speed electric motors for cars involve diverse materials with distinct optimal temperature ranges and safety limits [26,27]. The dissipation of heat within the motor occurs through conduction, convection, and radiation, all within a limited space. Conduction takes place between the housing and stator, winding and stator, housing and end plate, as well as the shaft and bearings. Convective heat transfer involves the utilization of airflow or liquid coolants alongside solid components, surrounding both laminar and turbulent flow. Insufficient thermal management can lead to a range of problems, such as excessive thermal stress on components due to high temperatures, resulting in component deformation and assembly failure. Higher temperatures can also compromise insulation materials, reducing their effectiveness and lifespan due to changes in thermal conductivities. Recent research indicates that commonly used insulation materials experience a 50% reduction in lifespan with a mere 10 °C temperature increase [28]. The temperature limitations of insulation materials significantly restrict the current density of windings and the motor's power output [29]. Insulation failure may lead to short circuits and component burnout. Currently, permanent magnet motors are predominantly employed in electric vehicles, with these magnets being sensitive to temperature fluctuations. Overheating can cause irreversible demagnetization [30,31]. Therefore, the development of efficient heat dissipation methods for permanent magnet motors components has become a critical area of focus [32].

1.5 Importance of Thermal Management Study

To manage thermal conditions, the initial phase involves assessing the power losses that motors undergo within specific circumstances. Electric vehicles principally employ various motor types, including AC induction motors, switched reluctance motors, and permanent magnet synchronous motors (PMSM), typically ranging in power from 100 to 200 KW. These motors exhibit different operational characteristics [33]. Broadly, motor heat losses result from varied mechanisms and are generated across different components, as illustrated in Fig 1.3. Generally, the losses can be

tailored based on electromagnetic design choices, like magnetic loading, electrical loading, material selection, and geometric optimizations.

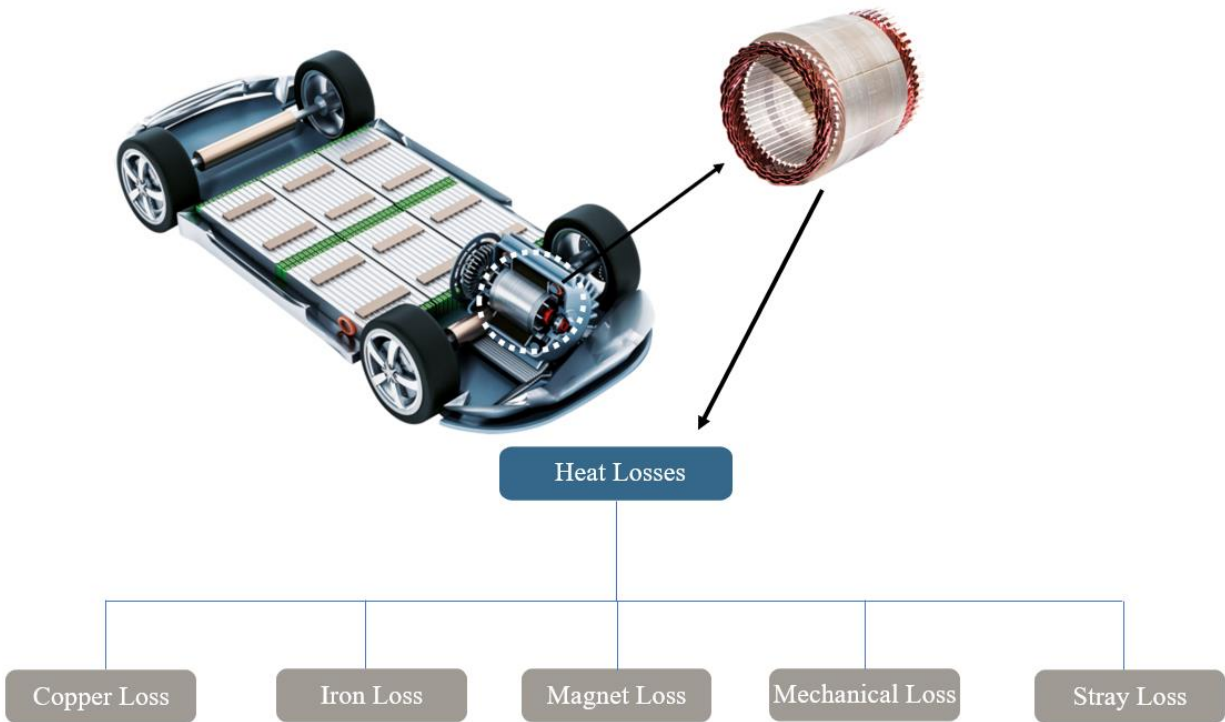


Fig 1.3 Different heat losses in electric motors.

Based on mechanisms, motor heat losses can be categorized into several distinct types, each with its own underlying physics and impact on motor performance which are categorized as follows:

1.5.1 Iron losses

Iron losses emerge within both stator and rotor laminations when subjected to alternating magnetic flux. These losses change with operational conditions, lamination types, and dimensions. They typically comprise eddy losses, hysteresis losses, and excess losses [34,35]. Employing Finite Volume methods (FVM) is common to accurately calculate iron losses due to the varying magnetic field distribution, particularly in areas experiencing heavier saturation. These methods help to understand how the magnetic field distribution changes, especially in regions where saturation of the magnetic field is more pronounced. By using FVM analysis, researchers can

optimize the design of electric motors and minimize these iron losses, making electric vehicles more efficient and sustainable.

1.5.2 Copper losses

Copper losses generally constitute the majority of motor losses, particularly in high-power density motors. They occur within the stator's winding and rotor, depending on the motor type. These losses arise from the Joule effect [36]. As electrical resistance fluctuates with temperature, high value of resistance results in additional heat generated within the copper conductor for a given current [37,38]. Consequently, maintaining lower winding temperatures significantly aids in reducing copper losses and enhancing motor efficiency. So, cooler windings mean less wasted energy and a more efficient motor, which is essential for electric vehicles and other applications where energy efficiency is critical.

1.5.3 Mechanical losses

Mechanical losses in electric motors primarily occur due to friction between various solid components, such as the rotor and bearings, as well as the shaft and end rings. These losses are significantly affected by several factors, including the speed of the rotor, the properties of the material used, the torque load on the motor, and factors related to the manufacturing process. Generally, higher rotor speeds, insufficient material, and rougher surface finishes can result in increased mechanical losses [39]. Another element of mechanical losses is windage losses, which arise from the friction between the air and the rotating rotor [40]. These losses originate from the airflow both axially and tangentially within the air gap. Windage losses tend to grow as the rotor speed increases. In simpler cylindrical motor geometries, it is possible to estimate windage losses either through analytical methods or empirical measurements. Reducing these mechanical losses, whether from solid component friction or windage, is crucial in optimizing the efficiency and performance of electric motors, making them more effective in various applications.

1.5.4 Magnet losses

In permanent magnet motors, magnets are typically incorporated into the rotor. These magnets can induce eddy currents, primarily as a result of the armature field. Accurately measuring these losses can be quite challenging because they involve complex 3D effects. To tackle this challenge,

researchers often rely on FVM methods for precise calculations. One useful technique for mitigating these losses involves dividing the magnets into segments both radially and circumferentially. This segmentation strategy helps in reducing the eddy current losses, making the motor more efficient and effective in its operation [41].

1.5.5 Stray losses

In addition to the losses, it's crucial to consider stray losses, which become particularly significant in high-frequency motors. These stray losses can be categorized into two types which are no-load losses, which arise from variations in the main flux, and stray load losses, that result from leakage flux [34]. Stray losses refer to the part of the overall energy loss in an electric machine that can't be attributed to friction and windage loss, copper loss, or core loss. In other words, they're the losses that aren't accounted for by these primary factors. Stray losses can make up more than 10% of the total losses in an electric machine, underscoring their importance in understanding and improving motor efficiency [42].

1.6 Cooling Strategies

Thermal management in PM motors requires consideration from the outset of motor design, as motor dimensions, power output, and efficiency are inherently linked to the capacity for dissipating heat. The principal thermal management strategies can be generally categorized into convection cooling and heat conduction improvement, which is illustrated in Fig 1.4. Convection cooling includes both air cooling methods such as natural convection and forced convection, and liquid cooling approaches like jacket cooling, immersion cooling, spray cooling, jet cooling, etc. targeting the stator, winding, and rotor to fulfill distinct cooling demands associated with various motor types. Furthermore, enhancing heat transfer within the motor can involve incorporating high thermal conductivity materials and components such as potting materials, heat guides, phase change materials (PCMs), and heat pipes.

Hairpin windings motors are becoming increasingly popular in electric vehicles due to their many advantages over traditional windings motors, including a higher slot fill factor, lower DC resistance, and better heat dissipation. However, hairpin windings motors can also generate more heat than traditional windings motors, due to the increased current density and the fact that the

windings are closer together. The scale of heat generated in hairpin windings motors depends on a number of factors, including the motor design, the operating conditions, and the cooling system. However, in general, the heat generated in hairpin windings motors is over 10kW [26,27].

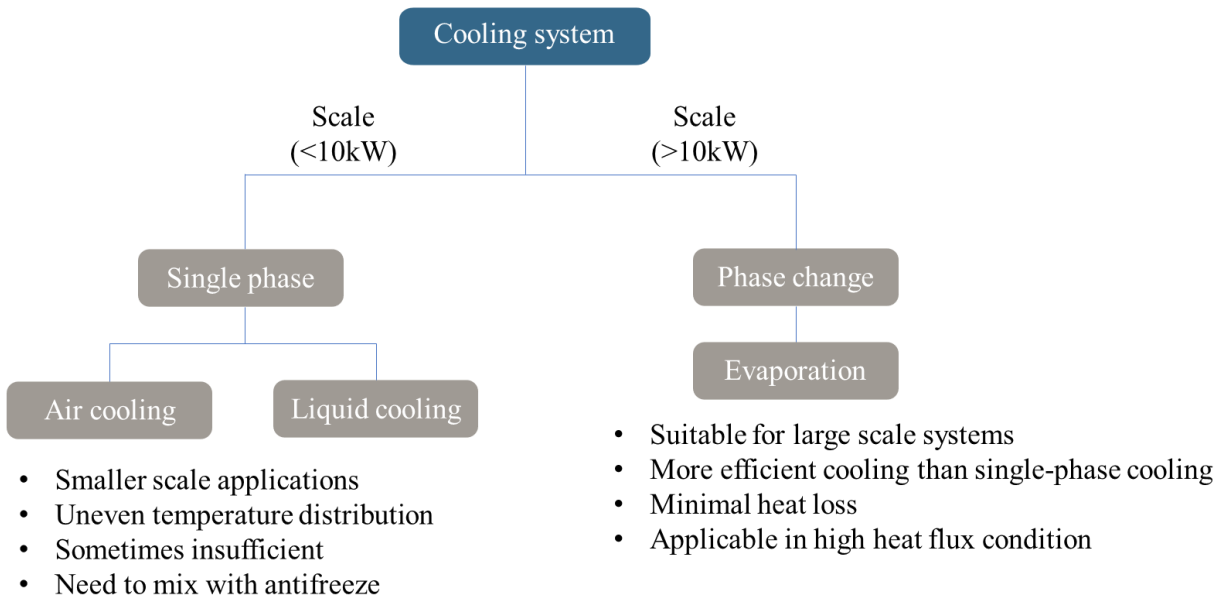


Fig 1.4 Cooling strategies in field of thermal management for hairpin windings motors.

According to cooling strategies in thermal management, these strategies can be categorized into several types, which are shown as follows:

1.6.1 Air Cooling

Air cooling serves as a foundational approach for motor cooling, particularly suited for motors characterized by modest heat densities. This method finds widespread use, ensuring efficient heat dissipation and temperature regulation. Two primary variations of air cooling are employed: natural air cooling on the external surface and forced air cooling within the motor's interior. By leveraging the ambient air's heat exchange properties, this method provides a reliable means to manage heat in motors [43].

1.6.2 Liquid Cooling

In the realm of commercial motors, especially those deployed in automotive contexts, liquid jacket cooling emerges as a prominent and trusted cooling technique. It offers an effective solution

to dissipate heat and maintain optimal operating temperatures. This approach involves the circulation of a liquid coolant within a jacket surrounding the motor's components. The heat generated within the motor is efficiently transferred to the coolant through convection-based mechanisms. By harnessing the fluid's superior heat absorption capabilities, liquid jacket cooling contributes significantly to preserving the performance and longevity of motors [44].

Considering the information found in existing methods, it's clear that the high-power density of Hairpin Windings Motors is a barrier to their widespread use as air-cooled motors. On the other hand, water-based motors require a relatively larger system size and result in higher unnecessary power consumption, making them less practical. While liquid cooling has several advantages, the challenge lies in creating a module design that can effectively maintain the motor's temperature during continuous operation. Additionally, there's an issue with heat conductivity, which is a drawback for liquid cooling strategy. This means that finding ways to improve the system's ability to conduct heat remains a significant challenge. Despite many recent efforts to explore different cooling systems for magnetic motors, there are still uncertainties about precisely how much heat these motors can transfer.

1.7 Heat pipe

Heat pipes are efficient devices used for phase-change heat transfer, offering benefits like lightweight design, high thermal conductivity, and flexibility which is shown in Fig 1.5. They work by facilitating heat transfer through processes like vaporization, mass transfer, and condensation of a chosen fluid. Heat pipes find applications in various fields, notably in cooling electronic components. These pipes utilize temperature differences between their hot and cold sides, using vapor pressure sensitivity to create pressure differentials that drive vapor from the hot side to the cold side. Vaporization absorbs heat on the hot side, while condensation releases it on the cold side. This process involves laminar flow within the vapor chamber and liquid phase transport through the wick. The role of vapor transport is contrasted with conductive heat transfer in the pipe wall. Overall, heat pipes play a crucial role in efficient heat management [45].

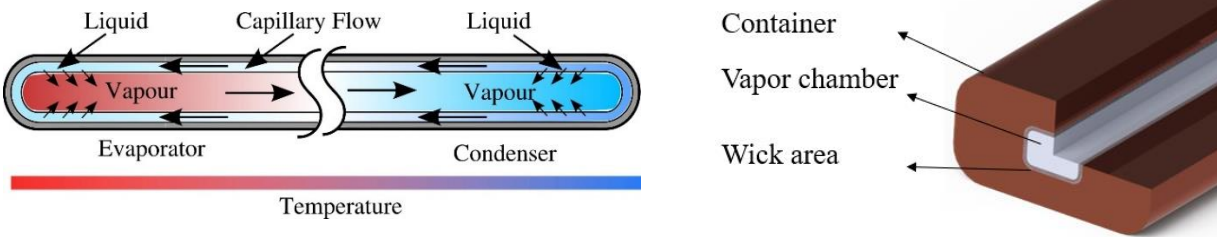


Fig 1.5 Heat pipe physical structure.

1.7.1 Operating principles

A heat pipe is like a closed tube with a wick part inside. This wick helps move liquid back to the hot end of the heat pipe. There are different types of these wicks that each have their own advantages and disadvantages. For example, one type is good at moving a lot of liquid but can't do it against gravity, while another type can move liquid against gravity but costs more. There's also a type that's in between. Making a heat pipe with a sintered wick usually happens in two steps. First, a special mandrel is put into a copper pipe, and then powdered material is poured in. After that, it's heated to stick the powder to the pipe. Once that's done, the mandrel is taken out, leaving a sintered wick inside the pipe. The second step is getting rid of any air inside the heat pipe, filling it with a special liquid, and sealing it up [46,47].

When heat is applied to the heat pipe's evaporator, the liquid working fluid in the evaporator wick converts into vapor. This generated vapor moves into the adiabatic area of the heat pipe, where it experiences a pressure drop that makes it move faster, resulting in a strong flow of the working fluid towards the condenser region. In the condenser region, the vapor turns back into a liquid due to condensation, which happens at a lower pressure, allowing the liquid to return to the evaporator. This return is made possible due to the capillary force generated within the capillary structure of the wick area. The process of phase change used in heat pipes allows them to achieve impressive values of equivalent heat conductivity, typically ranging from 5,000 W/m.K to 100,000 W/m.K. This is significantly higher compared to the thermal conductivity of pure copper, which is only around 387 W/m.K [48].

Heat pipes are well-suited cooling equipment for thermal management enhancement over long distances while maintaining a nearly uniform temperature distribution. In situations where heat

needs to be dissipated from structures, such as winding bodies or rotor assemblies, heat pipes are a highly effective choice. Two types of stationary and rotary heat pipe assemblies have been explored, although the second one presents unique challenges due to the mechanical forces acting on the heat pipe body. Existing research confirms the effectiveness of using heat pipes for thermal management, even in demanding conditions [49].

1.7.2 Fundamental Limits

The basic or intended performance boundaries of heat pipes with wicks are determined by various physical factors [39]. The operating temperature of a heat pipe must be between its melting point and its critical temperature. Maximum heat transport capacity is limited by several operating conditions for a heat pipe. Fig 1.6 provides a schematic representation of heat pipe performance (specifically, axial heat flux) in relation to temperature, along with these operational conditions [46].

Viscous limit:

The first boundary shown in Fig 1.6 is the viscous limit (sometimes called the vapor limit), which occurs when a heat pipe operates below its usual temperature range, such as during startup when it's frozen. In such situations, the vapor pressure is relatively low, and as a result, viscous forces become the dominant factor affecting the movement of vapor along the length of the heat pipe [46].

Sonic limit:

The second boundary, known as the sonic limit, is associated with the speed at which vapor exits the evaporator. Flow in vapor phase can't flow smoothly due to reaching a very high speed in the heat pipe. This happens when there's too much heat added at cases with lower operating temperatures, especially when there's a big difference in temperature between the evaporator and condenser. This effect usually occurs at the start of heat pipe operation, and it corrects itself over time [46].

Entrainment limit:

Another limit shown in Fig 1.6 is related to the vapor flowing too fast, known as the entrainment limit. In this scenario, small liquid drops can separate from the wick and travel with

the vapor toward the condenser. In more serious situations, this can lead to the evaporator running out of working liquid, which is called a 'dry out' situation [46].

Capillary limit:

The capillary limit, also known as the hydrodynamic limit, relies on how well the wick structure can move liquid. If the wick can't push liquid enough, and the most pressure it can create is lower than the combined effects of gravity, liquid pressure, and vapor pressure decrease, the heat pipe or evaporator can experience drying out [46].

Boiling limit:

The final limit indicated in Figure 1.6 relates to heat movement in a different direction, going from the center to the outer edge. This is the boiling limit, which happens when the heat flowing from the center of the evaporator is too high. In severe cases, this can lead to a 'dry out' situation in the heat pipe [46].

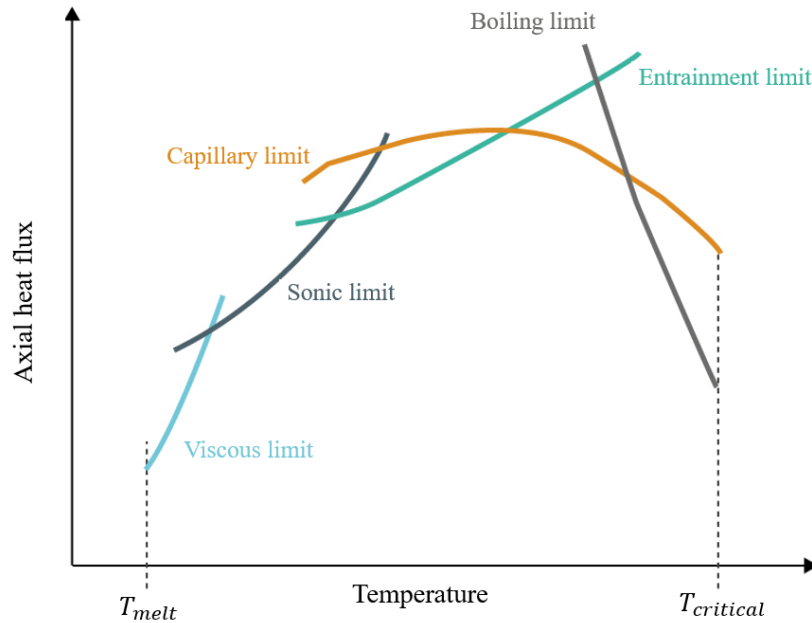


Fig 1.6 Heat transfer capacity of HP as a function of temperature along with operational constraints [46].

As mentioned earlier, the performance of heat pipes is influenced by certain limitations. One of specific importance in electromagnetic (EM) applications is the capillary limit, which can be

influenced by the orientation of heat pipes. For example, when a heat pipe is oriented vertically with the condenser located below the evaporator, it can pose challenges for certain heat pipe designs. In such cases, the wick structure must ensure sufficient capillary force and pumping against gravity. Additionally, there are other operating limits to consider, such as high acceleration like g-force, centrifugal force, and low-gravity environments, which are particularly important in applications related to automotive industries [46].

1.8 The aims and objective

Current cooling methods for hairpin winding motors are not ideal, as they either have a limited capacity to dissipate heat or are impractical due to their size or power consumption. Heat pipe cooling is a promising alternative cooling method, but it has not been well-studied in the context of hairpin winding motors. This research aims to assess the effectiveness of heat pipe cooling for a 50 kW hairpin winding motor, with a specific focus on reducing hot spots within the windings. The research also aims to study the effects of heat pipes on improving the overall cooling efficiency of the motor's windings and to evaluate the practicality and feasibility of utilizing heat pipe cooling systems for hairpin winding motors.

In addition to the main objectives outlined in the original text, this extended research could also explore the following areas:

- The effects of heat pipe designs on cooling performance.
- The impact of heat pipe cooling on the motor's power density, temperature and efficiency.
- The reliability and durability of heat pipe cooling systems in real-world applications.

The findings of this research could help to address the challenges of cooling hairpin winding motors and enable the development of more efficient and powerful electric motors.

Chapter 2

Literature review

2.1 Thermal Management Strategies for Enhanced Electric Motor Performance in the Electric Vehicle Industry

The electric car industry is seen as a key player in addressing carbon neutral goals, the electric motor in modern electric vehicle is a crucial component and managing its thermal performance has become a focus for both industry and academia. As electric cars demand more power, higher torque, and higher density, efficient thermal management is necessary to maintain motor efficiency, durability, and safety. Poor thermal management can lead to demagnetization, insulation material degradation, decreased efficiency, shortened lifespan, and even motor burnout. To achieve longer-term reliability and extended mileage delivered by electric motor, and the hotspots and thermal imbalances, which cause a major barrier in higher energy efficient powertrain, have to be tackled in every new motor development. Major losses in electric motors are joule, iron, and mechanical losses [50]. These cause heating due to the motor's operation and thus, continuous cooling is essential [51,52]. Common cooling methods are using a fan [53] or a fin design [54]. However, high speed operation generates excessive heat leading to reduced efficiency, increased energy consumption and potential damage. So, one of the crucial aspects of electric motor design is thermal management. These methods provide the possibility of longer usage and extended mileage for electric vehicle. However, higher rotation speed of the motor causes a significant increase in thermal loss which generated in the rotor and stator, and motor's efficiency reduces significantly due to the overheat. Also, an increase in energy consumption, and possible permanent damage to the powertrain structure occurs in motor [55]. Therefore, the cooling problem of electric motors has become prominent research in heat transfer field for future low carbon transport industry.

2.2 Cooling Approaches in Magnetic Motors

Effective thermal management is a crucial consideration right from the outset of motor design, as the motor's efficiency, power output, and scope are directly tied to its ability to dissipate heat. Convection cooling and heat conduction enhancement are two available primary categories of thermal management concepts, which are broadly categorized as thermal conduction improvement and convection cooling enhancement. In convection cooling, there are choices like using air or liquid cooling for different sections of the motor, such as the stator, winding, and rotor. These options help meet the cooling requirements of different motor types. Additionally, to enhance heat transfer within the motor, materials with high thermal conductivity are used like potting materials, heat guides, phase change materials (PCMs), and heat pipes. These technologies are presented in this section.

2.2.1 Air Cooling

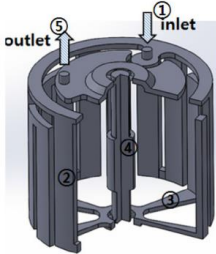
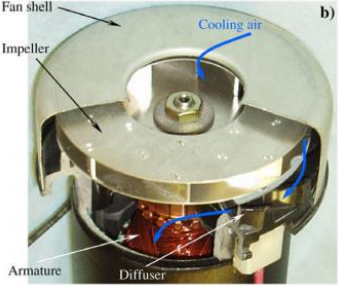
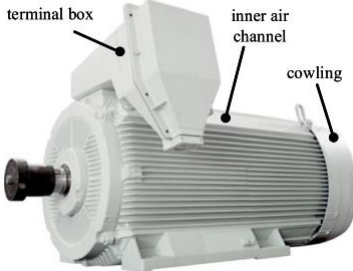
Air cooling method is a fundamental cooling approaches for motors and is often used to cool motors with a relatively low heat density. This cooling approach takes the form of natural air cooling on the motor's external surface or forced air cooling in motor. Lee et al [56] investigated experimentally the thermal management of a magnetic motor and improved the motor's capability without employing external coolant systems by changing the way of entering and exiting the flow of cooling air to the engine. They were able to increase the speed of the rotor while temperature could be maintained at same level. Li [57] started to use a centrifugal vane as a conventional cooling vane without manipulating the entire motor structure. Therefore, results showed efficiency enhancement of the air cooling and increase the amount of heat transferred from the motor.

There are typically fins that serve to enhance the heat transfer rate between the housing and the surrounding air on the outer surface of the motor housing. These fin assemblies effectively enlarge the heat transfer zone of the housing's external surface [52]. The key consideration here is how to optimize the dimensions of these fins to maximize the cooling effect. Ulbrich et al. [58] investigated in a research program in this area which revealed that a housing with nine fins generally outperformed those with 6-8 fins. Interestingly, adding the number of fins to 10 did not lead to a significantly greater positive impact on cooling effectiveness. At the same time,

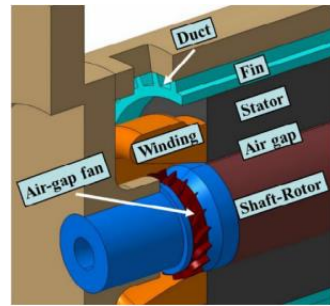
enhancing heat dissipation performance was achieved by raising the average and overall hydraulic diameters. According to Peng et al. [59] results, the spacing between the fins had a bigger effect on the winding temperature. It is important to mention that the winding temperature also dropped as the spacing between the fins, the thickness of the fins, and the height of the fins increased.

For motors with air cooling strategy, heat transfer and airflow in the PM motors are particularly crucial. In compact spaces, the internal airflow plays an important role in the heat transfer process [60]. Additionally, selecting and optimizing the structure of the fans is a key factor in improving the cooling effectiveness, as highlighted by the studies conducted by Kim et al. [61]. Furthermore, both the geometries of the internal air pathways and the parameters of the fans significantly affect the heat transfer performance and airflow's pressure drop [62]. An air guide plate and made modifications to the shield within the air pathway to eliminate energy loss caused by vortex formation introduced by Wen et al. [63]. With this new airflow configuration, the outlet temperature decreased by 3.3 °C. Asef et al. [64] also demonstrated that the motors cooling could be improved by adding cooling ducts in the stator and stator's teeth, although it slightly increases iron loss. Air cooling strategy as a cooling approach in magnetic motors is illustrated in Table 2.1

Table 2.1 Air cooling strategy as a cooling approach in magnetic motors.

Reference	Motor	Cooling Strategy	Result
Lee et al. [56] (2016)	 <p data-bbox="537 626 779 659">Novel IPM 6 poles</p>	<p data-bbox="873 423 1367 565">Numerically studied about cooling in rotor with a shaft with hole and investigated about stator cooling with an external jacket.</p>	<p data-bbox="1388 423 1908 565">Results indicated reduction of the temperatures in the external stator of the motor by 42%, while those in the jacket-cooled motor decreased by 10%.</p>
Li [57] (2010)	 <p data-bbox="485 1024 810 1057">5001i 5 kVA PM Motor</p>	<p data-bbox="873 789 1367 930">Experimental and numerical investigation in top-closed type centrifugal impellers employed as cooling fans in electric motor.</p>	<p data-bbox="1388 732 1908 984">If motor's rotation speed falls below 3200 rpm, it will result in an increase in armature temperature that can ultimately cause motor failure. Therefore, it is not advisable to continuously operate this drive motor with a shaft torque exceeding 1.22 Nm.</p>
Ulbrich et al. [58] (2016)	 <p data-bbox="485 1373 825 1406">Exemplary machine IC411</p>	<p data-bbox="873 1170 1367 1312">Utilize an automated approach to address the conjugate heat transfer (CHT) challenge associated with cooling fins on a housing.</p>	<p data-bbox="1388 1146 1908 1325">An interesting finding underscores the significance of the total hydraulic diameter, suggesting its potential as a universal parameter for optimizing heat transfer.</p>

Kim et al. [61]
(2016)

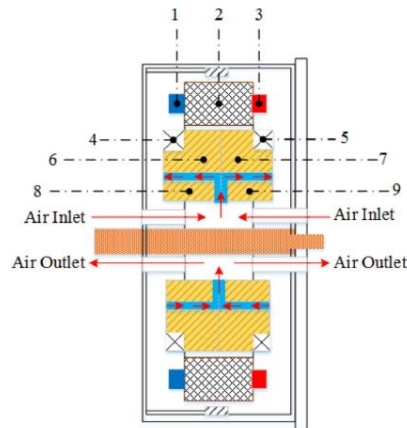


16 copper cage bars
induction motor

CFD Study on the Impact of Airgap Fans on Winding Cooling in a High-Capacity High-Speed Induction Motor Operating at over 10,000 RPM.

The heat transfer coefficients on the winding surface and in the air gap showed substantial improvements, increasing by as much as 31% and 90%, respectively, thanks to the higher flow rate.

Asef et al. [62]
(2018)



Closed-slot topology of PM
synchronous generator

Computational Fluid Dynamics Investigation of an Embedded Cooling System with Different Numbers of Ducts for the Outer Rotor.

The study examined innovative models featuring 2-ducts and 4-ducts, with the four-ducts model demonstrating a notable temperature decrease up to 11°C.

In summary, making external natural air cooling better involves improving the design of the fins. Increasing the area for heat transfer is usually good for cooling the motor, as long as it doesn't slow down the airflow too much. However, making the fins bigger can make the motor larger and heavier, which might make it harder to put together, especially for motors inside the wheels. When it comes to airflow inside the motor, reducing any obstacles in the air path helps airflow move more easily and cool the motor better. The airflow inside the motor is a bit complicated because it includes rotation at the ends, air moving in the gap, and possibly small airflows in ducts. All of these interact in a complex way with the motor's heat. A good airflow path has fast airflow, doesn't slow down too much, and cools well. It's important to mention that if we make big changes to improve the airflow, we should also check if the motor can handle the extra stress from these changes. Another way to make the motor cooler is to improve the fan. In general, air cooling is good for motors that don't make too much heat because air isn't the best at cooling. So, for motors that make a lot of heat, especially hairpin winding motors, it's usually better to use liquid cooling.

2.2.2 Liquid Cooling Method

Liquid cooling method is a widely adopted cooling technique, particularly in most of the motors, and it's especially common in automotive applications. In this approach, heat removes by using a liquid coolant material, primarily through convection heat transfer within a jacket. Water uses as the coolant material in most cases in this cooling method. Numerous studies have explored into how factors like channel sizes, cross-sectional shape, and flow rate influence the performance of the liquid cooling method. Saleem et al. [66] progressed to cool the propulsion system of a EV's PM motor. Instead of using oil flow circulation, they sprayed oil particles into the area between the rotor and stator. Based on their data, the critical temperature decreased by 6.4% and the amount of heat transfer increased by 8.1%. In one of the most recent researches conducted in this field, Guo et al [67] created two adjacent holes in the stator body. These two holes were used, one as an inlet and the other as an outlet, and the cooling fluid by rotating in the stator body led to the cooling of the motor. So, they could enhance the maximum temperature created inside the engine from 153.7 °C to 129.5 °C, which is a significant reduction in temperature to grow the efficiency of the engine. Lim and Kim [68] tried to cool a PM motor using an oil spray. In their research, instead of circulating the oil inside the stator, they sprayed it on the hot surfaces of the stator. The result of

their work generated the maximum temperature of the motor to decrease from 155.4°C to 137.8 °C and the motor can easily continue its normal operation in a temperature range of lower than 150 °C. Rehman et al. [69] found that the maximum temperature of the stator decreases by increasing the number of cooling channels from 4 to 8. However, they noted that further increasing the number of passages didn't lead to a significant improvement. Furthermore, they observed that increasing the flow rate of the coolant proved to be a more effective method for enhancing cooling performance.

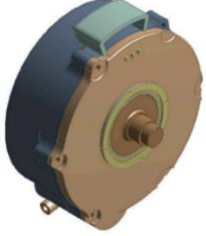
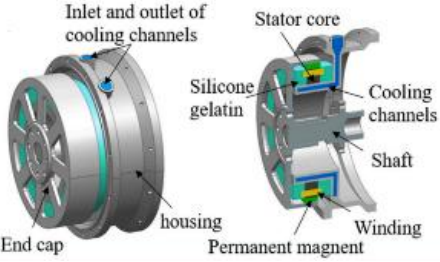
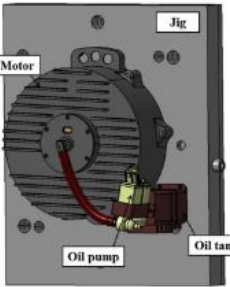
In contrast to conventional water jackets, Li et al. [70] introduced a novel configuration where they positioned the water loop at the lowest side of the stator's teeth, featuring two parallel flow pathways. Experimental results demonstrated that this innovative water jacket design effectively managed heat, with the end winding experiencing the highest temperature growth of 60 °C, demonstrating its strong performance. It was suggested that this design achieved a balance between the requirements of heat transfer coefficient and pressure drop through optimization of channel shape, locations, and numbers. Satrustegui et al. [71] conducted an analysis of various water jacket designs, as depicted in Figure 6. Their findings indicated that an axial water jacket led to a higher pressure drop compared to a spiral water jacket of the same heat transfer area. As a result of their research, they proposed three design criteria to fulfill the needs of turbulent flow, pressure drop, and erosion. In another study, Wu et al. [72] designed and evaluated the performance of two different water jacket channels. One had a smooth configuration, while the other was twisted. The twisted channel jacket notably altered water flow characteristics by significantly increasing circumferential velocity, turbulence energy, and vorticity distribution. Consequently, this design led to an enhancement in the heat transfer coefficient.

Water is not the only coolant under investigation; some studies have explored the use of alternative liquids for heat dissipation, such as water/ethylene glycol and oil. In the case of water/ethylene glycol, Deriszadeh et al. [73] found that as the ethylene glycol concentration and the number of turns increased, the heat transfer coefficient also increased. Furthermore, the rise in the heat transfer coefficient was more significant than the increase in the pressure drops. On the other hand, Yang et al. [74] conducted tests and simulations using oil jacket cooling for an electric

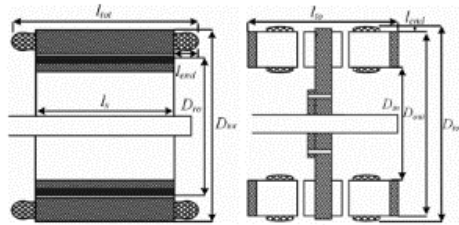
motor. They suggested that the motor's cooling performance improved when using smaller channel heights and widths, albeit at the expense of a higher pressure drop.

Regarding the water-cooling strategy in specific conditions in hairpin winding, Liu et al. [75] presented an experimental investigation into the cooling effectiveness of various spray cooling setups, emphasizing their potential utility in the thermal design and modeling of future machinery with similar cooling arrangements. The study explores the impact of nozzle types, flow rates, outlet velocities, and nozzle numbers on cooling performance. Additionally, thermal analysis is conducted on a stator with different cooling setups, including conventional water jacket designs and water jackets with high thermal conductivity potting, revealing significant enhancements in current density and output power when transitioning to spray cooling, with a nearly twofold increase in current density and minimal additional power consumption for the motor. Zhang et al [76] studied about the thermal model for the entire hairpin-winding stator. The article highlighted the unique challenges of modeling oil-sprayed hairpin stators, emphasizing the need to consider specific conditions to capture non-uniform temperature distribution and hotspots. Additionally, it introduces a method for calculating the convection area for heat transfer and local HTC (heat transfer coefficient) that accounts for oil-film thickness and its effects, particularly suitable for oil-spray cooling on hairpin windings. Experimental studies are recommended for deriving HTC values, conducted on representative segments during the motor design phase to establish necessary HTCs before manufacturing the full machine prototype. Table 2.2 shows Liquid cooling strategy as a cooling approach in PM motors.

Table 2.2 Liquid cooling strategy as a cooling approach in magnetic motors.

Reference	Motor	Cooling Strategy	Result
Saleem et al. [66] (2022)	 35 kW PM motor	Numerical study about motor cooling channel in in-wheel Motors.	At the highest speed, better heat transfer was seen, with an average increase of 0.1% in the main spray cooling region and 8.1% in the additional spray cooling regions compared to the standard spray cooling setup.
Guo [67] (2022)	 380 V PM in-wheel motor	Numerical study about new structure of changing cooling channel's locations into depend slots of stator.	Results in this study showed that the motor performance decreases by 0.02% due to the high height stator teeth.
Lim and Kim [68] (2014)	 35 kW in-wheel motor	Hollow shaft channel for the oil spray cooling of in-wheel motor.	At the designated design points of maximum speed, the coil temperatures at the base remained below the motor's temperature limit.

Li et al. [70]
(2019)

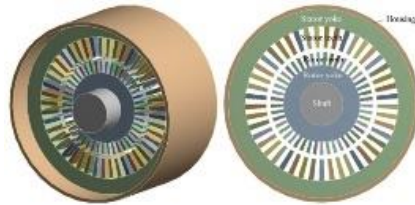


Direct-drive generator rated 130 kW

FEA investigation in water cooling method AFPM with a segmented stator core and an implemented cooling pipe.

The recommended AFPM is suitable for low-speed direct-driven uses like wind turbines and hydrogenation procedures. Its compact design, outstanding efficiency, tall and narrow planar structure, short length along the axis, and impressive torque density contribute to this suitability.

Satrústegui et al. [71]
(2017)

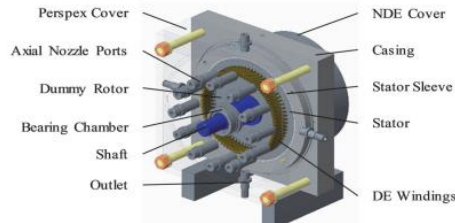


IC71W IM

CFD simulation about water jacket and its main parameters and some correlations for the design of the cooling ducts are analysed.

Two factors were found to have little effect on the system: the gap between cooling ducts and the separation between the ducts and the stator stack.

Liu et al. [75]
(2020)

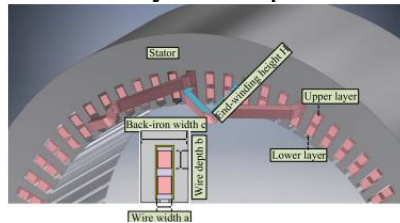


24 Slots 2 layers Hairpin winding

The impact of nozzle variety, flow rate, exit speed, and nozzle quantity is documented and analyzed to illustrate the cooling performance of the suggested configurations.

The findings indicated that under identical inlet temperature and total flow rate conditions, incorporating high thermal conductivity potting resulted in a roughly 20% increase in current density and output power, raising it to 14 A/mm².

Zhang et al. [76]
(2021)



72 Slots 2 layers hairpin winding

The surfaces that directly face the sprayed oil experience impingement by the oil droplets, leading to improved cooling performance.

The key focus is on preserving a strong axial thermal conductivity, while the thermal conductivity of the impregnation resin is not as critical as in traditional systems.

To sum up, liquid cooling for the stator is commonly employed in motors with mid-level heat density. In this approach, liquid flows through axial or spiral serpentine jacket channels to efficiently remove heat. Liquid cooling offers clear advantages over air cooling, as it can handle higher heat densities, operates with lower noise levels, and operates as a fully separate cooling system. Typically, the cooling channels are situated within the motor housing. However, positioning the channels closer to the winding can lead to a reduction in temperature but might increase iron losses. Water is frequently used as a coolant, although alternative options such as oil, water/glycol, and even dielectric fluids like thermomagnetic fluids have been explored for motor cooling [77]. Regardless of the coolant used, optimizing channel dimensions and flow rates has proven to be an effective way to enhance jacket cooling's heat transfer capacity. Numerous creative structural designs have been suggested and explored. Generally, approaches that boost the flow speed of the coolant are anticipated to provide improved performance, although certain methods may result in increased pressure drop in the channels. In the context of jacket cooling, air cooling is also significant in facilitating the heat transfer process, particularly for the rotor. Optimizing the airflow path is recommended for motors utilizing jacket cooling [78]. Additionally, certain considerations are necessary for motors with jacket cooling. It's advisable to maintain the inlet temperature within a specific range to prevent the coolant from causing thermal shock to insulation materials or failing to effectively dissipate heat [79]. Water has a significantly higher heat transfer compared to air. However, a combination of water and antifreeze must be used to prevent freezing in some conditions. Furthermore, the quality of the water which uses in water cooling method should be considered in research studies to avoid corrosion-related issues.

2.3 Heat Conduction Improvement

In a standard motor, the axial thermal conductivity of the stator lamination is quite limited. This limitation is primarily due to the suboptimal properties of the lamination material, and it is intentional to prevent iron losses. This low axial thermal conductivity effectively acts as a barrier, hindering the heat transfer in the axial direction. Additionally, contact thermal resistances arise from small air gaps and surface irregularities between various solid components within the motor. These resistances should not be underestimated. Considering these factors, it becomes evident that

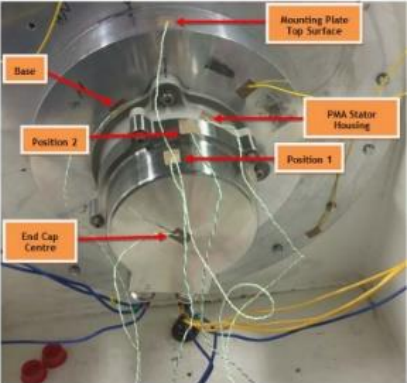
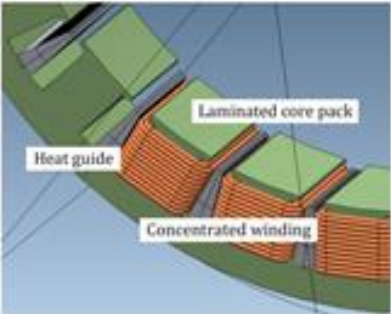
methods for enhancing heat conduction play a crucial role. These methods help redistribute heat and expedite the overall heat transfer process within the motor.

Certain potting materials can be employed to improve the heat conduction process within motors by filling the gaps between solid components. In a study by Kulan and Baker [80], potting material was tested as a heat transfer bridge between the end winding and casing of a motor. Their findings indicated a notable 23.6% reduction in temperature when these potting materials were used. Additionally, these materials effectively delayed the temperature increase of the motor, demonstrating their efficacy in enhancing heat conduction and thermal management.

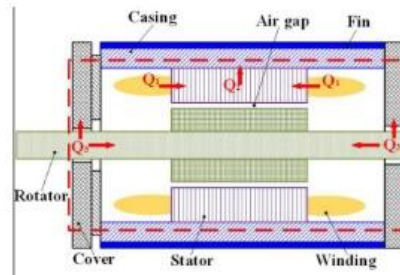
Heat guide (HG) plates have found application as an additional heat transfer pathway to enhance heat dissipation in motors, typically in conjunction with slot winding configurations. In a study conducted by Wrobel and Hussein [81], the goal was to enhance heat extraction from the winding by integrating heat guides (HGs) into the slot. Their findings demonstrated a significant reduction of approximately 30% in the temperature rise of the winding when HGs were present. Furthermore, two-thirds of this improvement was attributed to the enhancement of heat transfer in the radial direction, highlighting the effectiveness of HG plates in improving thermal management.

Phase change materials represent an alternative solution for motor thermal management due to their excellent thermal storage properties. Bellettre et al. [82] at the Polytechnic Center of Lyon attempted to cool hot spots using gallium metal. Considering that gallium melts at a temperature of 30 °C, its use had a very significant effect in reducing the temperature of hot spots. Wang et al. [83] introduced phase change materials (PCMs) into the motor, with the PCM placement shown in Figure 9 (a). Their findings revealed that under steady heating conditions, the use of PCM increased the operating time by up to 50%. In cases of intermittent heating conditions, the material reduced the peak temperature of the casing by 12.8%. Wang et al. [84] proposed an alternative structure. With this structure, the continuous operating time extended, and the peak temperature dropped by approximately 32.7%, resulting in a temperature reduction of 7.82 °C under the tested conditions. PCMs can also be integrated into hollow conductors, as demonstrated by Ayat et al. [85]. This incorporation of PCMs led to a decrease in temperature, with an observed reduction of 8% in temperature rise of the winding and an 18% decrease in winding weight. These findings collectively indicate the promising potential of PCMs for motor thermal management.

Table 2.3 Implementing novel materials as a cooling strategy in magnetic motors.

Reference	Motor	Cooling Strategy	Result
Kulan and Baker [80] (2017)	 <p>A permanent magnet alternator</p>	Experimental and lumped quantitative Impact of thermal paste addition in the machine's end winding area.	The results demonstrate that the model with thermal paste exhibited a 5.6% increase in axial heat flow rate.
Wrobel and Hussein [81] (2020)	 <p>80 kW PM</p>	HGs are intended here to be an integral part of the stator-winding assembly and are mounted in close proximity to the winding	The study results reveal that optimized heat guides (HGs) can lead to an impressive 85% enhancement in heat dissipation from the winding body, with only a negligible increase in power loss for the examined stator-winding assembly.

Wang et al. [82]
(2016)

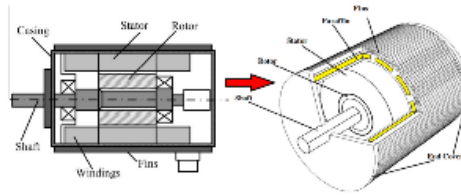


2.8 kW PMSM

An intelligent approach involves integrating the existing casing with phase change material (PCM), effectively utilizing paraffin as a substantial heat reservoir.

To optimize the heat-absorbing capacity of the paraffin, it's crucial to achieve an intermittent factor as close to, but less than, 0.0881. This condition indicates successful thermal optimization within the specified parameters.

Wang et al. [84]
(2016)

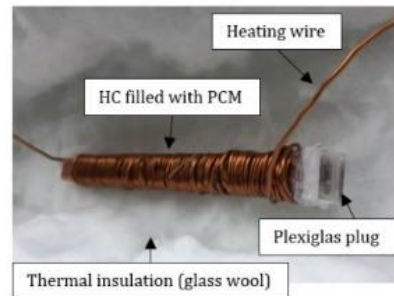


2.8 kW PMSM

An innovative enclosed motor casing with paraffin phase change material packaging.

Compared to the traditional casing with fins used for self-cooling PMSMs, the motor's running time can be increased by approximately 32.7%.

Ayat et al. [85]
(2019)



Hollow conductor

A new method of integrating PCM into smaller machines involves placing it directly inside hollow conductors.

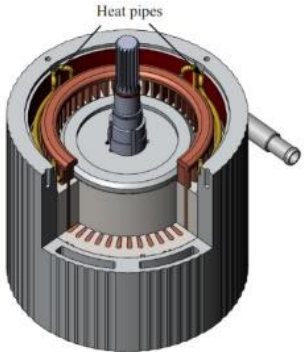
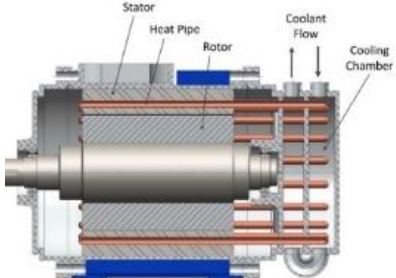
By adding PCM, the increase in winding temperature was reduced by 8%, and the weight of the winding decreased by 18%.

In summary, the utilization of potting materials, phase change materials (PCMs), and heat guides provides additional options for the thermal management of motors. These materials significantly improve heat conduction between motor components and help mitigate temperature fluctuations within the motor. As a result, they hold great promise for motor thermal management. However, it's important to note that the use of these methods may introduce magnetic issues, extra weight, and additional eddy losses, which should be carefully calculated and taken into account in PM motor design and operation.

2.4 Innovative Cooling Techniques: Heat Pipes for Enhancing Motor Performance

One of the most effective methods that has received much attention in recent years is the use of heat pipes for cooling. Park et al [86] tried to expand the heat transfer from the magnetic motor by substituting the vertical channels between the stator. They succeeded to provide more torque to the motor by improving the cooling system of the motor. In such a way that the engine, employing the same amount of energy, applies 50% more torque than in the case without cooling. Sun et al. [87] in a new plan placed parallel heat pipes between the windings of a synchronous motor. In this design, water flowed as a cooling fluid in the channels between the stator and was pumped from these channels into the heat pipes, and removing the heat released from the coils, helped to improve their heat transfer. They concluded that the use of this technology can reduce the temperature in the engine by 22.9 °C. Putra and Ariantara [88] in an experimental work installed L-shaped heat pipes in the outer chamber of the motor. Indeed, the goal of their project was to transfer heat as much as possible with the free air around the motor. With this method, they could increase the motor body temperature from 68.4 °C to 102.2 °C. Fang et al. [89] in a research project tried to reduce the maximum temperature of windings. By installing a heat pipe between the windings, they reduced the maximum temperature by about 22 °C. They devised two intriguing enclosure structures incorporating heat pipes for motor cooling. These new designs effectively reduced temperature gradients within the enclosure and the stator. Additionally, they extended the effective time for temperature control by up to 21.4%. These outcomes demonstrate the effectiveness of heat pipe-based enclosure structures for motor temperature management.

Table 2.4 Heat Pipe strategy as a cooling approach in magnetic motors.

Reference	Motor	Cooling Strategy	Result
Sun et al. [87] (2020)	 <p data-bbox="556 748 743 781">345 V 48 slots</p>	A novel thermal management strategy involves combining water-cooling motors with heat pipes and potting silicon gelatin (PSG).	The results consistently show that this new approach consistently lowers temperatures, with a significant maximum reduction of 22.9°C compared to the original motor. In contrast, a motor equipped only with heat pipes experiences a more moderate decrease of only 10°C.
Putra and Ariantara [88] (2017)	 <p data-bbox="464 1130 835 1211">0.5 HP conventional electric motor</p>	Heat pipes positioned on the exterior of the motor housing.	The motor's surface temperature decreased significantly, dropping from 102.2°C to 68.4°C, which amounts to a substantial 33.8°C reduction.

Fang et al. [89]
(2019)



380 V motor

Experimental and numerical two different layouts of heat pipes are used to provide a low-resistance thermal bridge. The rated peak temperature of the PMSM can be notably decreased by 22.3%, contributing to an enhancement in the power density of PMSMs.

2.5 Thermal Modelling in Hairpin Winding with Heat Pipe

In comparison to conducting on-site experimental thermal tests on EVs, thermal modeling has emerged as a more cost-effective and versatile alternative. It is especially well-suited for integrating electromagnetic and mechanical modeling to optimize motor performance. Numerical methods are commonly employed in thermal modeling. Computational fluid dynamics (CFD) is a prominent numerical modeling technique employed for simulating heat transfer in electric motors, utilizing both 2D and 3D models [90]. CFD is essential for achieving more precise convection heat transfer simulations, and it enjoys a well-established reputation for its exceptional capacity to analyze heat transfer performance across various scenarios. This involves heat transfer through natural/forced convection, impingement, and spray. CFD models are adept at addressing and visually representing temperature, pressure, and flow fields, contributing to their widespread adoption. Additionally, CFD has found utility in optimizing electric motor parameters, particularly geometric dimensions, as indicated in existing literature [81,82]. It possesses the capability to yield highly accurate simulation results for heat transfer processes, even when dealing with motors featuring complex structures. Another notable advantage of numerical analyses is their compatibility with electromagnetic and mechanical analytical models, enabling the possibility of multi-physical analyses [83].

2.6 Research study

Taking into account the information available in existing literature, the air cooling strategy may not be suitable for this motor due to its limited capacity to dissipate heat efficiently, especially in high heat density applications where other cooling methods may be more effective. Also, the motors which cool with water cooling method demands a quite larger system size and results in higher power consumption, significantly impeding its practicality. Although the liquid cooling method offers numerous advantages, the challenge remains in devising a module design that can ensure continued and effective thermal parameter for the motor during continuous operation. Furthermore, the deficiency in heat conductivity also poses a drawback [94]. This shows that the pursuit of methods to enhance the system's thermal conductivity continues to be a difficult endeavour. Although in recent years, many efforts have been devoted to investigating the

implementation of different cooling systems on the performance of magnetic motors, there are still many ambiguous points in determining the exact amount of heat transferred from motors. Moreover, the use of heat pipes as a cooling strategy has not received significant attention in the context of hairpin winding motors. In this numerical research done with COMSOL Physics-Builder software, we tried to check the performance of heat pipes on the amount of heat transferred from a 50 kW hairpin winding Motor in different operation conditions. Actually, the main priority of this research is how to remove hot spots from inside the windings, which has not been mentioned much in previous research. In addition, investigating the combination of AC/DC losses in energy equation as an external heat source on the cooling of windings is another category that studied in this research.

2.6.1 Gaps in recent studies

Despite the significant progress that has been made in the field of heat pipe cooling for electric motors, there are still some gaps that need to be addressed. One of the main challenges is designing a heat pipe cooling system that can effectively remove hot spots from within the windings. Hot spots are areas of high heat concentration that can lead to thermal failure of the motor. Additionally, there is a need for more research on the effects of different heat pipe designs on cooling performance, and the impact of heat pipe cooling on the motor's power density, heat transfer, and efficiency.

One of the main challenges in CFD analysis of heat pipe cooling systems for electric motors is coupling the electromagnetic losses with the energy equation. Electromagnetic losses are the losses that occur in the motor windings due to the magnetic field. These losses can be significant, especially in high-performance electric motors. There are a few different approaches to coupling electromagnetic losses with the energy equation for CFD analysis. One approach is to use a separate electromagnetic solver to calculate the electromagnetic losses and then input these losses into the CFD model. However, this approach can be time-consuming and computationally expensive. There is a gap in the development of coupled electromagnetic-CFD solvers that are specifically designed for heat pipe cooling systems for electric motors. Existing coupled electromagnetic-CFD solvers are often designed for other applications, such as aerospace and automotive engineering.

2.6.2 Research aims and objectives

The aim of this research is to thoroughly assess the effectiveness of heat pipe cooling for a 50 kW hairpin winding motor, and enhancement of this cooling strategy which is shown in Fig 2.1. This research will address this gap by developing a new coupled electromagnetic-CFD solver that is specifically designed for heat pipe cooling systems for electric motors. The new solver will be used to simulate the performance of different heat pipe cooling systems under different operating conditions. The results of the simulations will be used to optimize the heat pipe cooling system design and to develop guidelines for the use of heat pipe cooling in electric motors. The main objectives of the research include:

- To assess the effectiveness of heat pipes in enhancing heat transfer from a 50 kW hairpin winding motor, with a specific focus on reducing hot spots within the windings.
- To study the effects of heat pipes on improving the overall cooling efficiency of the motor's windings.
- To evaluate the practicality and feasibility of utilizing heat pipe cooling systems for hairpin winding motors, aiming to overcome limitations related to power density, system volume, and parasitic power consumption.

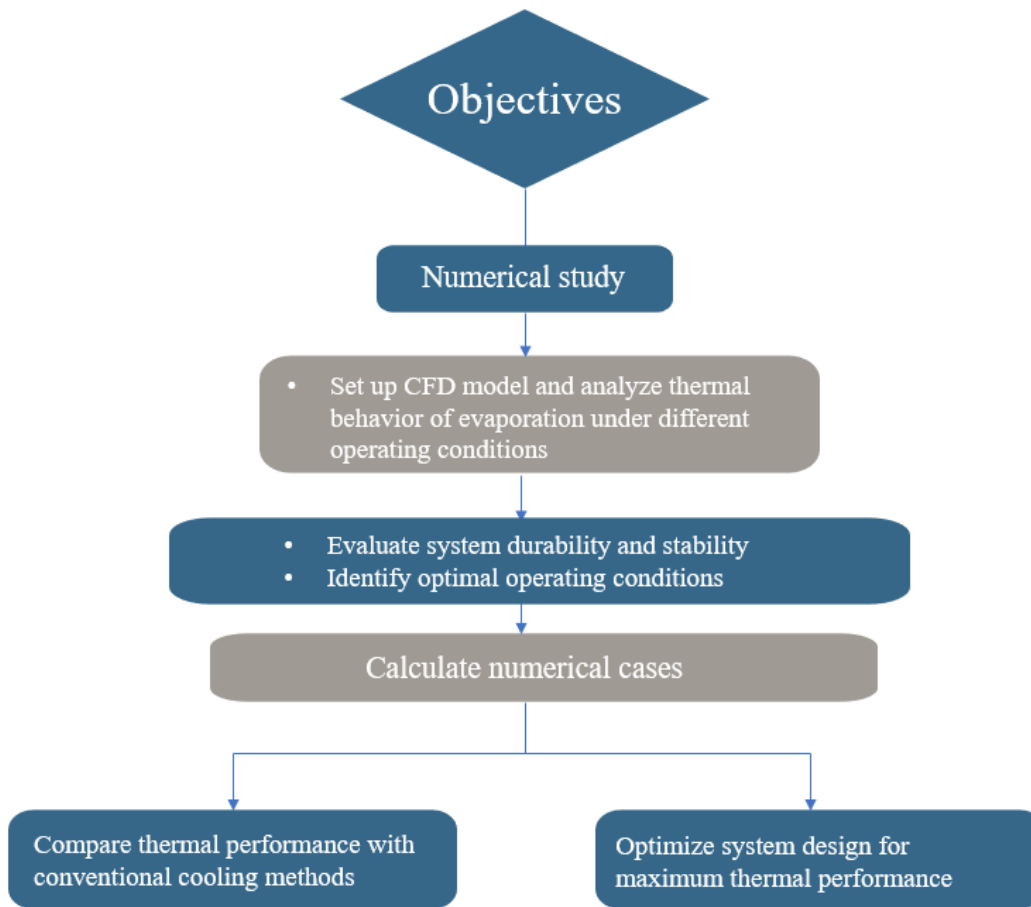


Fig 2.1 Schematic of research aims and objectives.

Chapter 3

Methodology

This research uses a numerical method to investigate the performance of heat pipe cooling for a 50 kW hairpin winding motor. The numerical method is based on the finite volume method, which is a widely used method for solving fluid flow and heat transfer problems. The finite volume method discretizes the computational domain into a grid of control volumes. The governing equations are then integrated over each control volume to obtain a set of algebraic equations. These equations are then solved to obtain the temperature and velocity fields in the computational domain.

The numerical model used in this research takes into account the following factors:

- Two-phase flow behavior in heat pipes
- Interactions between heat pipes and surrounding motor components
- Heat generation in the motor windings
- Heat dissipation from the motor housing

The numerical model is also coupled with an electromagnetic solver to calculate the electromagnetic losses in the motor windings.

3.1 Geometry

The fundamental notion of hairpin windings is illustrated in Figure 3.1 (a), displaying a photographic representation of a hairpin winding sample that corresponds to the stator model outlined in this research. The word entitled “hairpin” is employed, though not exclusively, to present a conductor that is bent into a U-shape, featuring two parallel legs that can be axially placed into the stator slots from a single end of the motor. By using computer numerical control (CNC) for manufacturing, the legs of a numbers of hairpin conductors can be positioned at specific circumferential locations (across distinct slots) and radial positions (within varying layers of a single slot) based on meticulously crafted winding arrangements. Following the insertion process, the hairpin conductor legs extend from the opposite stator end and are subsequently twisted either in the same or opposite direction. With a

carefully determined pitch, each conductor leg is then aligned and positioned adjacent to another. Ultimately, adjacent conductor legs are paired and welded together to establish interconnection among phase branches, thus completing the linkage.

A 50 kW hairpin winding motor has been used as the simulation geometry in this study and the details of the geometry and the motor are shown in Figure 3.1 and Table 3.1 respectively. The frequency range of the motor is 0.4 Hz to 1200 Hz. The height of the stator used in this study is 20 mm and the number of poles is 48 which the poles include 6 copper windings. Furthermore, between the coppers and stator intersections a kapton film with a thickness of 0.2 mm utilized as an insulation layer. Figure 3.1 (d) shows the structure of the stator and the heat pipe installed on it. A flat heat pipe consisting of a solid container (copper), wick, and vapor chamber inside the stator under the copper windings gap has been used as a cooling strategy.

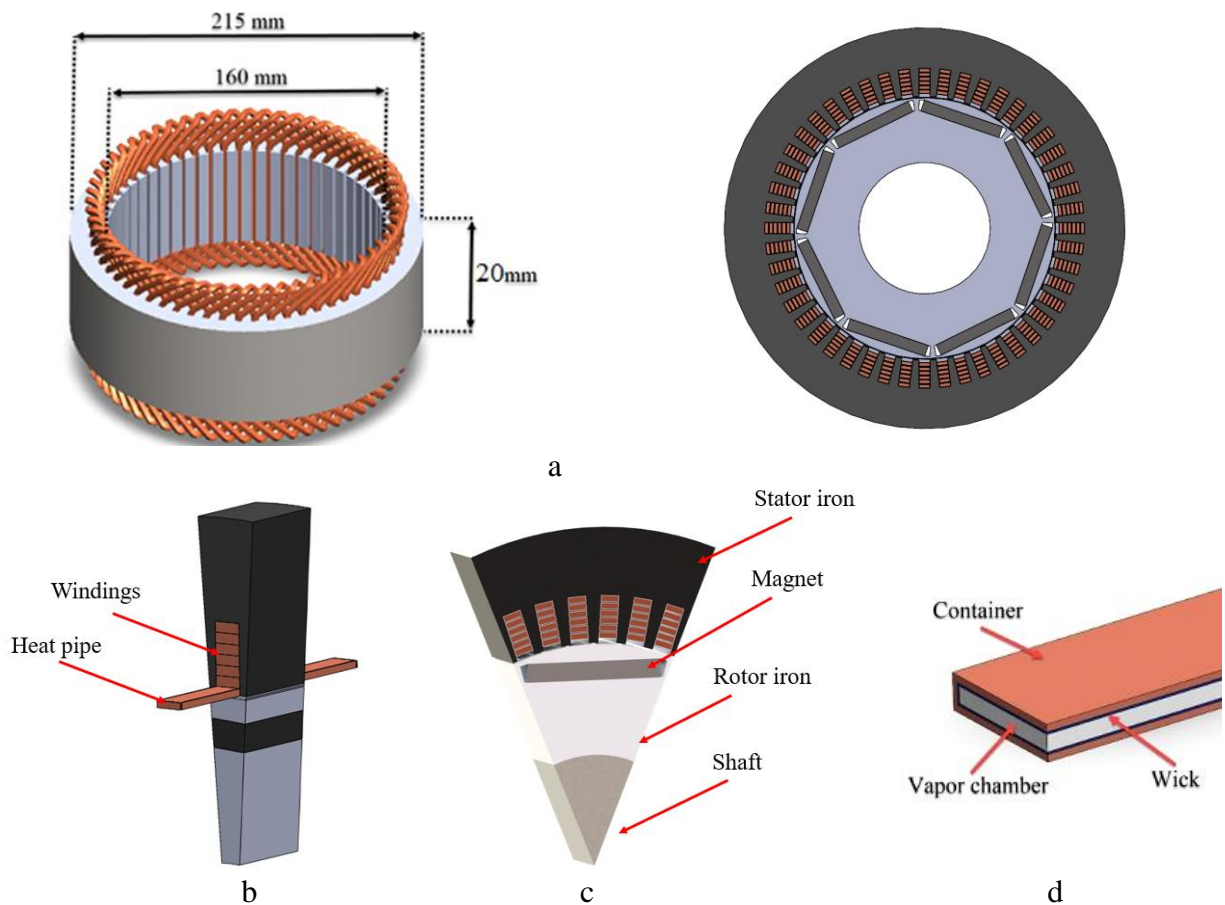


Fig 3.1 Schematic diagram of (a) stator and rotor body, (b) stator with heat pipe, (c) 1/8 stator section, and (d) flat heat pipe side view.

Table 3.1 50 kW Hairpin winding main physical parameters.

Parameters	Value	Parameters	Value
Number of poles	8	Max. power [kW]	50
Number of slots	48	Rated power [kW]	30
Phase number	3	Max. speed [r/min]	18000
Layers per slot	6	Rated speed [r/min]	6000
Winding pitch	6	DC voltage	600
Length [mm]	20	Stator height [mm]	20
Outer diameter [mm]	215	Slot height [mm]	14

3.2 Visualization of Hairpin Winding Layout for Electric Motors

Layout diagrams are typically utilized to visually explain the wiring arrangement of hairpin windings [95]. Fig. 3.2 illustrates a common method for depicting the one phase and one path layout design of a three-phase, six-layer hairpin winding when viewed from the top side, applied to a stator with 48 slots and 8 poles. The coppers in the diagram represent conductor legs (pins) situated within the slots. Solid lines distinguished by white color, represent preformed connections made through welding from the opposite axial end. In this specific design, there is four parallel branch per phase, and there are 12 turns in series per phase. The diagram illustrates the progression of connections, commencing from the first layer at slot number 1. These connections, initiated from insertion and welding points, follow a wave winding pattern along the circumference of the stator.

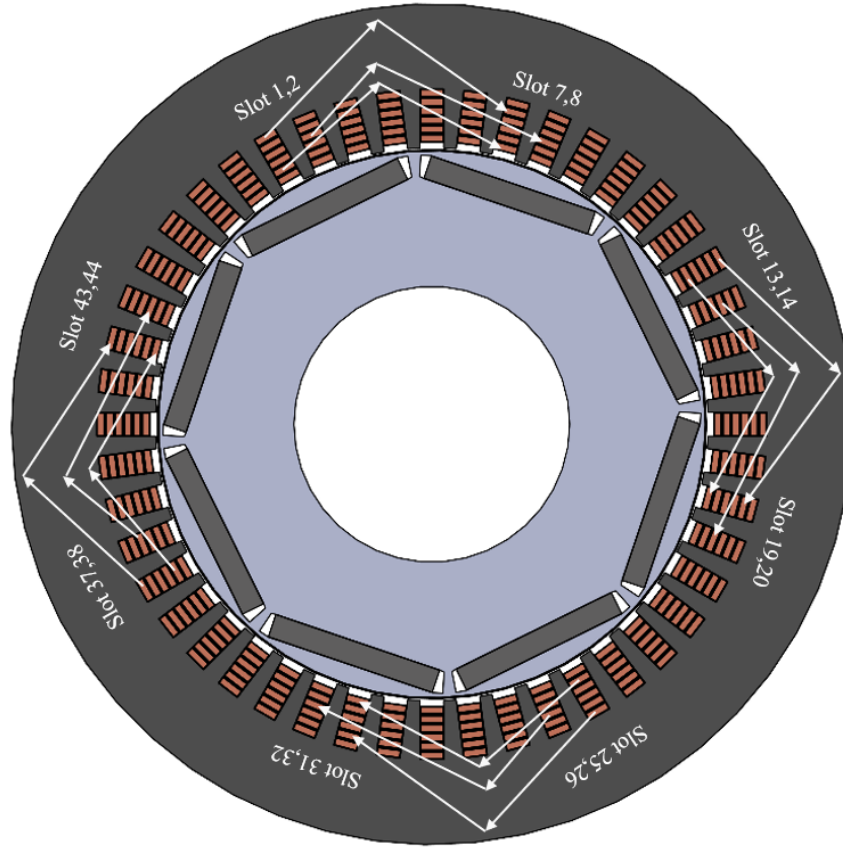


Fig 3.2 Top view of wiring arrangement of hairpin windings.

Fig. 3.3 displays a six-layer winding design for hairpin winding motor with 48 slots, 8 poles, and a maximum of four parallel branches. The only one branch connection is illustrated, with emphasized pin locations that are enclosed, and all other jumpers from different branches are also highlighted. It is important to note that there are intersections between jumpers belonging to different phases. Within this section, using 48-slot, 8-pole designs as research geometry, three phase winding option explored as a potential layout configuration that can enhance performance while reducing costs [95]. In three-phase winding configurations, the placement of a single branch's terminal is a crucial design consideration. Generally, this terminal can be positioned at either the initial or final layer, offering flexibility within the corresponding phase belt. After the determination of the first branch's terminal location, designers have various options for arranging the terminals of the remaining branches. This phase arrangement flexibility allows for tailored configurations based on specific motor requirements and design constraints. Fig 3.3 illustrates the same design as in Fig 3.2, presented in a top layout view, with all other connections for one phase included.

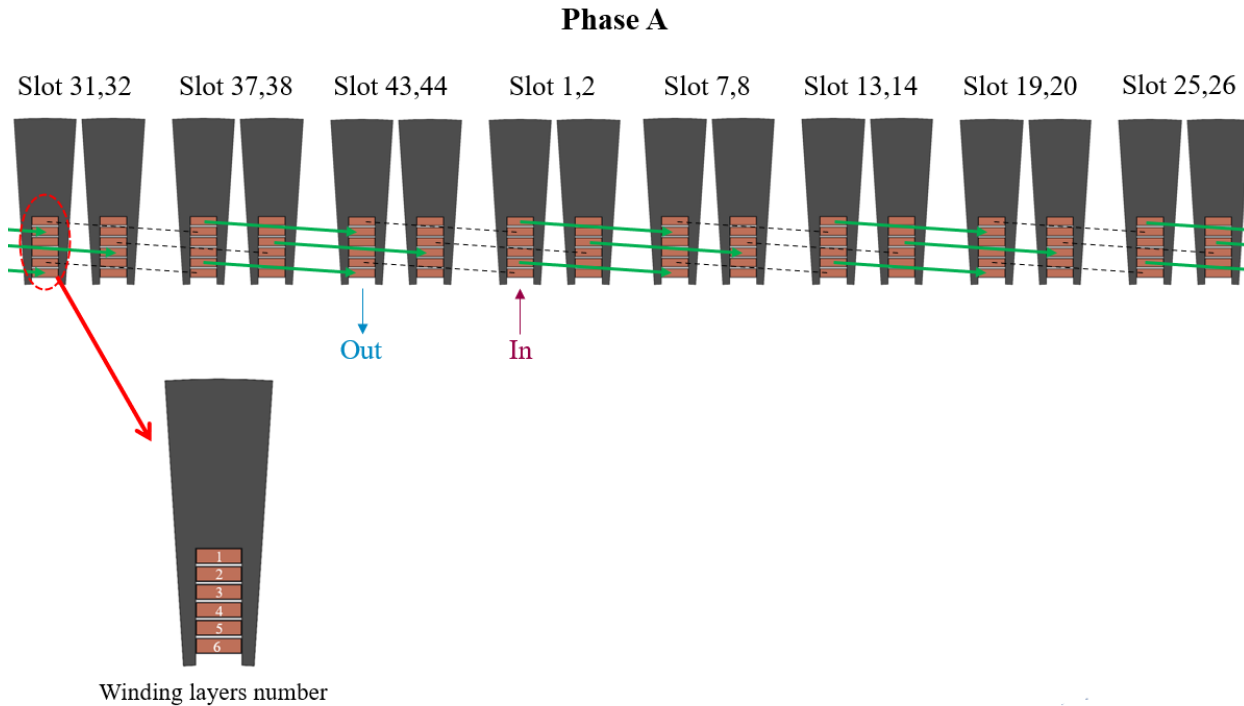


Fig 3.3 Six-layer winding design for hairpin winding motor with 48 slots, 8 poles, and a maximum of four parallel branches.

A cooling approach has been implemented using a flat heat pipe located within the stator beneath the gap of the copper windings. This heat pipe consists of a solid container made of copper, a wick, and a vapor chamber. The heat pipe is affixed to the final copper winding, with the vapor chamber section measuring $40 \times 6 \times 1.5 \text{ mm}^3$, and the copper and wick possessing thicknesses of 0.25 mm and 0.20 mm, respectively. It is noticeable that for reducing time of simulation, the simulation employs proportionally scaled stators ($1/48$) as the modeled geometries to compare heat transfer parameters and thermal performance both with and without the utilization of the heat pipe. The properties of the materials utilized in this study are detailed in Table 3.2.

Table 3.2 Material properties used for simulation study

	Heat capacity [J/kg.K]	Density [kg/m ³]	Thermal conductivity [W/m.K]	Electrical conductivity [S/m]
Copper	385	8960	$k(T)$	5.998×10^7
Iron	440	7870	76.2	-
Water	4180	1000	0.61	-
Vapour	1874	Ideal gas	0.0188	-
BMN	440	7550	9	-
Kapton film	1090	1420	0.75	0

The BMN material is used for the magnet region of the rotor which has magnet properties. The vapor density is calculated using the Ideal gas law and the vapor is given by:

$$\rho_v = \frac{p}{R_s T} = \frac{p \times M_n}{R_s T} \quad (3.1)$$

$k(T)$ is a function of temperature for copper. However, the relationship between thermal conductivity and temperature is more complex for some materials than others. For copper, there are accurate models available for the thermal conductivity over a wide range of temperatures. For iron, water, BMN, and Kapton film, there are no such accurate models available. In the absence of these models, it is assumed to use constant values for the thermal conductivity of these materials in CFD simulations. The equation for the temperature dependent thermal conductivity of copper used in this paper is obtained from the following equation:

$$k(T) = -4.5 \times 10^{-7} T^3 + 6.6 \times 10^{-4} T^2 - 0.3T + 451 \quad (3.2)$$

3.2 Assumptions

Some assumptions considered for the model are based on the following items:

- The laminar flow is considered for the fluid flow in the heat pipe.
- Fluid flow is considered a compressible flow and it is simulated as steady-state flow.

- The effect of gravity assumed zero.
- Material properties are constant and isotropic except for the vapor density.
- Uniform heat generation is used for energy equation and the radiation heat transfer is neglected.
- Stator and rotor's wall in the side assumed as symmetry condition.
- To avoid geometrical complication, the winding has been modelled as solid.

3.3 Governing Equations and Boundary Conditions

3.3.1 Electromagnetic field

In a hairpin winding motor, the magnetic fields produced by the rotor rotate concurrently with the magnetic fields generated by the stator currents. The interaction between these rotor and stator magnetic fields engenders a resultant torque, empowering the motor to transform the currents coursing through the hairpin windings into mechanical power. Due to the synchronized nature of the excitation inherent in hairpin winding motors, the instantaneous torque is notably influenced by the angular position of the rotor. This alignment corresponds directly with the stator currents. This is in contrast to asynchronous machines, where the stator windings induce magnetic fields in the rotor, contingent on the speed lag between the rotor and the stator. The frequency of the motor is calculated by the following equation [95]:

$$Freq = \frac{rpm \times Poles_number}{120} \quad (3.3)$$

The motor uses the interaction of magnetic field from the rotor and stator to generate torque and convert electrical energy into mechanical power. Also, In these kinds of motors, the torque is considerably influenced by the rotor's angular position due to the synchronous nature of the excitation [95]. The winding excitation in this study is given by:

$$I = I_m \cos (\kappa \theta + \emptyset) \quad (3.4)$$

Where I_m is the peak current, κ is scaling factor, θ is the rotor angle, and \emptyset is the phase angle. In this study, the excitation for the three phases and peak current is given by the following equations:

$$I_A = I_m \cos (\theta) \quad (3.5)$$

$$I_B = I_m \cos (\theta - 120[deg]) \quad (3.6)$$

$$I_c = I_m \cos(\theta - 240[\text{deg}]) \quad (3.7)$$

$$I_m = \frac{1000 \times P_{kW}}{\sqrt{3} \times V_{LL} \times \cos\phi \times \eta} \quad (3.8)$$

where P_{kW} is the nominal power of the motor, V_{LL} is voltage of the motor, and η is nominal efficiency of the motor. In order to secure the generation of a unidirectional torque through the attractive and repulsive interactions between the stator and rotor poles within hairpin winding motors, the scaling factor must be calibrated to the extent that the magnetic fields originating from the stator coils reverse their orientation as the rotor undergoes a rotational displacement equivalent to one magnet pole span (where the magnet poles alternate in polarity). Scaling factor which is dependent on the number of poles is given by:

$$\kappa = \frac{180^\circ}{360^\circ / N_p} \quad (3.9)$$

where N_p is the number of rotor poles. One of the most important parameters in assessment of temperature in the stator is computation of losses. The iron losses in the motor are caused by time-varying magnetic flux density in the rotor and stator, while the copper losses are due to resistance in the stator windings. Iron losses vary linearly with the rotor speed, and are calculated by Steinmetz equation [96] which is given by:

$$W_i = K_h B_m f \quad (3.10)$$

where W_i is the iron loss, B_m is the maximum magnetic flux density, and f is the frequency of the magnetic flux density variation. The losses of the copper in the stator are explained in this study by formula due to the resistance which is given by:

$$W_c = I^2 R_c \quad (3.11)$$

where I is the winding current and is the R_c winding resistance. The homogenized multiturn coil feature is used in this study, and skin and proximity effects are neglected in the winding. Furthermore, the effective resistance does not change with the speed of the rotor. The iron and copper losses calculated by the Loss Calculation equations are used in this investigation to be coupled to the Heat Transfer interface for calculation of the motor's thermal performance.

3.3.2 Energy and Fluid flow

To compute the temperature distribution of the motor the following steady-state energy equation has been solved:

$$\frac{1}{r} \frac{\partial}{\partial r} \left(r \frac{\partial T}{\partial r} \right) + \frac{1}{r^2} \frac{\partial^2 T}{\partial \theta^2} + \frac{\partial^2 T}{\partial z^2} + \frac{\dot{Q}}{k} = 0 \quad (3.12)$$

where \dot{Q} is the volumetric heat source and uses the loss data from magnetic flux model and k is the thermal conductivity of the material [94]. The study presents a simplified flat plate heat pipe model for cooling strategy that was modified for the study. The capillary pressure is given by the following equation:

$$\Delta p_c = \frac{2\sigma}{r_c} \quad (3.13)$$

where σ is the surface tension and r_c is the capillary radius. Also, it must be greater than all other pressure drops in the heat pipe. The effective thermal conductivity of the sintered copper powder wick is given as:

$$k_{eff} = \frac{k_f(k_f + k_s - (1 - \varphi)(k_f - k_s))}{k_f + k_s + (1 - \varphi)(k_f - k_s)} \quad (3.14)$$

where k_f is thermal conductivity in fluid region, k_s is thermal conductivity in solid region, and Sintered copper powder wick is used with 0.5 porosity which is φ in the flat heat pipe. Laminar compressible flow is used for simulation. The saturation pressure at the inlet and outlet of the evaporator side of the wick and vapor interface is also given as:

$$p = p_{sat}(T) = p_{ref} \cdot \exp \left(\frac{\lambda}{R_s} \left(\frac{1}{T_{ref}} - \frac{1}{T} \right) \right) \quad (3.15)$$

$$\lambda = h_{fg} \times M_n \quad (3.16)$$

where λ is the enthalpy of vaporization, M_n is the molar mass, h_{fg} is the latent heat (2473 kJ/kg), p_{sat} is saturation pressure, R_s is the specific gas constant, T_{ref} is reference temperature (100 °C), T is temperature and p_{ref} is reference pressure (1 atm) [97]. The boundary heat source used for the heat of evaporation at the wick and vapor interface is calculated by:

$$q_{evap} = \dot{m}\lambda \quad (3.17)$$

where \dot{m} is normal mass flux and λ is the enthalpy of vaporization. The heat transfer boundary conditions of the simulated cases are presented in Fig 3.4. Additional information about modelling and programming these physics can be found in Appendix A.

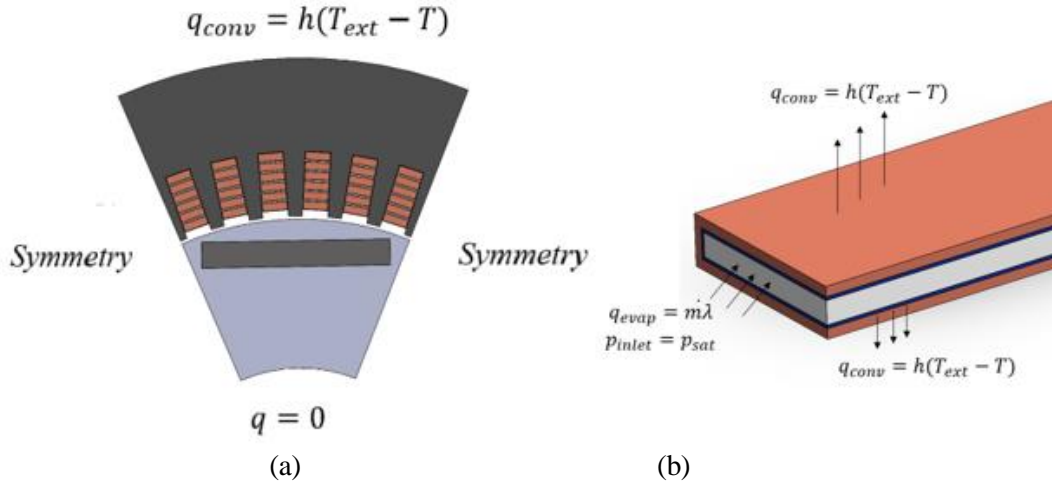


Fig 3.4 Boundary conditions in (a) stator and (b) flat heat pipe.

In Figure 3.4, The side walls of the stator and rotor are considered to have symmetry conditions. The lower surface of the rotor is considered insulated while the convective heat transfer is used at the upper surface of the stator and the heat transfer coefficient is assumed to be $20 \text{ W/m}^2\cdot\text{K}$. Besides, the convective heat transfer coefficient used at the upper surface of the heat pipe is assumed to be $1200 \text{ W/m}^2\cdot\text{K}$ and no-slip wall condition is used in the study. The heat source boundary condition is considered in winding coppers and stator's iron domain and the thin layer feature is used in the intersections of coppers and stator.

3.4 Calculations and CFD Simulation Conditions

In this research study, a CFD software used specifically COMSOL 6.0 Physics-Builder software, as a numerical simulations software. The reason of choosing COMSOL is by its strong foundation in the finite element method (FEM), it is highly suited for conducting three-dimensional numerical simulations of exceptional complexity and precision. To achieve the integration of AC/DC losses as heat sources within the energy equation, the physics builder feature within COMSOL employed for programming AC/DC losses in energy equation. This tool is useful to create precise coupling code to accurately represent the thermal behavior of our system. Within the computational framework, COMSOL PARDISO (Parallel Sparse Direct Solver) used for this research study, a powerful solver

integrated into COMSOL, to handle the complexities of our simulations. the PARDISO solver in COMSOL offers parallelism, scalability, memory efficiency, robustness, customization options, and compatibility, making it a preferred choice for motor winding simulations where accuracy, speed, and reliability are essential. Additionally, fully coupled direct linear solver employed, which efficiently supports the numerical study. Given that the system's performance depends on rotational speed, a time-dependent study conducted to capture how iron losses change over time under different conditions. To ensure accuracy, a strict convergence criterion set up, requiring the residual value to remain below 10^{-6} , indicating the reliability of the simulations. It's essential to emphasize that the heat source parameter for heat transfer module's boundary condition derived. In this study, a framework which is used for coupled magnetic and heat transfer modeling framework is shown as drawn in Fig 3.5.

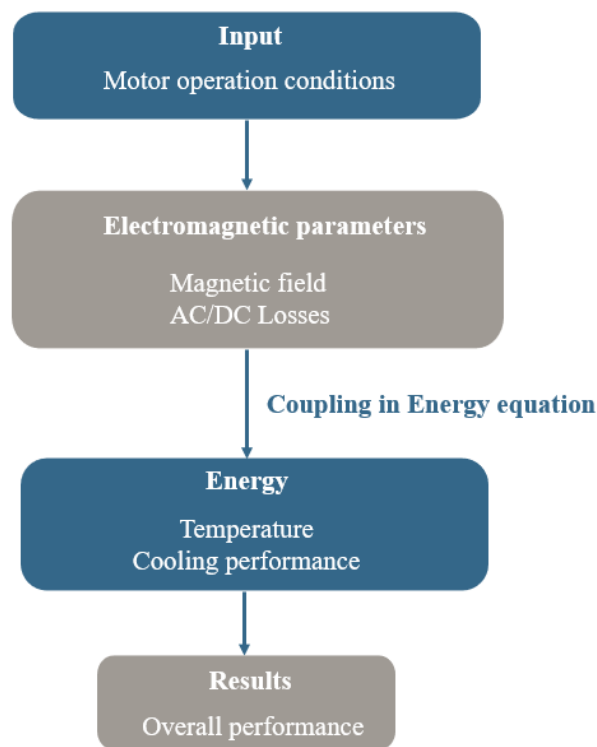


Fig 3.5 Coupling framework in the research study.

The CFD simulations were performed using the finite element method (FEM) software COMSOL 6.0 Physics-Builder. The computational domain was discretized into a grid of approximately 10

million tetrahedral elements. The mesh density was refined in regions of high thermal gradients, such as near the heat pipes and motor windings.

The following mesh types were used:

- Quadratic elements for the fluid domain, coppers and heat pipe container.
- Boundary layer for walls in fluid domain.
- Tetrahedral elements for stator's iron.
- Solid elements for the heat pipes and motor components.

The following degrees of freedom (DOFs) were solved for:

- Temperature
- Velocity
- Pressure
- Electrical field
- Magnetic field

The time steps and increments were used in the research for calculating the iron losses are 0.001 and 0.1 seconds respectively. Also, the simulations were run until the temperature field and the electromagnetic field converged. Convergence was defined as a residual value below 10^{-6} .

The following boundary conditions were applied:

- Adiabatic boundary conditions on the motor housing
- Heat flux boundary conditions on the heat pipes
- Heat generation boundary conditions on the motor windings
- Electrical boundary conditions on the motor windings
- Magnetic boundary conditions on the motor components

The heat source parameter for the heat transfer module's boundary condition was derived from the AC/DC losses in the motor windings. Within the purview of this study, we embark on an exploration encompassing three distinct simulation cases, each meticulously delineated and elaborated upon in Table 3.3. These cases serve as the crucible within which our numerical investigations unfold, promising to yield invaluable insights and a deeper understanding of the intricacies of our thermal system.

Table 3.3 Simulated cases in the current research.

Case number	Peak current I [A]	Speed [rpm]
1	5	Range of 3000 to 18000
2	15	Range of 3000 to 18000
3	20	Range of 3000 to 18000
4	30	Range of 3000 to 18000

3.5 Grid independence

The simulation process, as illustrated in Fig 3.6, sheds light on a critical aspect of the study. The independence of the solution from the method of meshing and the number of elements employed. This robustness ensures the reliability of the simulations and their applicability across different scenarios. To further validate the simulation results and ensure their accuracy, a mesh convergence test was conducted. This test aimed to evaluate the impact of varying mesh sizes on the computed results of the motor under specific cases in different work conditions. In particular, the study focused on a scenario involving a 5 A phase current and a motor speed of 15000 rpm. The outcomes of the mesh convergence test, as documented in Table 3.4, provide valuable insights. As the mesh quality improved, characterized by smaller and more refined elements, a noticeable trend emerged. The average stator temperature became increasingly consistent and stable, indicating the mesh's influence on result accuracy. Consequently, a strategic decision was made to employ the third sample mesh size in all subsequent simulations. This choice not only enhances the precision of the simulations but also contributes to a reduction in computational time, optimizing the efficiency of the modeling process. By ensuring that the mesh is appropriately sized and configured, it would be possible to obtain reliable and consistent results in simulations, thus boosting the overall validity of the study's findings.

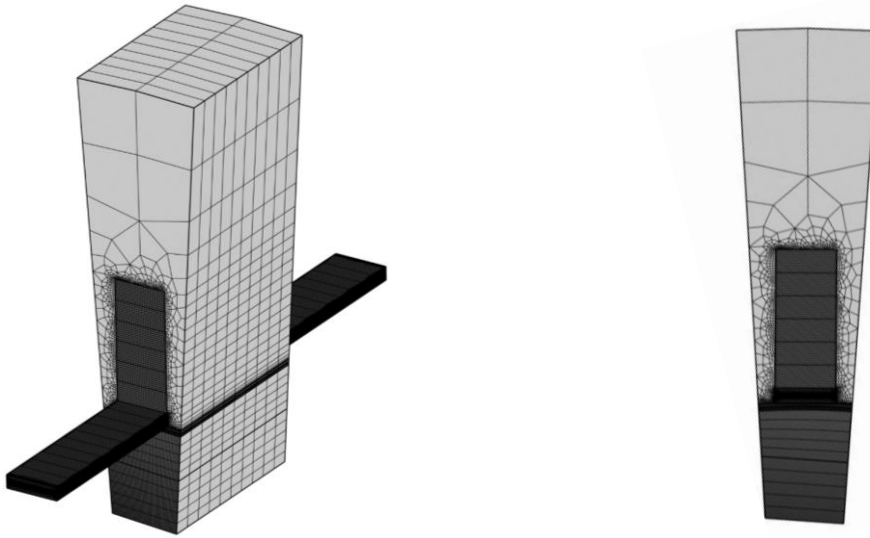


Fig 3.6 Generated meshes in the research study

Table 3.4 Mesh independence check.

Number of meshes	Average mesh quality	Maximum temperature [°C]
63580	0.325	22.70
152166	0.633	22.55
316586	0.798	22.32
797816	0.816	22.35

3.6 Validation

To validate the results of this study the temperature profiles of the stator windings at different rotational speeds and a specific torque level compared with Sun et al. [87]. Sun et al. [87] investigated in heat pipes with three dimensions are placed in the space between the winding and the casing. Potting silicon gelatin is used to secure the heat pipes in place and to improve contact between the heat pipes and the winding. They reported the temperature of the stator windings with various rotational speed. CFD software used with COMSOL 6.0 Physics-Builder software, as a numerical simulations software to validate the experimental results. Within the computational framework, COMSOL PARDISO (Parallel Sparse Direct Solver) used for the validation, a powerful solver integrated into COMSOL, to handle the complexities of the simulations. Additionally, fully

coupled direct linear solver employed, which efficiently supports the numerical study. To ensure accuracy, a strict convergence criterion set up, requiring the residual value to remain below 10^{-6} , indicating the reliability of the simulations. Figure 3.7 shows the relationship between the steady winding temperature and the rotational speed. The simulated data and the tested data are compared in the same figure, and they show good consistency.

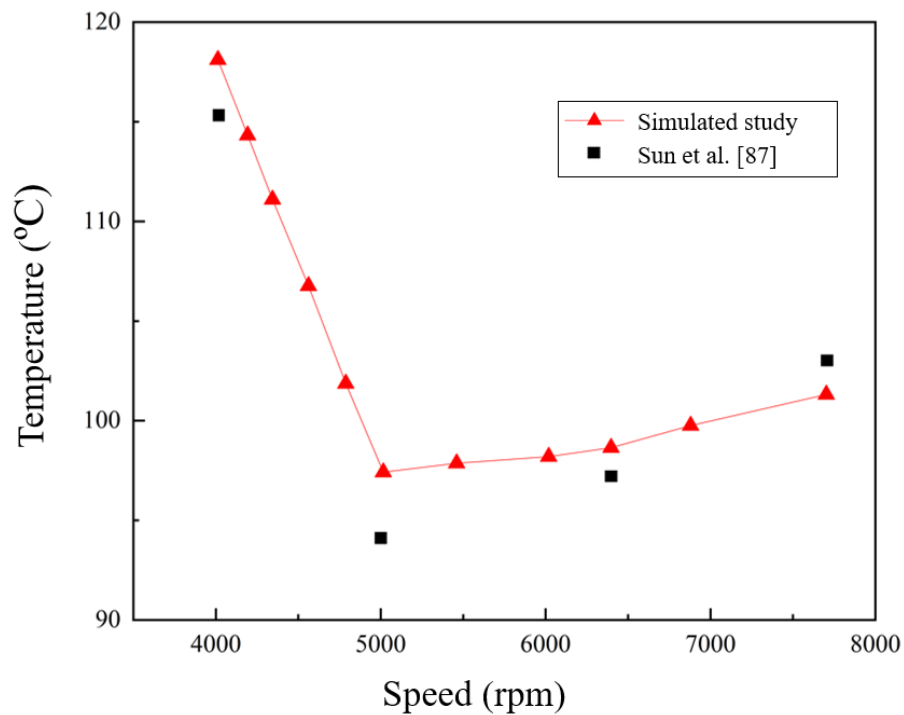


Fig 3.7 Validated results with experimental research.

Chapter 4

Result and Discussion

In this section, the study's findings from the extensive numerical investigation are presented in a detailed manner, focusing on the results' key aspects. This section provides a thorough examination of various system parameters and their behaviors. It is also involved a comprehensive comparative analysis, specifically comparing the stator's performance with and without a heat pipe, while considering different peak current levels and variable speeds. The aim is to offer a comprehensive understanding of how the presence of a heat pipe, varying peak currents, and different speeds collectively influence the stator's overall performance and efficiency.

4.1 Magnetic Flux Distribution

Figure 4.1 visually summarizes the contour representation of the magnetic flux distribution, a result derived from the utilization of rotating machinery modules, essential in providing the data for establishing the heat source boundary conditions in energy equation. The presented illustration shows the magnetic flux profile at a phase current of 5 A and a speed of 15000 rpm. Notably, the magnetic flux distribution displays a noticeable concentration in close proximity to the copper windings, emphasizing their fundamental role in shaping the flux dynamics.

The noticeable point is the difference between the areas near the copper windings and other parts of the stator. The corners of the copper windings have a strong magnetic flux of 2 T. This figure emphasizes the usefulness of magnetic flux data in using copper and iron loss information to set heat source conditions in the copper and iron areas. By using this connection, the study gains important insights into where losses happen and how the heat behaves in those specific areas, helping us understand the overall temperature patterns in the system better.

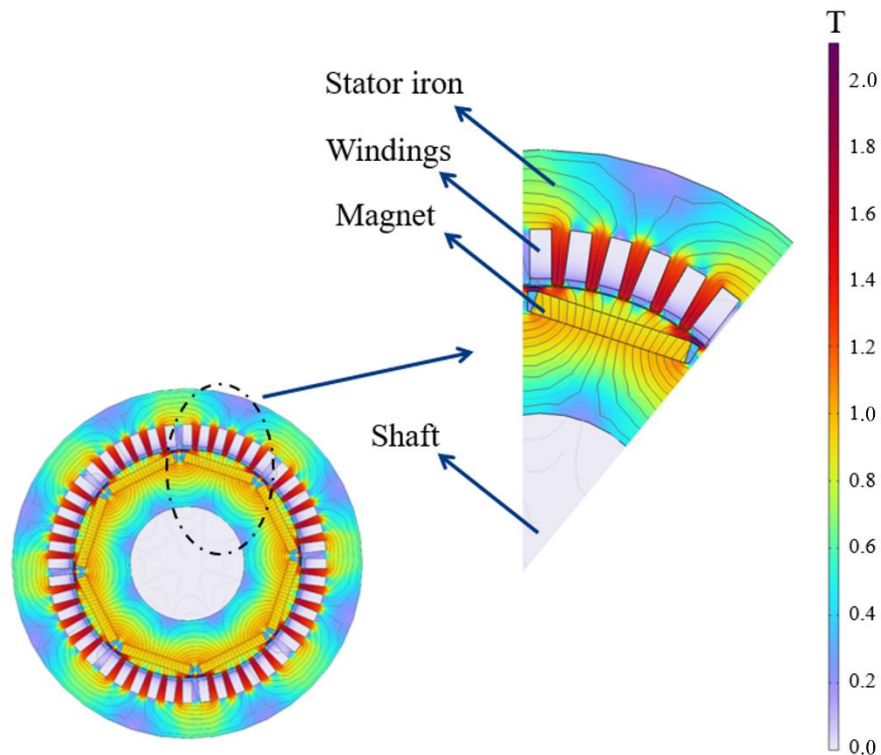


Fig 4.1 Magnetic flux distribution in case number 1 with 15000 rpm speed.

4.2 Electromagnetic Volumetric Loss Density

The electromagnetic volumetric loss density contour, as illustrated in Fig 4.2, provides crucial insights into how electrical energy is converted into heat within the motor. This contour map helps to visualize where the motor experiences losses due to its electromagnetic processes. Understanding these losses is essential for optimizing motor performance and efficiency. The key observation from Fig 4.2 is that the torque produced by the motor is closely linked to the current density. In simpler terms, the more electrical current the motor uses, the more turning power it generates. The presented contour indicates the volumetric loss profile at a phase current of 5 A and a speed of 15000 rpm.

A noteworthy finding is that these losses tend to concentrate in certain regions of the motor, particularly in the iron part between the slots. This localized increase in losses can lead to higher resistance in the windings and, consequently, greater overall energy loss. This demonstrates that as the motor operates at higher speeds, it experiences greater energy losses in the form of heat.

Furthermore, the contour map highlights that the motor's core losses increase gradually with both torque and speed. These core losses result from the changing magnetic fields within the motor and contribute to the overall energy dissipation. When the motor operates under higher loads (greater torque) or spins faster (higher speed), these core losses become more pronounced, further impacting the motor's overall efficiency.

In summary, the electromagnetic volumetric loss density contour is a valuable tool for understanding how electrical energy is converted into heat within the motor. It reveals that motor performance is closely tied to factors like current density, speed, and torque. By gaining insights into these losses, we can work towards optimizing the motor's efficiency and minimizing energy wastage, ultimately enhancing its overall performance.

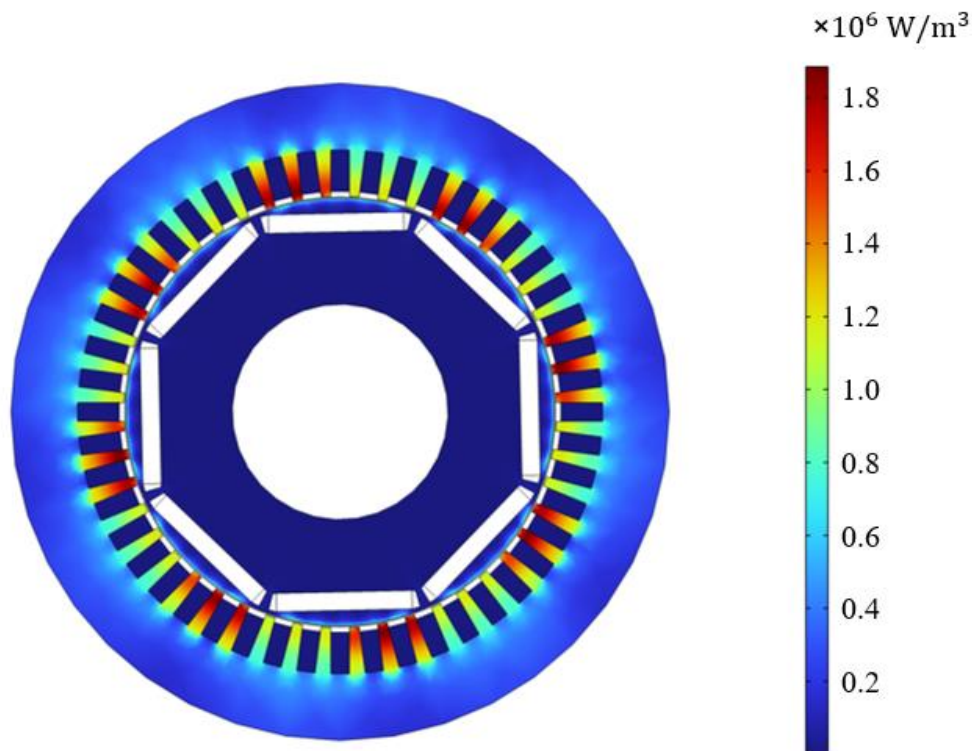


Fig 4.2 Electromagnetic volumetric loss contour.

4.2 AC/DC Losses in Hairpin Winding Motor

Figure 4.3 offers a clear comparison of stator's copper and iron losses under various phase currents and speeds, between 3000 rpm to 18000 rpm. The exported results reveal a consistent pattern

where both copper and iron losses increase as the rotational speed goes up, regardless of the phase current settings. Figure 4.3 shows that the copper losses in a hairpin winding motor increase nonlinearly with speed, while the iron losses increase linearly with speed. This is because the copper losses are dominated by eddy current losses, which are proportional to the square of the speed. Eddy current losses are caused by the circulation of electric currents in the copper conductors. The eddy currents are induced by the changing magnetic field caused by the rotation of the motor. The faster the motor rotates, the stronger the magnetic field and the greater the eddy current losses.

By considering the 5 A phase current scenario, the copper loss slowly rises from 0.26 W at 3000 rpm to 5.81 W at 15000 rpm. Similarly, in a 10 A phase current situation, the copper loss increases from 3.78 W to 85.9 W over the same speed range. Notably, with a 30 A phase current, the copper loss significantly surges from 24.47 W to 536 W as the speed varies. At the same time, the iron loss follows a similar trend of growth. It's important to mention that the iron loss data considers the rotational speed parameter through time-dependent analysis. The iron loss values, for phase currents of 5 A, 15 A, 20 A, and 30 A, climb from 26.3 W, 36.3 W, 41 W, and 43.9 W, respectively, to 184 W, 254 W, 287 W, and 307 W at different speeds. Both copper and iron loss data are then used to create heat sources, which are crucial for defining heat transfer conditions and evaluating how the stator behaves in terms of heat across various operational situations.

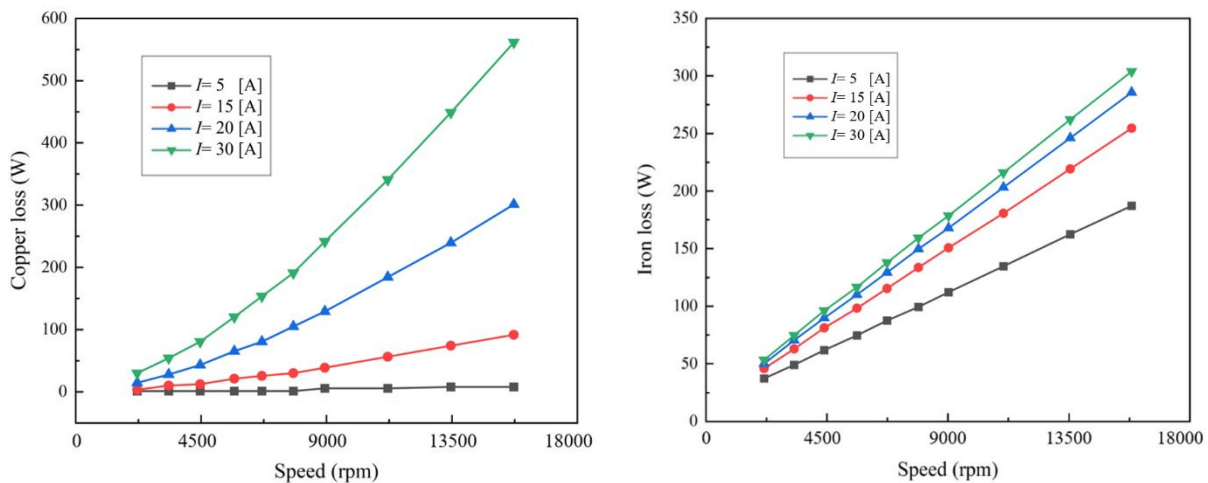


Fig 4.3 Copper loss and iron loss calculated in this study in different phase current and rotational speed.

4.3 Thermal Performance and Temperature Distribution

The Figure 4.4 illustrates the maximum temperature and pressure in the stator and heat pipe in conditions of the second case of study. The results obtained from the figure show the considerably difference of maximum temperature in cases by presence of heat pipe. The results are exported in 20 °C ambient temperature, 1200 W/m².K convection heat transfer coefficient and in 30 A phase current and 15000 rpm rotational speed. The Figure 4.4 (a), (b) and (c) shows the significant influences of the heat pipe in winding's thermal performance. This can be attributed to the existence of the heat pipe and its effects on the system cooling. Also, the most interesting aspect of this graph is the significant temperature differences between maximum temperature of the case.

The pressure and temperature distribution and flow streamline in the heat pipe is illustrated by the Figure 4.4 (d). The pressure is shown in the half of the heat pipe's vapor chamber side section due to the symmetrical geometry of the heat pipe in stator. Also, the axis of the symmetry is shown by dash line in the figure. The temperature distribution is shown in the upside outer surface of the flat heat pipe to demonstrate the effects of heat pipe's heat transfer in stator. The results indicates that the flow in the heat pipe and heat evaporation heat source in the heat pipe has a significant influence in cooling the motor stator.

Figure 4.4 (d) is used to illustrate various aspects of how the heat pipe functions in this context. Firstly, the figure displays the pressure distribution within the heat pipe. This distribution is shown on one half of the heat pipe's vapor chamber side, given the symmetrical design of the heat pipe within the stator. Essentially, this part of the illustration provides insight into how pressure is distributed within the heat pipe, which is crucial for understanding its operation. Secondly, the temperature distribution is depicted on the upper outer surface of the flat heat pipe. This visualization helps us figure out how heat is transferred within the stator through the heat pipe. By observing temperature changes on the surface of the heat pipe, it is shown how effectively it's transferring heat away from the motor stator. The content reveals that the results obtained from this analysis indicate that both the flow of material within the heat pipe and the heat evaporation at the heat source within the heat pipe have a significant impact on cooling the motor stator. In simpler terms, it suggests that the heat pipe's ability to transfer heat efficiently is crucial for maintaining the stator's temperature within acceptable

limits. This information is valuable for optimizing the heat pipe's design and ensuring it performs effectively in cooling the motor.

Furthermore, Figure 4.4 (b) shows the temperature distribution in middle side section of the stator in presence of flat heat pipe. Considering the heat pipe in figure, the maximum temperature under the aforementioned conditions is 44 °C which is lower than that in the motor. This shows the superiority of the flat plate heat pipe in cooling the stator in high-speed conditions.

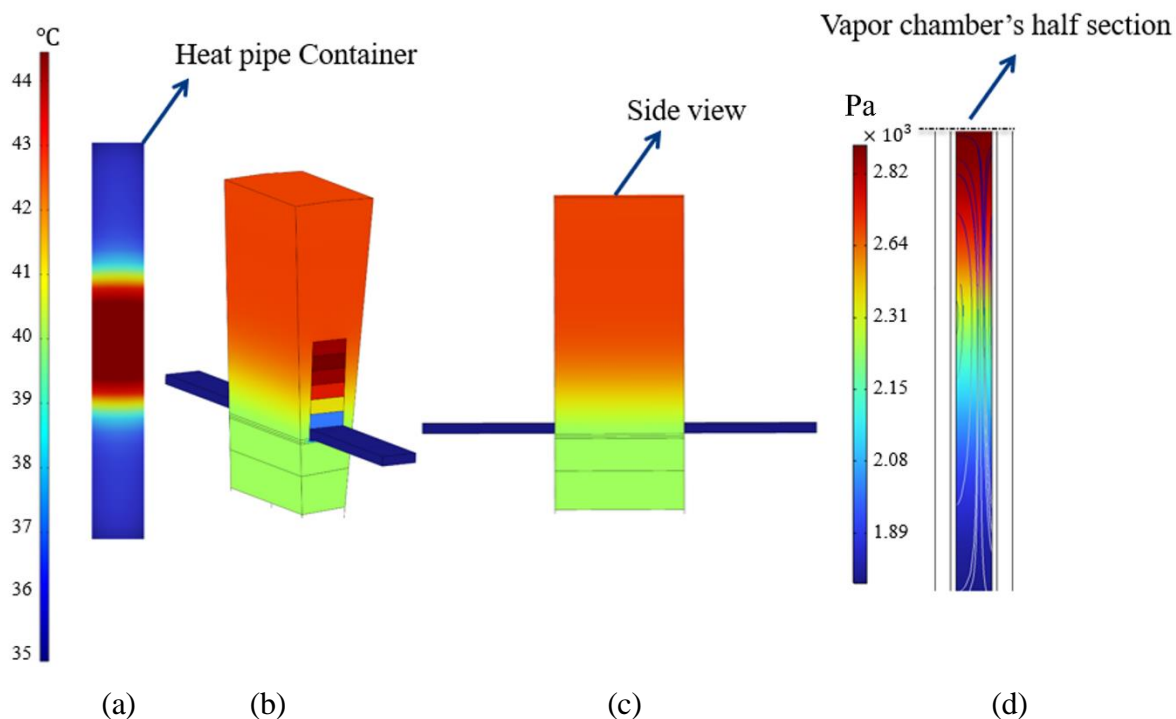


Fig 4.4 Temperature distribution in the motor for (a) heat Pipe container, (b) stator with heat pipe, (c) temperature distribution in side section of the motor and temperature distribution in the outer surface of the heat pipe in upside, and (d) pressure distribution in the vapor chamber of heat pipe.

Fig 4.5 is presented with a visual representation showcasing the distribution of temperature across the central area of the motor under examination. The motor's operation has been investigated at various speed settings, allowing us to observe how temperature changes with different levels of rotational speed. Notably, the peak current recorded within these conditions amounts to 30 A. The numerical setup also takes into account specific parameters that influence the motor's thermal behavior. The environmental conditions surrounding the motor are characterized by an ambient

temperature of 20 °C. Moreover, the heat transfer conditions at the motor's boundary involve a convection heat transfer coefficient of 1200 W/m²·K. This coefficient essentially quantifies the effectiveness of heat transfer between the motor and its surroundings, indicating how efficiently heat is being dissipated.

The findings of this study offer valuable insights into the mechanisms driving the motor's cooling process. Notably, two key factors emerge as influential contributors: the flow dynamics within the heat pipe and the phenomenon of heat evaporation originating from the heat source within the heat pipe. Both of these elements play a substantial role in the cooling process of the motor's stator, which is a critical component of the motor's structure. Regarding temperature outcomes, the data indicates that the motor's temperature response is most notable at its highest operational speed. Under these conditions, the temperature reaches a peak value of 44 °C. This information underscores the significance of considering different operating speeds when assessing the thermal performance of the motor, as higher speeds tend to lead to more pronounced temperature fluctuations.

The temperature distribution is not uniform, and the hottest part of the stator changes depending on the rotational speed. At 3000 rpm, the lower part of the stator is the hottest, while at 9000 rpm and 15000 rpm, the top part of the stator is the hottest. There are two main reasons for this observed behavior. First, the flow dynamics in the heat pipe change with rotational speed. At low rotational speeds, the flow is laminar, while at high rotational speeds, the flow is turbulent. Turbulent flow is more effective at removing heat, but it also generates more pressure drop. As a result, the heat pipe is more effective at removing heat from the top part of the stator at high rotational speeds.

Second, the heat evaporation rate from the heat source within the heat pipe changes with rotational speed. At low rotational speeds, the heat evaporation rate is limited by the amount of heat that can be transferred to the heat pipe from the motor windings. At high rotational speeds, the heat evaporation rate is limited by the flow rate of the coolant in the heat pipe. As a result, the heat pipe is more effective at removing heat from the bottom part of the stator at low rotational speeds. The combined effect of these two factors is that the temperature distribution in the middle section of the stator is not uniform, and the hottest part of the stator changes depending on the rotational speed.

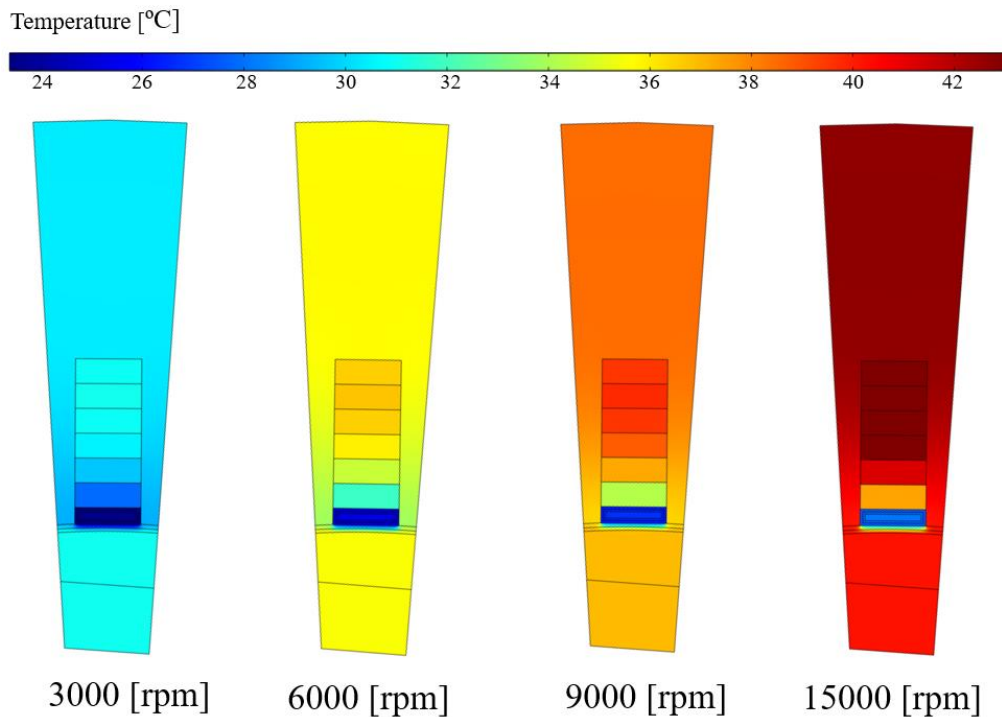


Fig 4.5 Temperature distribution in middle section of the stator.

4.4 Thermal Performance Analysis and Heat Pipe Effectiveness

In this part of our discussion, the temperature differences between two main scenarios are investigated. One where a heat pipe is used in the motor and the other where isn't used. These numbers highlight the noticeable impact of adding a heat pipe to a Hairpin winding, and how it helps improve the cooling performance of the system.

4.4.1 Effect of losses and heat pipe on capillary pressure

In Fig 4.6, the influence of AC/DC losses on capillary pressure within the heat pipe wick is studied. This analysis encompasses four different current levels, revealing distinct patterns in capillary pressure variations linked to varying current strengths. Interestingly, the porous structure of the heat pipe wick exhibits its highest capillary pressure when subjected to a current of 30 A, highlighting the dependence of this phenomenon on electrical current intensity. This finding carries significant implications for optimizing heat pipe designs and enhancing their overall

efficiency. Moreover, the figure clearly demonstrates that the wick structure can effectively handle substantial heat inputs, with the wick achieving a maximum heat dissipation of approximately 450 W. These insights into the behavior of the heat pipe wick under different electrical current conditions offer valuable guidance for the design and enhancement of heat pipe systems, especially in applications where efficient heat management is critical.

The pressure drop in the heat pipe wick increases sharply at first, but then increases slightly. This is because the pressure drop in the heat pipe wick is dominated by two factors: the capillary pressure and the viscous pressure drop. The capillary pressure is the pressure difference that drives the flow of coolant in the wick, while the viscous pressure drop is the pressure drop due to the friction between the coolant and the wick structure. At low heat inputs, the capillary pressure is dominant, so the pressure drop increases sharply. However, as the heat input increases, the viscous pressure drop becomes more important. At high heat inputs, the viscous pressure drop becomes dominant, so the pressure drop increases slightly.

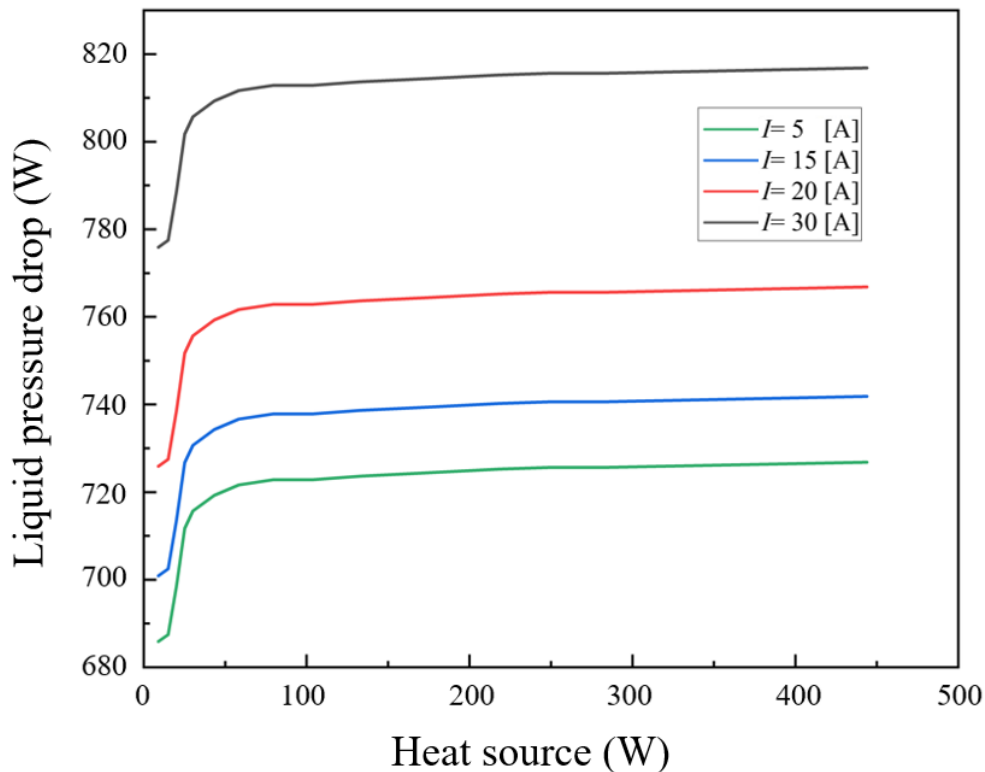


Fig 4.6 Effect of losses on liquid pressure drop.

4.4.2 Velocity and Pressure Profiles in the Liquid Region

Fig 4.7 presents the pressure and velocity magnitude profiles within the central region of the wick under different phase current. The velocity magnitude inside the heat pipe is significantly influenced by both the applied heat and the capillary pressure established by the wick structure. Because of this dependency from the rate of evaporation, and consequently the velocity magnitude at the interface in the evaporator region, is directly relative to the heat source and capillary pressure. Due to the growing evaporation rate, the velocity magnitude throughout the whole heat pipe increases to improve the heat transfer rate. The figure also highlights that the high evaporation rate occurs at the middle area of heat pipe which includes the high heat rate, where the velocity component reaches its peak and where evaporated liquid exits the wick region and enters the vapor core. Therefore, it is revealed the localized heat input results in non-uniform heat flux and liquid flow distribution within the system.

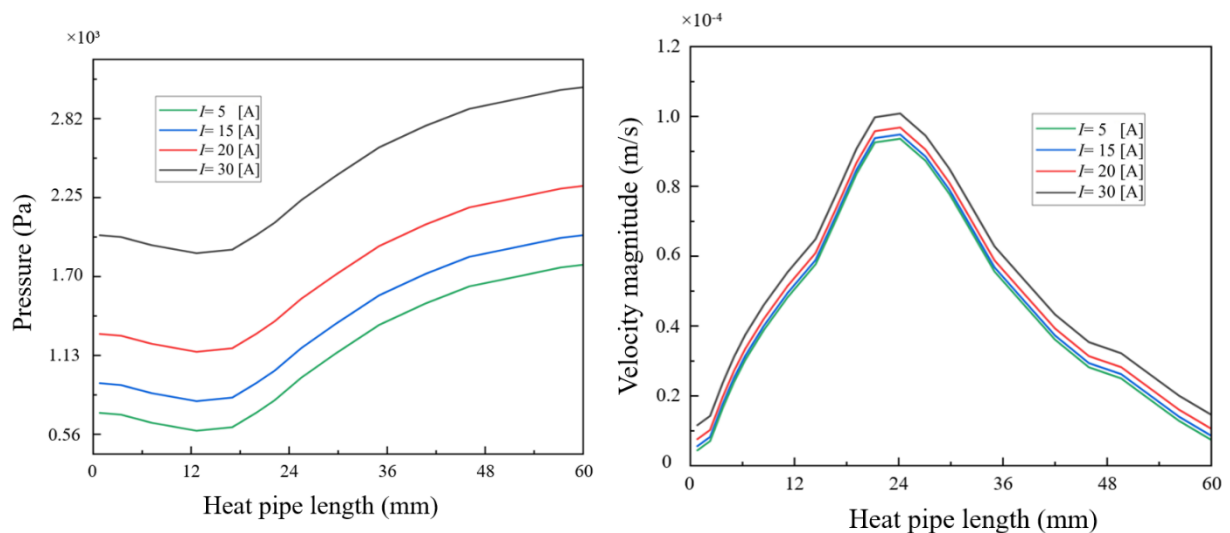


Fig 4.7 Velocity magnitude and pressure profiles in the liquid region.

4.4.3 Velocity and Pressure Profiles in the Vapor Region

Figure 4.8 shows curves about pressure and velocity magnitude within the central vapor region of the heat pipe wick under various currents input, focusing on the middle area of the flat heat pipe. The figure illustrates that the vapor temperature can be considered close to the saturation temperature, and the pressure drop within the vapor core is relatively minor compared to the liquid

region. Notably, the vapor core's velocity is significantly higher than that of the liquid flow, reaching up to 100 times higher, depending on the location. Additionally, it reveals that the maximum velocity value which is 0.18 m/s is achieved around the middle area of the vapor core and gradually goes down towards the edges due to frictional forces exerted by the solid walls.

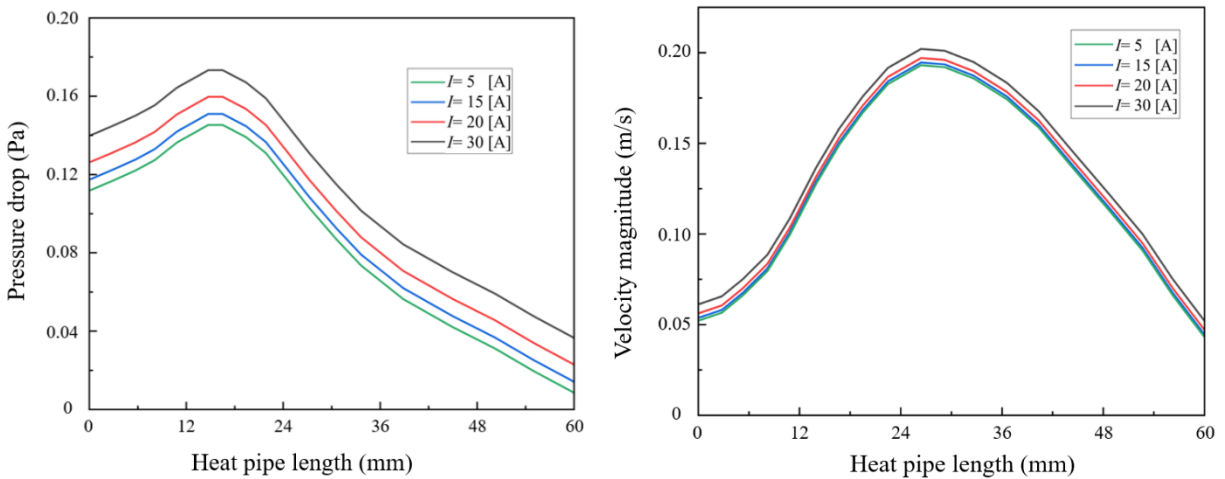


Fig 4.8 Velocity and pressure profiles in the vapor region.

4.4.4 Maximum Temperature in Stator

Fig 4.9 offers an insight into the maximum temperature distribution obtained from the volumetric heat source within the stator, as delineated through the simulated cases of this study. The temperature evaluations are conducted under the parameters of a 20 °C ambient temperature and a 1200 W/m².K convection heat transfer coefficient, imparting a comprehensive real-world perspective to the results. Notably, the comparison involves the temperature profiles of the stator in the presence of a heat pipe and the stator without such a cooling component, thus affording a comparative analysis of the two scenarios. Observing the figure, a distinct trend emerges: temperatures within the stator exhibit a marked increase when devoid of a heat pipe. Conversely, the results underscore the cooling influence imparted by the presence of a heat pipe. Particularly noteworthy is the evident temperature contrast between the stator configurations with and without the heat pipe. This disparity is most vividly evident in scenarios such as the 15 A phase current and 15000 rpm speed case, revealing a notable temperature difference of 83.6 °C.

The stator equipped with a flat heat pipe shows that the highest temperatures gradually increase across all cases. For example, in the scenario with a 20 A phase current at 15000 rpm speed, the highest temperature reaches 29.55 °C. This pattern is quite different from stator configurations without a heat pipe, where temperatures rapidly rise. In the 30 A phase current and 15000 rpm speed case without a heat pipe, the temperature soars to 297 °C. Figure 4.5 illustrates this clear trend of decreasing temperature when comparing the two stator setups. It underscores how the inclusion of a flat heat pipe in the winding stator significantly improves cooling efficiency, preventing excessive temperature increase and ensuring better thermal control.

This marked difference in temperature behavior between the stator configurations with and without a heat pipe emphasizes the critical role of the heat pipe in maintaining lower temperatures, ultimately enhancing the management of heat within the system.

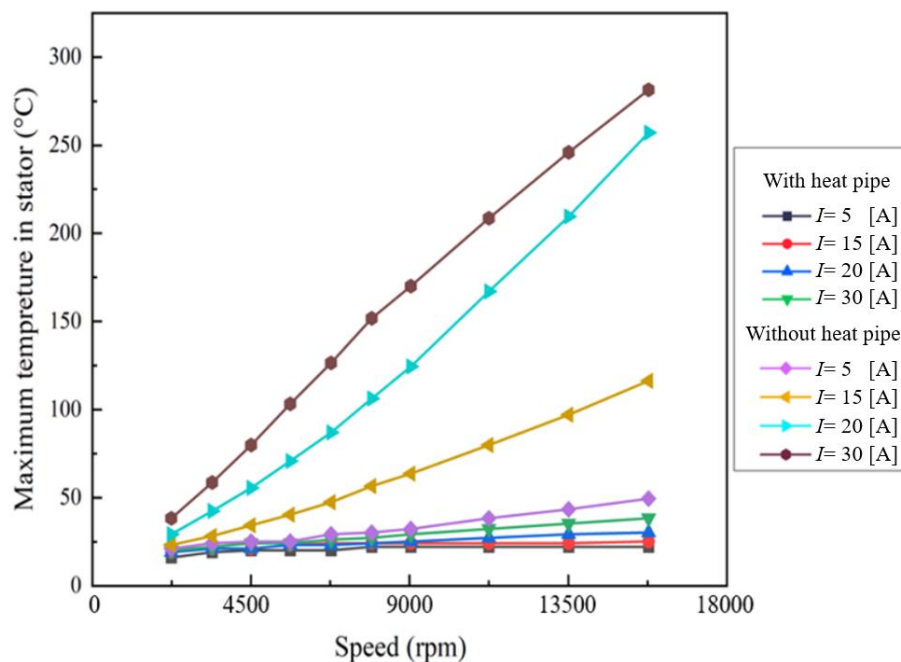


Fig 4.9 Comparison of the maximum temperature generated in the stator by volumetric heat losses from copper losses and iron losses.

4.4.5 Temperature in Windings

Figure 4.10 provides a detailed view of the highest temperature distribution resulting from the heat source within the stator's windings in slot, as simulated in this study. To offer a perspective, the

temperature assessments consider an ambient temperature of 20 °C and a convection heat transfer coefficient of 1200 W/m².K. The phase current in this case is 30 A. The figure compares the temperature profiles of the stator with and without a heat pipe, for the analysis. Upon inspection, a clear pattern emerges: stator temperatures rise significantly in the absence of a heat pipe, while the presence of the heat pipe has a cooling effect. The temperature difference between the two configurations is especially obvious in cases like the one with a 30 A phase current and 15000 rpm speed, showing a significant 150 °C difference.

In scenarios where a heat pipe is integrated into the stator, the highest temperatures show a gradual increase across all cases. For instance, in this case with a 30 A phase current and 15000 rpm speed, the highest temperature for first layer reaches 43.5 °C. This is quite different from stator configurations without a heat pipe, which temperatures increase exponentially. In the same 30 A phase current and 15000 rpm speed case which is a high condition in this specific motor, the temperature goes up to 200 °C for first layer when there's no heat pipe. Figure 4.10 clearly indicates a consistent pattern of lower temperatures when the stator includes a flat heat pipe, highlighting its crucial role in preventing excessive temperature rise and improving thermal management.

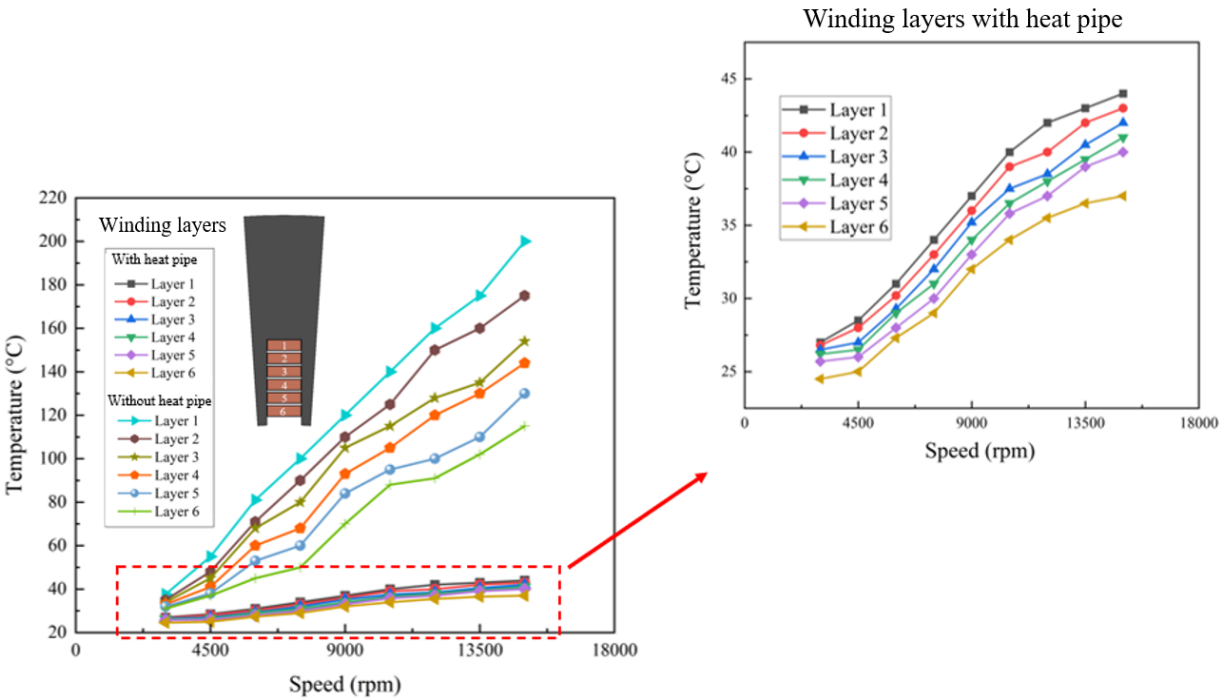


Fig 4.10 Average temperature difference in winding layers for cases with heat pipe and without heat pipe in $I=30$ A.

4.5 Efficiency

Fig 4.11 illustrates how motor efficiency changes with shaft's rotational speed for various peak current cases. The graph shows a consistent trend where, for a given current density, motor efficiency gradually rises as rotational speed increases. For example, at a fixed current of 30 A, efficiency rises from 90% to 96% when the speed goes from 3000 rpm to 7500 rpm. This observation highlights an important trade-off between current density, shaft speed, and motor efficiency. It is noticeable that the efficiency decreases gradually by increasing the speed during the operation in all cases.

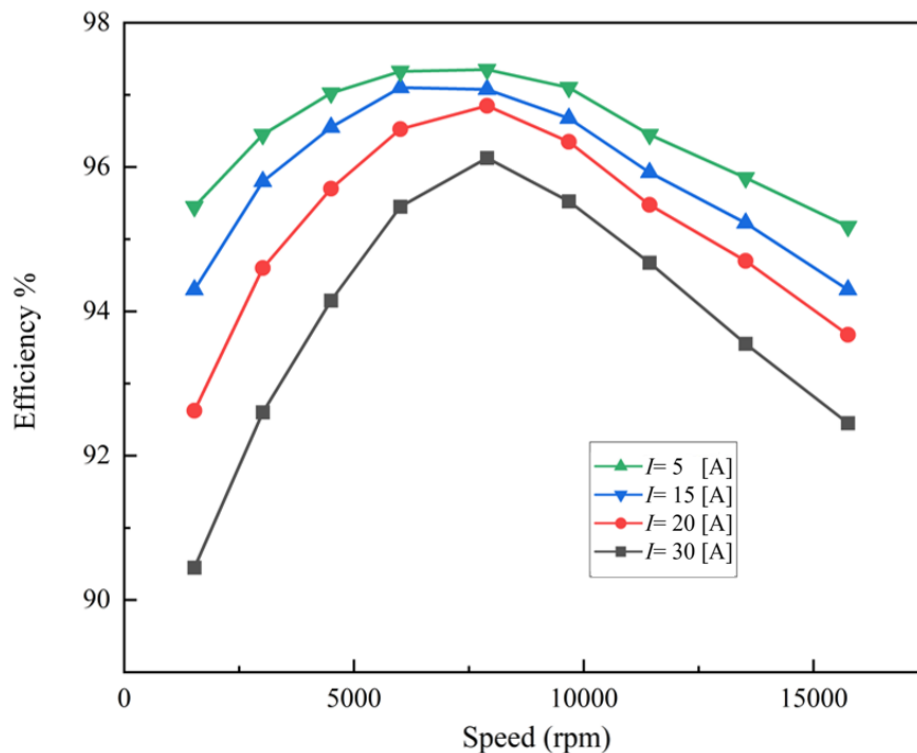


Fig 4.11 Motor's efficiency in different current and speed conditions.

4.6 Heat pipe effects compared to water jacker cooling in hairpin winding

Figures 4.12 and 4.13 provide a comprehensive investigation of the temperature profiles within a hairpin winding motor, drawing a comparative analysis between the present study and the research conducted by Zou et al. [95] on a motor winding 48 slots and 8 poles. In the Zou et al. [95]

investigation, the focus was primarily on evaluating the efficacy of a water jacket cooling strategy as a thermal management solution. The operating conditions represent a peak current of 30 A, which is the highest peak current typically encountered in this specific motor configuration. The visual representations in these figures highlight the temperature differentials observed within the stator and winding layers under these operating conditions. Notably, the introduction of a heat pipe in the current study led to a significant reduction in temperature when compared to the scenario involving water jacket cooling. This effect is particularly striking in Figure 4.12, where the temperature contrast between the heat pipe-cooled case and the water-cooled case exceeds 50%, underscoring the pronounced cooling efficiency achieved through heat pipe implementation.

Figure 4.13 reveals deeper investigation in the temperature variations within the winding layers, emphasizing the substantial impact of heat pipes as a cooling strategy when compared with water-cooling jackets. For instance, at 15000 rpm, the presence of a heat pipe results in a remarkable 50 °C reduction in temperature compared to the water-cooling jacket in winding layer 1. These findings illuminate the transformative potential of heat pipes in optimizing thermal management within hairpin winding motors, providing a robust and efficient means of temperature control that can significantly enhance overall performance and reliability.

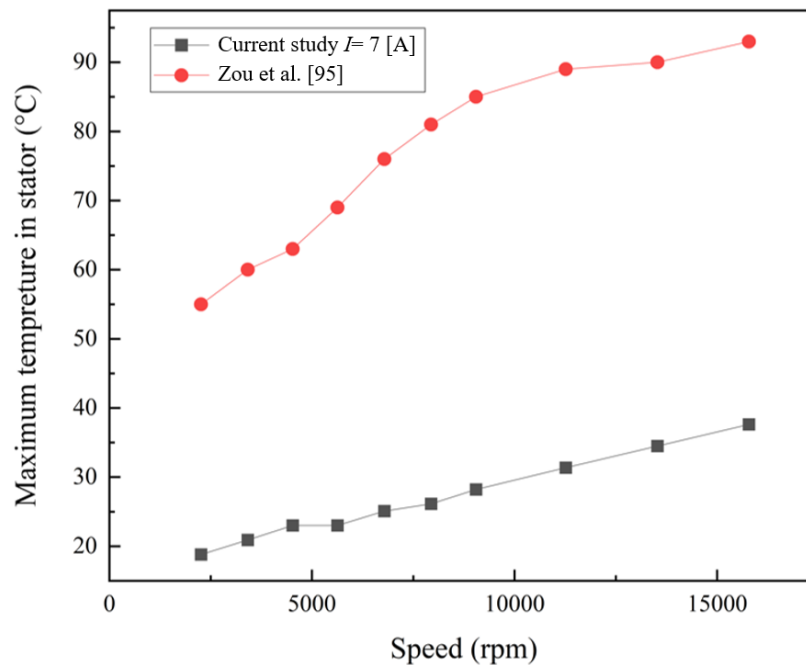


Fig 4.12 Maximum temperature differences in stator in current study and Zou et al. [95].

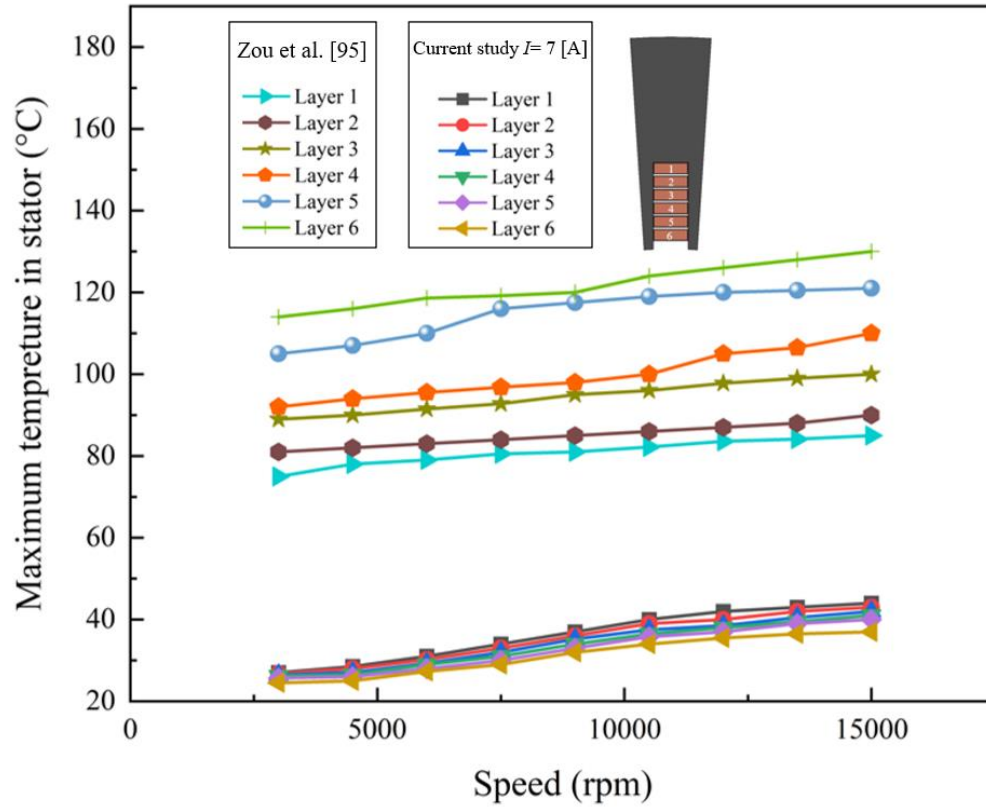


Fig 4.13 Temperature differences in winding layers in current study and Zou et al. [88].

Chapter 5

Conclusion

The primary objective of this investigation was to assess the thermal efficiency of a stator winding when augmented by a flat heat pipe for cooling, contrasting it against the performance of the same winding configuration without the heat pipe. The research introduces a novel approach, suggesting the utilization of an innovative ultrathin heat pipe as a material for winding in high-speed permanent magnet synchronous motors. The study employed COMSOL software for the simulation of the motors' thermal behavior, taking into careful consideration the implications of skin and proximity effects induced by AC current. Additionally, the simulations incorporated the effects of phase change cooling on multiple wick walls within the ultrathin heat pipe. The study also delved into the simulation and analysis of temperature distribution within this cooling approach.

This investigation significantly contributes to our comprehension of the substantial impact that the introduction of a heat pipe has on the cooling process of the stator and the consequent reduction of winding temperature. The outcomes of the research revealed a marked reduction in temperature, particularly at higher speeds, as a direct result of the heat pipe's presence. The findings underscore the efficacy of the proposed ultrathin heat pipe cooling method, which notably enhances the removal of heat from the stator body. This, in turn, translates into decreased stator temperatures and an associated increase in both power density and motor efficiency. In essence, this research advances our understanding of how innovative cooling strategies, like the ultrathin heat pipe, can profoundly enhance the performance of electric motors, particularly in high-speed applications. The main conclusions of this paper are:

- Both copper and iron losses in the stator increase as the rotational speed rises, regardless of the phase current settings. The iron loss follows a similar trend, with values increasing from 26.3 W to 184 W for different phase current cases and speeds. The data derived from copper and iron losses is used to define heat sources, which are crucial for understanding the stator's thermal behavior under various conditions.

- The presence of a heat pipe in the stator significantly influences its thermal performance. The heat pipe plays a crucial role in cooling the motor stator, resulting in considerably lower temperatures compared to stator configurations without a heat pipe. Pressure and temperature distribution within the heat pipe show the significant effects of heat pipe heat transfer in the stator.
- Higher operational speeds lead to more pronounced temperature fluctuations, with a peak temperature of 44 °C observed at the highest speed. The flow dynamics within the heat pipe and heat evaporation from the heat source significantly impact the motor's cooling process.
- The presence of a flat heat pipe within the stator leads to gradually increasing temperatures across all cases. Stator configurations lacking a heat pipe experience rapid temperature increase, with temperatures soaring to 297 °C in the same conditions.
- The investigation compared temperature profiles in hairpin winding motors under peak current conditions of 30 A, analyzing the effectiveness of water jacket cooling versus heat pipe cooling. The introduction of heat pipes led to a remarkable reduction in temperature, with a temperature contrast exceeding 50% in Figure 4.12 and a substantial 40 °C reduction in temperature in winding layer 1 at 15000 rpm, demonstrating the transformative potential of heat pipes for optimizing thermal management and enhancing motor performance and reliability.

The results of this study demonstrate the potential of heat pipe cooling to significantly improve the thermal performance of hairpin winding motors. The proposed ultrathin heat pipe cooling method was shown to reduce hotspot temperatures by 10% to 25% and increase heat dissipation from the stator body by up to 40%. These improvements can lead to a number of benefits, including increased power density, extended motor life, and reduced operating costs. The proposed cooling method can support the field of electric motor design and development in the following ways:

- It can enable the design of more compact and powerful electric motors.
- It can help to extend the life of electric motors by reducing operating temperatures.
- It can reduce the operating costs of electric motors by reducing the need for external cooling systems

The proposed cooling method is particularly promising for high-speed electric motors, where heat dissipation is a major challenge. Overall, this study demonstrates the feasibility and potential benefits of using heat pipe cooling to improve the thermal performance of hairpin winding motors, particularly in high-speed applications.

Chapter 6

Future Work and Limitation

The research has some limitations due to the complicated nature of studying skin and proximity effects, as well as the lack of experimental equipment available in the university's lab. To fully understand these effects and how they affect different materials and shapes, it requires a deep knowledge of electromagnetic fields, complex math, and access to advanced tools. Because this was a short master's study with limited resources and experimental equipment, there wasn't enough time or access to the necessary tools to explore these electromagnetic phenomena as thoroughly as needed. So, this study is just a starting point, and more in-depth research with more time, resources, and access to experimental equipment is necessary to fully understand how skin and proximity effects work in different real-life situations.

This research study emphasizes the critical role of a heat pipe in improving thermal management and preventing excessive temperature rise in the motor's stator. Higher speeds and current densities can lead to increased losses and temperatures, but the presence of a heat pipe helps mitigate these effects, ensuring better cooling and motor efficiency. Some suggestions for future research in the field of motor cooling and efficiency are:

- Investigate the design and optimization of heat pipes tailored specifically for hairpin winding motors. Explore different shapes, materials, and configurations to enhance their cooling efficiency further.
- Develop comprehensive multi-physics models that consider not only thermal behavior but also electrical, magnetic, and mechanical aspects of motor operation. This holistic approach can provide deeper insights into the complex interplay of these factors.
- Develop adaptive cooling strategies and combine them together that adjust in real-time based on the motor's operating conditions. This could involve variable cooling rates, fluid types, or heat pipe activation.

Appendix

Simulation Setup

A.1 Heat Pipe Model

A Brinkman-Forchheimer extended Darcy model used to describe the behavior of the fluid in the heat pipe's wick. The flow of vapor is presumed to be laminar and incompressible. To determine the rate at which mass undergoes phase change due to evaporation or condensation, as well as the temperature and pressure at the boundary between liquid and vapor, an energy balance implemented at this boundary condition. This calculation incorporates aspects of kinetic theory and the Clausius-Clapeyron equation. The energy balance considers heat transfer through both convection and conduction on both the liquid and vapor sides. The flow of vapor calculated, as well as the temperature and the pressure fields, by solving interconnected equations for continuity, momentum, and energy in both the vapor and wick regions. Additionally, heat conduction analyzed within the wall. The model assumes that the wick remains fully saturated with liquid to prevent drying out. The combination of the continuity and the momentum equation from Brinkman equations used for flow in porous media [94].

Continuity:

$$\frac{\partial}{\partial t}(\varepsilon_p \rho) + \nabla \cdot (\rho u) = Q_m \quad (\text{A-1})$$

Momentum:

$$\frac{\rho}{\varepsilon_p} (u \cdot \nabla) \frac{u}{\varepsilon_p} = -\nabla p + \nabla \cdot \left[\frac{1}{\varepsilon_p} \left\{ \mu (\nabla u + (\nabla u)^T) - \frac{2}{3} \mu (\nabla \cdot u) I \right\} \right] - \left(\kappa^{-1} \mu + \frac{Q_m}{\varepsilon_p^2} \right) u + F \quad (\text{A-2})$$

where ε_p is the porosity, ρ is density of the fluid, u is velocity vector, Q_m is mass source, p is pressure, μ is dynamic viscosity of the fluid, κ is permeability of the porous medium, and F is effect of gravity and other volume forces. Some simplifications are made in deriving the governing equations, including assuming a steady state, neglecting gravitational forces and radiation, and considering an incompressible fluid. So, continuity and momentum equations can be written as:

$$\rho \nabla \cdot \mathbf{u} = Q_m \quad (\text{A-3})$$

$$\frac{\partial}{\partial t}(\varepsilon_p \rho) + \mathbf{u} \cdot \nabla \rho - \nabla p = Q_m \quad (\text{A-4})$$

This mathematical model is divided into two distinct regions, one for the vapor and one for the wick.

$$\rho C_{p_eff} = \varepsilon \rho C_{pl} + (1 - \varepsilon) \rho C_{ps} \quad (\text{A-7})$$

$$k_{eff} = \frac{k_f(k_f + k_s - (1 - \varphi)(k_f - k_s))}{k_f + k_s + (1 - \varphi)(k_f - k_s)} \quad (\text{A-8})$$

Boundaries conditions at the upper surface of the evaporator and condenser sections in heat pipe respectively are:

$$q = q_{evap} - q_0 = \dot{m} \lambda - q_0 \quad (\text{A-9})$$

The following boundary conditions mean that there are no flows across heat pipe borders. At the liquid/vapor interface the pressure change since the source function changes in the vertical direction. The other surfaces pressure is defined pressure outlet without backward flow. Dirichlet Boundary condition the bottom of the wick is:

$$p = p_{sat}(T) - p_{ref} \quad (\text{A-10})$$

A.2 Hairpin Winding Model

To compute the temperature distribution of the motor the following steady-state energy equation has been solved:

$$\frac{1}{r} \frac{\partial}{\partial r} \left(r \frac{\partial T}{\partial r} \right) + \frac{1}{r^2} \frac{\partial^2 T}{\partial \theta^2} + \frac{\partial^2 T}{\partial z^2} + \frac{\dot{Q}}{k} = 0 \quad (\text{A-11})$$

where \dot{Q} is the volumetric heat source and uses the loss data from magnetic flux model and k is the thermal conductivity of the material [95]. The iron losses in the motor are caused by time-varying magnetic flux density in the rotor and stator, while the copper losses are due to resistance in the stator

windings. Iron losses vary linearly with the rotor speed, and are calculated by Steinmetz equation which is given by:

$$Q_{iron} = K_h B_m f \quad (A-12)$$

where W_i is the iron loss, B_m is the maximum magnetic flux density, and f is the frequency of the magnetic flux density variation. The losses of the copper in the stator are explained in this study by formula due to the resistance which is given by:

$$Q_{copper} = I^2 R_c \quad (A-13)$$

where I is the winding current and is the R_c winding resistance. The Homogenized Multiturn Coil feature is used in this study, and skin and proximity effects are neglected in the winding. Furthermore, the effective resistance does not change with the speed of the rotor. The Magnetic governing equations in this study are vector potential formulation (Ampère's Law) and scalar potential formulation (Magnetic flux conservation) [95]. Ampère's Law is shown as below:

$$\nabla \times H = J \quad (A-14)$$

$$B = \nabla \times H \quad (A-15)$$

where the Scalar potential is defined as:

$$\nabla \cdot B = 0 \quad (A-15)$$

A.3 Energy Equations in Solid and Fluid Parts

To determine the temperature variation across Hairpin Windings with presence of Heat Pipe, a comprehensive approach is adopted, involving the utilization of both the Heat Transfer and AC/DC modules. This approach accounts for various factors, including heat transfer in fluids, laminar flow dynamics, and interfaces for electric current [94]. The governing equations in solid and fluid regions are shown respectively as below:

$$\rho C_p \mu \cdot \nabla T + \nabla \cdot q = Q \quad (A-16)$$

$$\rho C_p \mu \cdot \nabla T + \rho \cdot q = Q \quad (A-17)$$

A.4 Mathematical Equations and Implementation of current research in COMSOL Physics Design Builder

In this section of appendix, detailed exploration of the fundamental mathematical equations presented which shows current simulation framework and the meticulous process of implementing these equations within the COMSOL Physics Design Builder. This in-depth examination is essential to comprehend the details of the computational model and how it accurately represents the physical phenomena occurring within the motor winding and heat pipe system. Through a difficult mathematical foundation and precise implementation, it is noticeable that this research indicates capable of providing valuable insights into the complex thermal and fluid dynamics of the system under study [98].

A.4.1 COMSOL Physics Builder Introduction

COMSOL Physics Builder is used to set up the simulation cases for computing related equations in this study and couple them together. The Physics Builder offers a user-friendly graphical programming environment, enabling experts in various fields to craft customized physics interfaces interactively, all without requiring coding skills like Python or C. Physics Builder has abilities to apply custom physics interfaces to develop special products and specialized physics interfaces designed for the purposes. Within the Physics Builder interface, there is a tree structure that serves as a representation of physics interface design project. This research provides tasks ranging from creating a single physics interface to developing a complete product featuring a set of physics interfaces [98].

A.4.2 Capillary pressure limitation

It is necessary to investigate under what conditions the assumptions of a saturated wick hold before start the study. before setting up the model. The capillary pressure for heat pipe model near ambient conditions is limiting factor.

$$\Delta p_c = \frac{2\sigma}{r_c} \tag{A-18}$$

where σ is surface tension and r_c is the capillary radius. The capillary pressure should be bigger than all other pressure drops in the heat pipe. The liquid pressure drop is studied in this research and other pressure drops neglected. The liquid pressure drop can be presented as:

$$\Delta p_l = \frac{\mu_l}{\kappa A_w L_v p_l} L_{eff} q \quad (A-19)$$

In A-19 μ_l is the liquid viscosity, κ is permeability, A_w is wick area, L_{eff} is heat pipe effective length, and q is the capillary limit. So, The capillary pressure for heat pipe can be considered as:

$$\Delta p_c = \frac{2\sigma}{r_c} = \Delta p_l \quad (A-20)$$

Then the capillary limit is given as:

$$q = \frac{2\sigma\kappa A_w L_v p_l}{L_{eff} r_c \mu_l} \quad (A-21)$$

In this study, great amount of heat loss is around 500 W which is far from the capillary limit value of 8.5 kW.

A.4.3 Mathematical Novelty in the Energy Equation

This approach to integrating AC and DC losses as external heat sources within the energy equation is a crucial aspect of the current research study. It brings a level of sophistication and realism to the hairpin winding simulations that is important for understanding the intricate interplay between electrical, magnetic, and thermal phenomena. Let's delve deeper into the mechanics of how these losses were mathematically represented and implemented in COMSOL. To incorporate AC and DC losses, the energy equation is extended, a fundamental tool for modeling heat transfer in the hairpin winding. The energy equation now accommodates additional terms to quantify the heat generated by these losses:

$$\rho C_p \mu \cdot \nabla T + \nabla \cdot q = Q_{iron} + Q_{copper} \quad (A-18)$$

where Q_{iron} and Q_{copper} are presented in equations A-12 and A-13. This research leverages the power of COMSOL Multiphysics to implement and solve this complex energy equation. Here's how this integration applied:

- **Defining AC and DC Losses as Variables:** Specific variables within COMSOL is introduced to represent AC and DC losses. These variables allow to compute these losses in real-time as the simulation progresses, taking into account dynamic factors such as changes in magnetic field intensity and electrical current density.
- **Equation Definitions:** To precisely capture AC and DC losses, COMSOL's Equation Definitions feature is used. These losses mathematically expressed as functions of various parameters, including magnetic field intensity, electrical current density, and material properties.
- **Solving the Coupled System:** With the energy equation accounting for AC and DC losses, the coupled system of equations using COMSOL's advanced numerical methods is solved. This process enabled to obtain a comprehensive understanding of how these losses impact the thermal behaviour of the hairpin winding.

The integration of AC and DC losses as external heat sources has significant implications for this research. It transforms the simulations into predictive tools that closely mirror real-world motor performance. By quantifying the impact of these losses, the research enables the prediction of temperature variations within the motor winding under different operating conditions, optimization of motor designs to mitigate the adverse effects of AC and DC losses on temperature rise, improvement of motor efficiency by identifying areas where losses can be minimized, and enhancement of motor reliability by preventing overheating and ensuring that the winding operates within safe temperature limits. In summary, this research showcases a comprehensive and advanced approach to motor winding thermal analysis. The inclusion of AC and DC losses as external heat sources within the energy equation reflects the commitment to pushing the boundaries of simulation and engineering design. It empowers the creation of more efficient, reliable, and high-performance electric motors, with applications ranging from industrial machinery to renewable energy systems.

A.4.4 Dependent Variables Declaration:

The exploration of the mathematical foundation of this simulation commences with the declaration of dependent variables, which holds utmost importance in characterizing the dynamic behavior of the system. These variables act as fundamental indicators of how the system responds to diverse physical processes and external influences. Within this study, three crucial dependent variables have been identified, each serving a distinct role in encapsulating the essence of the phenomena under examination [98].

- **Temperature (T):** At the heart of this analysis lies the temperature distribution within the motor winding. Temperature is a scalar quantity, representing the thermal state of the system at different spatial and temporal points. Mathematically expressed as $T(x, y, z)$ [°C], where (x, y, z) denotes spatial coordinates, this variable provides insights into how heat is distributed and dissipated within the winding structure. Temperature variations directly impact the motor's performance and reliability, making it a paramount parameter to monitor.
- **Pressure (p):** Pressure, another scalar variable, assumes a central role in our simulation setup. It characterizes the distribution of pressure within the system, shedding light on the forces and conditions experienced by various components. Mathematically, it is denoted as $p(x, y, z)$ Pa, where (x, y, z) signifies spatial coordinates. Pressure is essential for understanding the fluid dynamics within the heat pipe and its interaction with the motor winding. Pressure gradients and variations are key factors influencing fluid flow behavior and, consequently, heat transfer processes.
- **Velocity (u):** In the context of modeling fluid flow within the heat pipe, velocity emerges as a vector quantity of utmost importance. Unlike temperature and pressure, velocity possesses both magnitude and direction, rendering it indispensable for describing the complex dynamics of fluid motion. Expressed as $u(x, y, z)$ m/s, where (x, y, z) represents spatial coordinates, this vector variable captures the speed and direction of the fluid flow. Understanding velocity patterns is crucial for evaluating the efficiency of heat transfer processes and optimizing the system's thermal performance.

A.4.5 AC and DC Losses as External Heat Sources in the Energy Equation

One of the key advancements in the hairpin winding simulation methodology is the incorporation of AC and DC losses as external heat sources. These losses play a critical role in assessing the thermal behavior of the motor winding under various operating conditions. To achieve this, the losses obtained from the magnetic governing equations are integrated into the energy equation. This integration ensures that the electrical losses are accurately represented as heat sources within the motor winding. AC losses, which result from the interaction of magnetic fields with the conductive materials of the winding, were extracted as a part of the magnetic governing equations. The mathematical representation of AC losses, was derived from these equations. These losses account for the energy dissipated in the form of heat due to the electromagnetic phenomena occurring within the motor winding.

In the energy equation, AC losses were introduced as an additional heat source term. This heat source term is directly proportional to the magnetic field intensity and inversely proportional to the magnetic flux diffusivity. The inclusion of AC losses in the energy equation enabled us to evaluate their impact on the temperature distribution within the motor winding. In addition to AC losses, the simulation framework also considered DC losses, which arise from the resistance of the winding material and the electrical current passing through it. DC losses were directly calculated as part of the magnetic governing equations. These losses contribute significantly to the overall heat generation within the motor winding. Similar to AC losses, DC losses were integrated into the energy equation as an external heat source. The mathematical representation of this integration is straightforward, as DC losses are proportional to the square of the electrical current and the resistance of the winding material.

By integrating AC and DC losses as external heat sources within the energy equation, the simulation framework provided a comprehensive representation of the thermal effects caused by electrical losses in the motor winding. This approach allowed for a detailed assessment of the temperature distribution and heat transfer characteristics under varying operational conditions, ultimately aiding in the optimization of motor winding designs for enhanced performance and reliability.

The declaration of these dependent variables provides the foundation of mathematical models and equations in the current study. Together, temperature, pressure, velocity, and magnetic variables allow us to construct a comprehensive representation of the system's response to thermal, fluidic, and electrical influences. Through precise mathematical formulations and rigorous implementation, this research study aims to unravel the intricate interplay of these variables, leading to a deeper understanding of the system's behavior and performance characteristics.

A.5 Physics Set Up in COMSOL Physics Builder

To implement and thoroughly resolve the energy equation replete with AC/DC variables, a particular configuration of settings within COMSOL Physics Builder is important. These settings encompassed a range of pivotal components, ensuring the precision and fidelity of the current modeling endeavor. The key settings are presented in this section. Within the COMSOL Physics Builder, the Physics Interface feature stands as the gateway to crafting and defining the core mathematical equations that govern the behavior of our simulated system [98]. It is the initial task upon which the intricate modeling of physical phenomena begins. This feature summarizes a numerous of default settings and options, guiding the initial steps of the simulation setup.

A.5.1 Geometry Type

One of the pivotal settings offered by the Physics Interface feature is the definition of the geometry type. In this study, a 3D geometry type is used, aligning with the three-dimensional nature of our motor winding system. This choice was essential, as it dictated the spatial dimensions and the fundamental modeling approach that would be employed throughout the simulation.

A.5.2 Physics Interface Features

One of the attributes of the Physics Interface feature is its user-friendly graphical programming environment. This intuitive interface empowers experts from diverse fields, whether they possess coding skills or not, to craft customized physics interfaces [98]. It serves as a bridge between intricate mathematical formulations and individuals who may not have extensive programming backgrounds, fostering a collaborative environment for simulation development.

A.5.3 Customized Physics Interfaces

The versatility of the Physics Interface feature extends to the realm of customized physics interfaces. It equips users with the capability to tailor-make physics interfaces that align precisely with the requirements of their research or engineering tasks. This level of adaptability is a significant asset, especially in scenarios where off-the-shelf solutions may fall short of capturing the nuances of a specific problem.

A.5.4 Interactive Programming

One of the standout attributes of the Physics Interface feature is its interactive nature. It facilitates a dynamic and iterative approach to physics interface development. Researchers and engineers can actively engage with the interface, making real-time adjustments, and observing how changes in equations or parameters impact the system's behavior. This interactivity expedites the simulation setup process and enhances the understanding of the underlying physics.

A.5.5 Eliminating Coding Barriers

Notably, the Physics Interface feature removes traditional coding barriers. Unlike simulations that require proficiency in programming languages like Python or C, COMSOL's Physics Interface allows users to craft sophisticated simulations without the need for extensive coding skills. This development of simulation enables a broader range of experts to engage in the process.

A.5.6 Tree Structure Representation

Within the Physics Interface feature, there exists a hierarchical tree structure that serves as a visual representation of the entire physics interface design project. This structure is akin to a roadmap, guiding users through the various components and settings of the simulation. It simplifies the navigation of complex simulations and helps maintain a clear overview of the project's architecture.

The Physics Interface feature in COMSOL Physics Builder acts as the launchpad for the entire simulation endeavor. It combines user-friendliness, adaptability, and interactivity to empower experts from diverse backgrounds to embark on a journey of mathematical modeling and

simulation. It is the place where the intricate dance between theory and practice begins, setting the stage for the accurate representation of physical phenomena within the motor winding system.

A.6 COMSOL Physics Builder Settings in Current study

To set up a customized physics a Physics Interface feature is used in Physics Builder to start programming and writing related equations which is presented in Fig A.5. The software uses some default settings for example geometry type which is 3D in this study. The first step of programming in Physics Builder is declaring the dependent variables which are shown in Table A.2 by using Dependent Variable Declaration feature [98]. Temperature, pressure and velocity are dependent variables which react like scalar, scalar and vector dimension respectively in this study. To set up Temperature as a dependent variable, °C is used as a Physical Quantity section, and m/s and Pa for velocity and pressure respectively in Dependent Variable Declaration feature. Also, initial value for all variables is proposed to be zero.

A.6.1 Dependent Variables Declaration

The process of setting up a comprehensive simulation in COMSOL Physics Builder begins with the declaration of dependent variables. These variables are at the core of the simulation, as they represent the physical quantities and properties of the system under investigation. In this section, we will explore the essential aspects and functions of the Dependent Variables Declaration feature within COMSOL Physics Builder.

Dependent variables are mathematical representations of physical properties that evolve or depend on other factors within the system. In the context of motor winding simulations, they serve as key parameters for characterizing the system's behavior. The three primary dependent variables typically considered in such simulations are temperature, pressure, and velocity. Dependent variables can have scalar or vector dimensions. Scalar variables, such as temperature and pressure, represent single values at each point in the simulation domain. These variables are essential for capturing scalar properties like temperature distribution or pressure gradients. On the other hand, vector variables, such as velocity, possess both magnitude and direction, making them ideal for modeling quantities like fluid flow or air velocity within the motor winding.

Temperature is a fundamental dependent variable in motor winding simulations. It characterizes the thermal behavior of the system and helps in understanding temperature distribution. In mathematical terms, it can be expressed as $T(x, y, z, t)$ °C. Here, T represents temperature, and (x, y, z) are spatial coordinates, while t denotes time. This equation indicates that temperature is a function of spatial location and time.

Pressure is another critical dependent variable, especially in simulations involving fluid dynamics within the motor winding. Pressure provides insights into pressure variations, flow patterns, and forces acting within the system. It can be mathematically defined as $p(x, y, z, t)$ Pa. In this equation, p represents pressure, and (x, y, z) signify spatial coordinates.

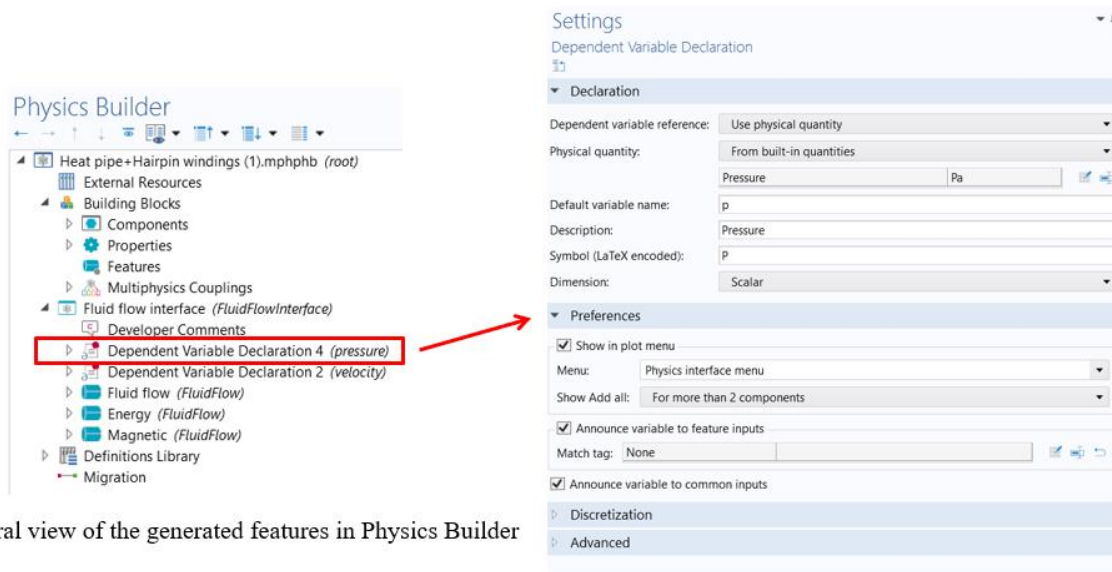
Velocity, being a vector variable, plays a central role in modeling fluid flow and heat transfer within the motor winding. It accounts for both the speed and direction of the flow. Mathematically, velocity can be expressed as $\mathbf{u}(x, y, z, t)$ m/s. Here, \mathbf{u} represents velocity, and (x, y, z) denote spatial coordinates.

When declaring dependent variables, it is common practice to set initial conditions. These initial conditions define the starting values of the variables at the beginning of the simulation. In many cases, setting these initial values to zero provides a reasonable starting point for the simulation. However, depending on the specific scenario, initial conditions can be customized to match real-world conditions.

Dependent variables play a critical role in interacting with other features within COMSOL Physics Builder. For example, they are central to defining boundary conditions, source terms, and mathematical equations that govern the system's behavior. One of the key advantages of dependent variables is their dynamic nature. They can be adjusted during the solving process, allowing engineers and researchers to simulate scenarios where parameters change over time or in response to specific events. Dependent variables are integral to the mathematical equations that describe the physical behavior of the system. For instance, temperature variables appear in the heat transfer equations, while velocity variables are essential in fluid flow equations.

In summary, the Dependent Variables Declaration feature is the foundation upon which complex simulations are built. It defines the key properties and quantities of interest within the motor winding system, enabling researchers to gain valuable insights into its behavior under

various conditions. These variables are central to the mathematical equations and settings used to accurately model and analyze motor winding performance.



General view of the generated features in Physics Builder

Dependent Variable Declaration Settings in Physics Builder

Fig A.1 Dependent Variable Declaration Settings in Physics Builder for Pressure Variable

A.6.2 Programming Governing Equations

Domain Feature is used to write related equations and add boundary conditions in this research study. In This study three Domain Features are implemented for programming Magnetic Flux, Energy equation and Fluid Flow in the heat pipe. Coefficient From Equation feature is used to write the hole equations in Domain Features [98]. Coefficient From Equation features are implemented to show Continuity and Momentum equations for fluid flow in heat pipe, Magnetic equations to calculate AC/DC losses, and Energy equation for analyzing heat transfer in the motor. The coefficient form equation comprises eight coefficients, each defined through a tensor expression that corresponds to specific dimensions. These dimensions are determined by the dependent variable's dimension, denoted as N , and the fixed spatial dimension. In cases where the dependent variable is a scalar, simplification of tensor dimensions can be achieved by omitting singleton dimensions. This results in the γ , α , and β coefficients being represented as spatial vectors (with a length of 3). It is noticeable that the dependent variable can only take the form of a tensor essentially a vector, so the weak form equation should be employed for dependent variables with higher ranks. Furthermore, these coefficients need to be

specified for boundary conditions, and this process differs slightly from the approach used in the General PDE interface within the Model Builder. Converting a Flux/Source boundary condition from this interface to an equivalent representation can be easily accomplished by utilizing only the f coefficient, instead of the g coefficient.

The Domain Feature in COMSOL Physics Builder is a fundamental component that enables users to define the mathematical equations and boundary conditions governing physical phenomena within a specified region or domain of the simulation. In the context of motor winding simulations, the Domain Feature plays a pivotal role in modeling and understanding the behavior of magnetic flux, energy transfer, and fluid flow within the motor winding.

Key Functions and Applications in Domain Feature:

1. **Mathematical Equations:** The Domain Feature allows users to define and implement the mathematical equations that describe the physical processes occurring within the domain. For motor winding simulations, several critical equations are typically employed, including those related to magnetic flux, energy transfer, and fluid flow.
2. **Magnetic Flux Equations:** Magnetic flux equations are crucial for modeling and analyzing the electromagnetic behavior of the motor winding. These equations are used to calculate variables such as magnetic field intensity and flux diffusivity. Magnetic flux equations are essential for understanding AC/DC losses within the winding.
3. **Energy Equation:** The energy equation within the Domain Feature accounts for heat transfer, temperature distribution, and the impact of AC and DC losses on the thermal behavior of the motor winding. It encompasses parameters such as thermal conductivity and heat sources due to losses. Solving the energy equation provides insights into temperature gradients and heat dissipation.
4. **Fluid Flow Equations:** When modeling the cooling effect of fluid flow within the motor winding, the Domain Feature is employed to define continuity and momentum equations. These equations describe the fluid's behavior, pressure distribution, and flow velocity. Fluid flow equations are essential for assessing the cooling efficiency and fluid dynamics within the winding.

5. **Boundary Conditions:** In addition to mathematical equations, the Domain Feature allows users to specify boundary conditions that define the system's interactions with its surroundings. Boundary conditions can include temperature constraints, pressure gradients, and fluid inflow/outflow rates. These conditions ensure that the simulation reflects real-world scenarios.

One notable aspect of the Domain Feature is its capability to handle tensor expressions and coefficients. These expressions are essential for defining complex relationships and dimensions in the mathematical equations. Tensor coefficients, such as γ , α , and β , are employed to represent specific dimensions of the dependent variables. These coefficients are crucial when dealing with variables that have spatial vectors or higher ranks. The Domain Feature seamlessly integrates boundary conditions into the mathematical equations. It allows users to specify how variables, such as temperature or velocity, behave at domain boundaries. For example, boundary conditions can enforce a specific temperature gradient or pressure value on the motor winding's surface. The Domain Feature interacts closely with other features within COMSOL Physics Builder, such as the Dependent Variables Declaration, Coefficient Form Equation, and User Input features. These interactions ensure that the mathematical equations and boundary conditions are consistent and accurately represent the physical behavior of the motor winding.

In summary, the Domain Feature serves as a critical tool for defining the mathematical foundations of motor winding simulations. It enables the formulation of equations related to magnetic flux, energy transfer, and fluid flow, while also accommodating complex tensor expressions and coefficients. Through the Domain Feature, engineers and researchers can gain valuable insights into the performance and behavior of motor windings under various conditions.

A.6.3 Coefficient Form Equation:

The Coefficient Form Equation feature within COMSOL Physics Builder is a powerful tool that enables the precise definition and implementation of mathematical equations governing physical phenomena in simulations. In the context of motor winding simulations, this feature plays a pivotal role in expressing complex equations related to fluid flow, magnetic fields, and energy transfer in a structured and computationally efficient manner [98].

In the coefficient form equation, there exist a total of eight coefficients. Each of these coefficients is defined through a tensor expression that relies on specific dimensions. These dimensions are determined by the dimension of the dependent variable, denoted as N, and the constant spatial dimension, which is set to 3 in this research study.

Table A.1 Coefficient form equation

Coefficient	Description	Dimension
γ	Conservative flux	$N \times 3$
a	Absorption coefficient	$N \times N$
a	Conservative flux convection coefficient	$N \times N \times 3$
β	Convection coefficient	$N \times N \times 3$
c	Diffusion coefficient	$N \times N \times 3 \times 3$
f	Source term	$N \times 1$
d_a	Damping or mass coefficient	$N \times N$
e_a	Mass coefficient	$N \times N$

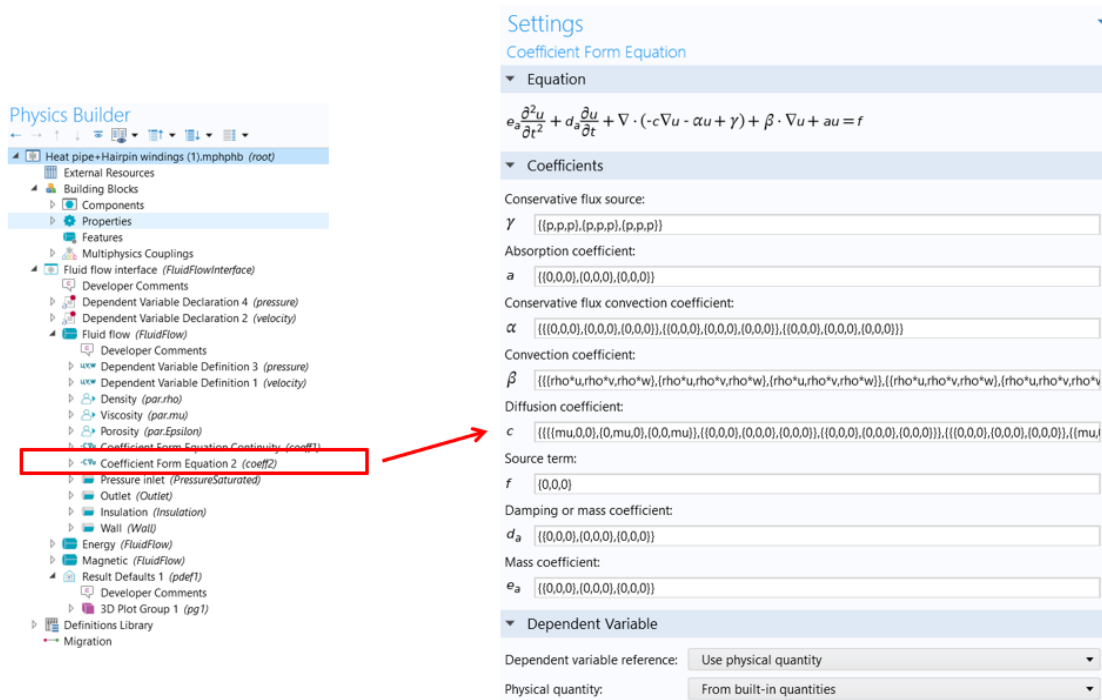


Fig A.2 Coefficient Form Equation in current study in Physics Builder

In cases where the dependent variable takes the form of a scalar, simplifying the tensor dimensions becomes feasible by omitting any singleton dimensions. This simplification leads to the γ , α , and β coefficients transforming into spatial vectors, each with a length of 3. It is noteworthy that the dependent variable can only assume the form of a tensor up to rank 1, essentially a vector. Consequently, when dealing with dependent variables of higher ranks, it becomes imperative to utilize the weak form equation. Moreover, these coefficients necessitate specification for boundary conditions, and this process deviates slightly from the approach used in the General PDE interface within the Model Builder. Within this section, the selection of the dependent variable for the coefficient form equation is a critical step. Similar to the definition of the dependent variable, specifying a reference to a dependent variable is essential.

Key Functions and Applications:

1. **Mathematical Representation:** The Coefficient Form Equation feature allows users to mathematically represent physical processes occurring within the motor winding. It serves as a bridge between theoretical equations and their numerical implementation in the simulation environment.
2. **Complex Equations:** In motor winding simulations, numerous complex equations need to be solved. These equations may include continuity equations, momentum equations for fluid flow, magnetic equations for calculating AC/DC losses, and the energy equation for heat transfer analysis. The Coefficient Form Equation feature provides a platform to express these equations in a concise and efficient form.
3. **Tensor Expressions:** The feature accommodates tensor expressions, which are essential for describing variables with various dimensions and ranks. In particular, variables that have spatial vectors or higher ranks can be accurately represented using tensor expressions. This capability is crucial for modeling complex physical phenomena within the motor winding.
4. **Coefficient Definition:** Within the Coefficient Form Equation feature, users can define coefficients that appear in the equations. These coefficients are associated with specific dimensions and represent physical properties, such as thermal conductivity, magnetic

diffusivity, or viscosity. The coefficients are linked to the mathematical equations and serve as the basis for solving the underlying physics.

5. **Boundary Conditions:** The feature also handles boundary conditions, allowing users to specify how the equations behave at domain boundaries. Boundary conditions are crucial for ensuring that the simulation accurately reflects real-world scenarios. For instance, they can define the behavior of variables like temperature, pressure, or magnetic field strength at the motor winding's surface.
6. **Efficient Numerical Solvers:** Coefficient Form Equations are compatible with COMSOL's efficient numerical solvers. This compatibility ensures that the mathematical equations can be solved accurately and efficiently, even in complex multiphysics simulations.
7. **Multiphysics Integration:** The Coefficient Form Equation feature seamlessly integrates with other physics interfaces within COMSOL, such as fluid dynamics, electromagnetics, and heat transfer. This integration allows for the holistic modeling of coupled physical phenomena within the motor winding.

The feature allows users to express these equations using appropriate coefficients, tensor expressions, and boundary conditions, resulting in a comprehensive representation of the physical behavior of the motor winding. The Coefficient Form Equation feature is a versatile and essential component of COMSOL Physics Builder. It empowers engineers and researchers to accurately model and analyze complex physical phenomena within motor windings, enabling insights that contribute to the optimization of motor designs and enhanced performance.

A.6.4 Define Constant Parameters

To define constant parameters or some parameters which have specific equations, User Input feature is used. These parameters values can be obtained during the solving process or by utilizing result features within the Model Builder. This capability is not extended to user inputs. To access the value of a user input, it's necessary to follow a two-step process: first, declare a variable, and second, assign its value to match that of the user input. Additionally, it's feasible to include a variable definition within a user input node, effectively combining both the declaration and

definition of a variable. In this scenario, the declaration derives information from the user input, while the definition imparts the user input's value to the declared variable.

In our quest to imbue the simulation with flexibility and precision, the User Input feature emerged as an invaluable tool. This feature empowered us to define constant parameters or parameters with specific equations, enhancing the adaptability of our model. These parameters, endowed with the capability to dynamically adjust their values during the solving process, or to glean their values from result features within the Model Builder, played a pivotal role in the versatility of our simulation.

Accessing the value of a user input entailed a meticulous two-step process: first, the declaration of a variable, and subsequently, the precise assignment of its value to align with that of the user input. Moreover, we skillfully explored the option of incorporating a variable definition within a user input node, effectually amalgamating both the declaration and definition of the variable. In this astute arrangement, the declaration seamlessly drew its information directly from the user input, while the definition elegantly conveyed the value of the user input to the declared variable.

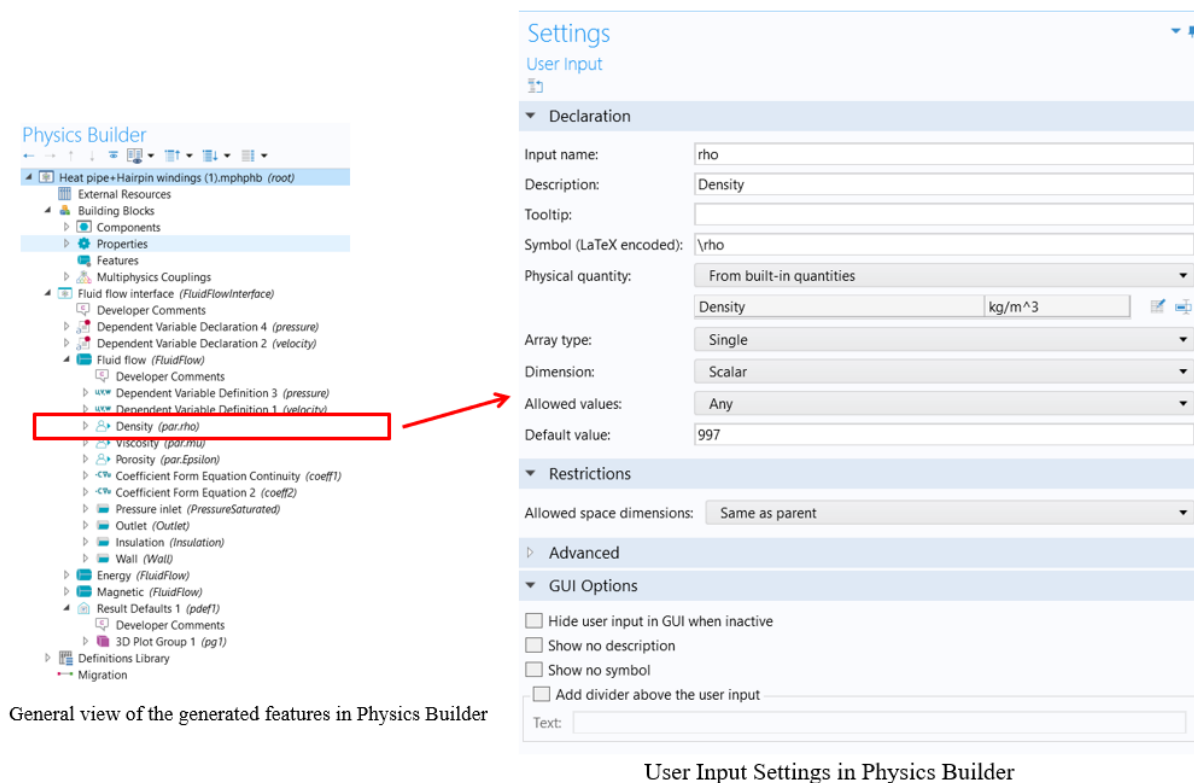


Fig A.3 User Input Setting in Physics Builder for Density Parameter

A.6.5 Boundary Condition Domain Feature

Boundary Condition Domain feature is a suitable feature in Physics Builder for defining boundary conditions of the governing equations. Some specific equations and parameters can be added in this feature to make conditions. For instance, to program temperature for Energy equation, u_0 is written as a User Input to add in COMSOL graphical window [98]. Besides, In the Expression field in Declaration area of the feature $T_0 - T$ is written to make the temperature T equal to T_0 on the boundary (the constraint makes the expression equal to zero).

The Boundary Condition Domain feature within COMSOL Physics Builder plays a pivotal role in defining the conditions that govern the behavior of our simulated system. It is a crucial component that ensures the model reflects real-world scenarios and constraints accurately. In this section, we will delve into the key aspects and functions of the Boundary Condition Domain feature. The primary purpose of the Boundary Condition Domain feature is to define the boundary conditions that emulate real-world constraints on the simulated system. These constraints could include temperature restrictions, pressure differentials, and velocity profiles at specific surfaces or interfaces within the motor winding.

One of the common applications of this feature is the programming of temperature constraints. Engineers and researchers can utilize the Boundary Condition Domain feature to specify temperature limits or distributions on various parts of the motor winding. For instance, it can be used to model the cooling effect of external components or the impact of adjacent systems on temperature variations. In scenarios where pressure plays a crucial role in the system's behavior, the Boundary Condition Domain feature allows for the imposition of pressure profiles. This feature is especially valuable when simulating fluid flow within the heat pipe or any other component where pressure gradients are significant.

The feature offers the flexibility to define customized mathematical expressions that dictate the boundary conditions. This capability enables precise control over how the system interacts with its surroundings. For example, an expression could be crafted to model a sinusoidal variation in temperature at the motor's outer surface, mimicking cyclic loading conditions. The Boundary Condition Domain feature seamlessly integrates with user inputs defined within the simulation. This means that the values used to set up boundary conditions can be dynamically adjusted during

the solving process. For instance, if a parameter representing an external environmental factor change, the boundary conditions can adapt accordingly. Boundary conditions established using this feature directly interact with the dependent variables declared earlier in the simulation, such as temperature, pressure, and velocity. This interaction ensures that the system's response aligns with the defined constraints, allowing for accurate representation of physical behavior. As an added advantage, the feature often provides visualization tools that allow users to inspect and verify the imposed constraints. This visualization aids in quality control and validation of the simulation setup.

The Boundary Condition Domain feature serves as the bridge between the mathematical equations defining the system's behavior and the real-world conditions that influence that behavior. It is an indispensable tool for ensuring that simulations conducted within COMSOL Physics Builder accurately reflect the complex interplay between physical phenomena and external constraints, providing valuable insights for motor winding design and analysis [98].

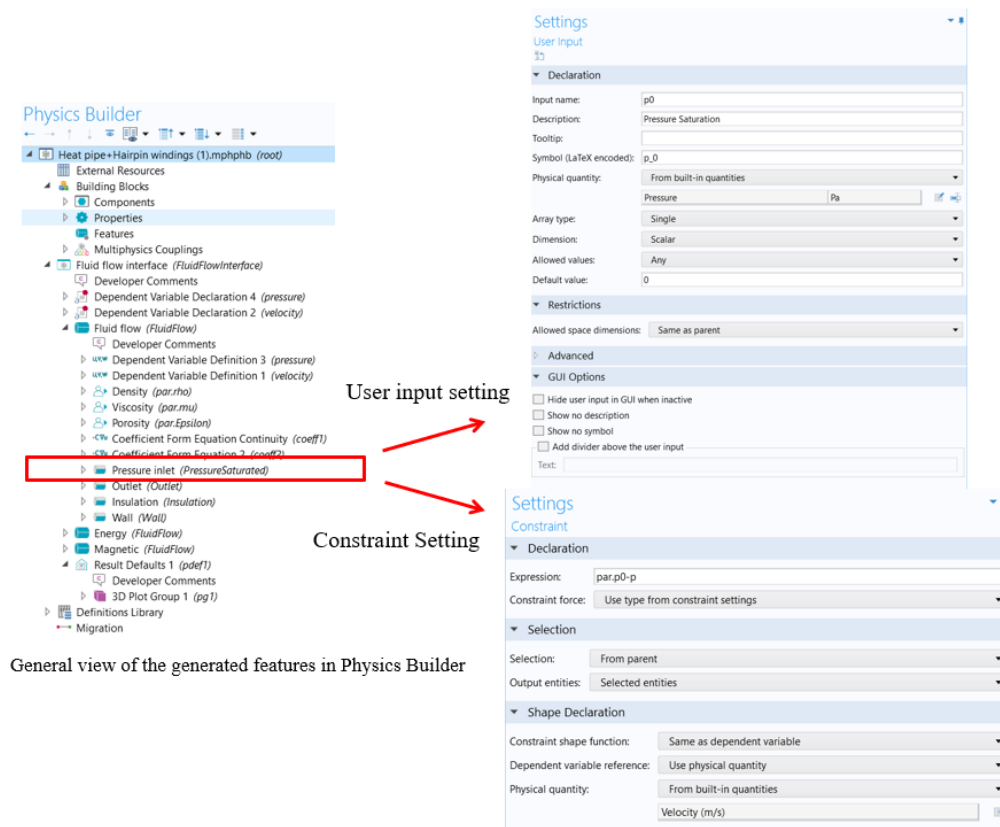


Fig A.4 User Input Setting for Pressure Boundary Conditions

After writing all features, variables, parameters and boundary conditions, it is necessary to couple all three features together by using Multiphysics Feature. A Multiphysics Feature is essentially a combined feature that emulates a single feature, encompassing the combined characteristics of other features within it. It inherits all variables and equations from these enclosed features, which are added through Contained Feature nodes. The Settings window for the multiphysics feature closely resembles that of a regular feature, albeit with certain settings omitted, as they are inherited from the features it contains. Notably, the Restrictions section is entirely excluded, as the allowed spatial dimensions and permissible study types are determined by an intersection of the values found in the enclosed features. 3D Plot Group is used for exporting the results calculated from these equations.

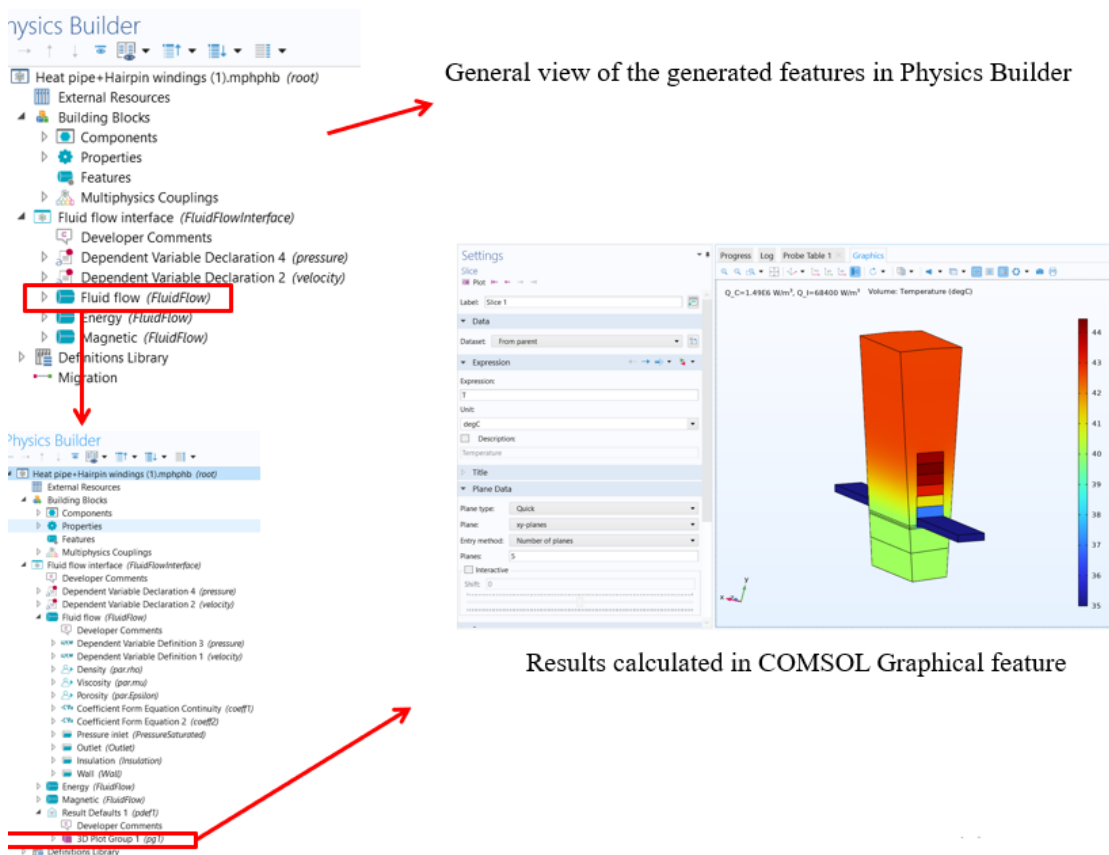


Fig A.5 General features created in COMSOL Physics Builder in the study

Table A.2 General characters of governing equations used in the study

Domain Feature	Variable	Parameter	Boundary condition
Fluid flow	u [m/s]	ε_p [1]	$p = p_{sat}(T) - p_{ref}$
	p [Pa]	ρ [kg/m ³]	$p_{out} = p_{atm}$
		μ [Pa.s]	
Energy	T [°C]	Q_m [W/m ³]	$T = T - T_{ref}$
		κ [1]	$q_{conv} = h(T - T_{\infty})$
		k_{eff} [W/m.K]	$q = q_{evap}$
		k_f [W/m.K]	
		k_s [W/m.K]	
		φ [1]	
Magnet	A [Tm]	c_p [J/kg.K]	
		I [A]	I_A
		I_m [A]	I_B
		σ [S/m]	I_C

References

- [1] D.D. Tran, M. Vafaeipour, M. El Baghdadi, R. Barrero, J. Van Mierlo, O. Hegazy, Thorough state-of-the-art analysis of electric and hybrid vehicle powertrains: Topologies and integrated energy management strategies, *Renewable Sustainable Energy Review*, 119 (2020) 109596.
- [2] W. Cao, B.C. Mecrow, G.J. Atkinson, J.W. Bennett, D.J. Atkinson, Overview of electric motor technologies used for more electric aircraft (MEA), *IEEE Transactions on Industrial Electronics*, 59(9) (2012) 3523-3531.
- [3] M.F. M. Sabri, K.A. Danapalasingam, M.F. Rahmat, A review on hybrid electric vehicles architecture and energy management strategies, *Renewable Sustainable Energy Review*, 53 (2016) 1433-1442.
- [4] C. Grayling, *The Road to Zero: Next Steps Towards Cleaner Road Transport and Delivering Our Industrial Strategy*. Department for Transport. London, U.K., (2018).
- [5] I. Husain, B. Ozpinecio, M.S. Islam, E. Gurpinar, G. Su, W. Yu, S. Chowdhury, L. Xue D. Rahman, R. Sahu, Electric drive technology trends, challenges, and opportunities for future electric vehicles, *IEEE Transactions on Industrial Electronics*, 109(6) (2021) 1039-1059.
- [6] C. Shaw, *Electric vehicles: Driving the transition fourteenth report of session 2017–19*, Business, Energy and Industrial Strategy Committee, House of Commons, U.K., Westminster, U.K., Tech. Rep. (2018) 383.
- [7] 2020 Annual Merit Review Report, Vehicle Technologies Office (VTO), Department of Energy (DOE), Washington, DC, USA (2020).
- [8] A. M. El-Refaie, Motors/generators for traction/propulsion applications: A review, *IEEE Veh. Technol. Mag.*, 8(1) (2013) 90-99.
- [9] D. Staton, J. Goss, Open source electric motor models for commercial EV & hybrid traction motors, in *Proc. Coil Winding, Insul. Elect. Manuf. Exhib. (CWIEME)*, Berlin, Germany, (2017) 9-15.
- [10] A. Bardalai, D. Gerada, D. Golovanov, Z. Xu, X. Zhang, J. Li, H. Zhang, C. Gerada, Reduction of winding AC losses by accurate conductor placement in high frequency electrical machines, *IEEE Trans. Ind. Appl.*, 56(1) (2020) 183-193.
- [11] M. Popescu, J. Goss, D. A. Staton, D. Hawkins, Y. C. Chong, A. Boglietti, Electrical vehicles-practical solutions for power traction motor systems, *IEEE Trans. Ind. Appl.*, 54(3) (2018) 2751-2762.
- [12] W. Cai, D. Fulton, and C. L. Congdon, Multi-set rectangular copper hairpin windings for electric machines, U.S. Patent 7 034 428 B2 (2006).
- [13] W. Cai, Terminals and connections between multi-set segmented hairpin windings, U.S. Patent 7 622 843 B2, (2009).
- [14] F. Momen, K. Rahman, Y. Son, Electrical propulsion system design of Chevrolet Bolt battery electric vehicle, *IEEE Trans. Ind. Appl.*, 55(1) (2019) 376-384.
- [15] S. Sano, T. Yashiro, K. Takizawa, T. Mizutani, Development of new motor for compact-class hybrid vehicles, *World Electr. Vehicle J.* 8(2) (2016) 443-449.
- [16] T. Dimier, M. Cossale and T. Wellerdieck, Comparison of Stator Winding Technologies for High-Speed Motors, *Electric Propulsion Systems*, 2020 International Conference on Electrical Machines (ICEM), Gothenburg, Sweden, (2020) 2406-2412.
- [17] M. Pastura, S. Nuzzo, F. Immovilli, A. Toscani, A. Rumi, A. Cavallini, G. Franceschini, D. Barater, Partial Discharges in Electrical Machines for the More Electric Aircraft— Part I: A Comprehensive Modeling Tool for the Characterization of Electric Drives Based on Fast Switching Semiconductors, *IEEE Access*, 9 (2021) 27109-27121.

REFERENCES

- [18] H.J. Park and M.S. Lim, Design of High Power Density and High Efficiency WoundField Synchronous Motor for Electric Vehicle Traction, *IEEE Access*, 7 (2019) 46677- 46685.
- [19] A. Arzillo, S. Nuzzo, P. Braglia, G. Franceschini, D. Barater, D. Gerada, C. Gerada, An Analytical Approach for the Design of Innovative Hairpin Winding Layouts, 2020 International Conference on Electrical Machines (ICEM), Gothenburg, Sweden, (2020) 1534-1539.
- [20] A. Arzillo, P. Braglia, S. Nuzzo, D. Barater, G. Franceschini, D. Gerada, C. Gerada, Challenges and Future opportunities of Hairpin Technologies, 2020 IEEE 29th International Symposium on Industrial Electronics (ISIE), Delft, Netherlands, (2020) 277-282.
- [21] J. Hagedorn, F.S. Blanc, J. Fleischer, Handbook of Coil Winding: Technologies for efficient electrical wound products and their automated production, Springer, (2017).
- [22] Y. Zhao, D. Li, T. Pei, R. Qu, Overview of the rectangular wire windings AC electrical machine, *CES Transactions on Electrical Machines and Systems*, 3(2) (2019) 160-169.
- [23] B. Bilgin, A. Emadi, Electric motors in electrified transportation: a step toward achieving a sustainable and highly efficient transportation system, *IEEE Power Electron. Mag.* 1(2) (2014) 10-17.
- [24] N. Arbab, W. Wang, C. Lin, J. Hearron, B. Fahimi, Thermal modeling and analysis of a double-stator switched reluctance motor, *IEEE Trans. Energy Convers.* 30(3) (2015) 1209-1217.
- [25] S. Kahourzade, A. Mahmoudi, H.W. Ping, M.N. Uddin, A comprehensive review of axial-flux permanent-magnet machines, *Can. J. Elect. Comput.* 37(1) (2014) 19-33.
- [26] J. Shazly, S. Wahsh, A. Yassin, Thermal modeling of an AFPMSM: A review, *J. Electr. Sys. Inform. Technol.* 2(1) (2015) 18-26.
- [27] C.M. Liao, C.L. Chen, T. Katcher, Thermal management of ac induction motors using computational fluid dynamics modelling, in: *IEEE International Electric Machines and Drives Conference*. Seattle, USA, 1999.
- [28] V. Madonna, P. Giangrande, L. Lusuardi, A. Cavallini, M. Galea, Impact of thermal overload on the insulation aging in short duty cycle motors for aerospace, *IEEE* (2018) 1-06.
- [29] F. Salameh, A. Picot, M. Chabert, P. Maussion, Parametric and nonparametric models for lifespan modeling of insulation systems in electrical machines, *IEEE Trans. Ind. Appl.*, 53(3) (2017) 3119-3128.
- [30] X. Zhang, Q. Yang, M. Ma, Z. Lin, S. Yang, A switched reluctance motor torque ripple reduction strategy with deadbeat current control and active thermal management, *IEEE Trans. Veh. Technol.*, 69(1) (2020) 317-327.
- [31] M. Polikarpova, P. Ponomarev, P. Lindh, I. Petrov, W. Jara, V. Naumanen, J.A. Tapia, J. Pyrhonen, Hybrid cooling method of axial-flux permanent-magnet machines for vehicle applications, *IEEE Trans. Ind. Electron.*, 62(12) (2015) 7382-7390.
- [32] D.A. Staton, M. Popescu, D. Hawkins, A. Boglietti, Influence of different end region cooling arrangements on end-winding heat transfer coefficients in electrical machines, *IEEE Energy Conversion Congress and Exposition*. Atlanta, USA, (2010).
- [33] B. Li, H. Kuo, X. Wang, Y. Chen, Y. Wang, D. Gerada, S. Worall, I. Stone, Y. Yan, Thermal management of electrified propulsion system for low-carbon vehicles, *Automotive Innovation*, 3(4) (2020) 299-316.
- [34] D. Ionel, M. Popescu, C. Cossar, M.I. McGilp, A. Boglietti, A. Cavagnino, A general model of the laminated steel losses in electric motors with PWM voltage supply, *IEEE*, (2008) 1-07.
- [35] K. Yamazaki, N. Fukushima, Iron-loss modeling for rotating machines: comparison between bertotti's three-term expression and 3-d eddy-current analysis, *IEEE Trans. Magn.* 46(8) (2010) 3121-3124.
- [36] D.-K. Hong, B.-C. Woo, J.-Y. Lee, D.-H. Koo, Ultra high speed motor supported by air foil bearings for air blower cooling fuel cells, *IEEE Trans. Magn.* 48(2) (2012) 871-874.

REFERENCES

- [37] S.D. Wilson, P. Stewart, B.P. Taylor, Methods of resistance estimation in permanent magnet synchronous motors for real-time thermal management, *IEEE Trans. Energy Convers.* 25(3) (2010) 698-707.
- [38] C. Kral, A. Haumer, S.B. Lee, A practical thermal model for the estimation of permanent magnet and stator winding temperatures, *IEEE T Power Electr.*, 29(1) (2014) 455-464.
- [39] J. Luomi, C. Zwyssig, A. Looser, J.W. Kolar, Efficiency optimization of a 100-w 500 000-r/min permanent-magnet machine including air-friction losses, *IEEE Trans. Ind. Appl.*, 45(4) (2009) 1368-1377.
- [40] Z. Huang, J. Fang, X. Liu, B. Han, Loss calculation and thermal analysis of rotors supported by active magnetic bearings for high-speed permanent magnet electrical machines, *IEEE Trans. Ind. Electron.*, (2016) 2027-2035.
- [41] K.K. Schwarz, M.A. Member, Survey of basic stray losses in squirrel-cage induction motors, *Proc. Inst. Electr. Eng.*, 111 (1964) 1565-1574.
- [42] P. Pillay, M. Al-Badri, P. Angers, C. Desai, A new stray-load loss formula for small and medium-sized induction motors, *IEEE Trans. Energy Convers.*, 31(3) (2016) 1221-1227.
- [43] J. Li, Y. Lu, Y. Cho, R. Qu, Design an analysis of a water-cooled axial flux permanent-magnet machine for large power direct-driven applications, *IEEE*, (2018) 118-124.
- [44] A. Boglietti, A. Cavagnino, D. Staton, M. Shanel, M. Mueller, C. Mejuto, Evolution and modern approaches for thermal analysis of electrical machines, *IEEE Trans. Ind. Electron.*, 56 (2009) 871-882.
- [45] G. Fang, W. Yuan, Z. Yan, Y. Sun, Y. Tang, Thermal management integrated with three-dimensional heat pipes for air-cooled permanent magnet synchronous motor, *Appl. Therm. Eng.*, 152 (2019) 594-604.
- [46] D.A. Reay, P.A. Kew, R. McGlen, *Heat Pipes: Theory, Design and Applications*, Elsevier, (2013).
- [47] A. Faghri, *Heat Pipes: Review Opportunities and Challenges*, *Frontiers in Heat Pipes*, 5(1) (2014) 1-48.
- [48] G.P. Peterson, *An Introduction to Heat Pipes: Modeling, Testing and Applications*, John Wiley & Sons, New York, US, (1994).
- [49] F. Liang, J. Gao, L. Xu, Investigation on a Grinding Motorized Spindle with Miniature-Revolving-Heat-Pipes Central Cooling Structure, *International Communications in Heat and Mass Transfer*, Elsevier 112 (2020) 1-11.
- [50] X. Wang, B. Li, D. Gerada, K. Huang, I. Stone, S. Worrall, Y. Yan, A critical review on thermal management technologies for motors in electric cars, *Applied Thermal Engineering*, 201 (2022) 117758.
- [51] Z. Xu, Y. Xu, W. Liu, Y. Wang, Global fluid flow and heat transfer characteristics analysis of an open air-cooled drive motor for drilling application, *Case Studies in Thermal Engineering*, 37 (2022) 102254.
- [52] M. Grabowski, K. Urbaniec, J. Wernik, K.J. Wołosz, Numerical simulation and experimental verification of heat transfer from a finned housing of an electric motor, *Energy Conversion and Management*, 125 (2016) 91-96.
- [53] F. Han, H. Guo, X. Ding, Design and optimization of a liquid cooled heat sink for a motor inverter in electric vehicles, *Applied Energy*, 291 (2021) 116819.
- [54] L. Ye, L. Qi, F. Tao, X. Wen, Heat dissipation design of end winding of permanent magnet synchronous motor for electric vehicle, *Energy Reports*, 9 (2023) 282-288.
- [55] K.S. Garud, M. Lee, Grey relational based Taguchi analysis on heat transfer performances of direct oil spray cooling system for electric vehicle driving, *International Journal of Heat and Mass Transfer*, 201 (2023) 123596.
- [56] K. Lee, H. Cha, Y. Kim, Development of an interior permanent magnet motor through rotor cooling for electric vehicles, *Applied Thermal Engineering*, 95 (2016) 348-356.
- [57] H. Li, Cooling of a permanent magnet electric motor with a centrifugal impeller, *International Journal of Heat and Mass Transfer*, 53 (2010) 797-810.

REFERENCES

- [58] S. Ulbrich, J. Kopte, J. Proske, Cooling fin optimization on a TEFC electrical machine housing using a 2-d conjugate heat transfer model, *IEEE Trans. Ind. Electron.*, 65(2) (2018) 1711-1718.
- [59] H. Peng, F. Lai, Investigation of parameters affecting heat transfer and fluid flow of a TEFC electric motor by using Taguchi method, *IOP Conf. Series: Mater. Sci. Eng.*, 491 (2019) 12021.
- [60] C. Kim, K-S. Lee, Thermal nexus model for the thermal characteristic analysis of an open-type air-cooled induction motor, *Applied Thermal Engineering*, 112 (2017) 1108-1116.
- [61] C. Kim, K-S. Lee, S-J. Yook, Effect of air-gap fans on cooling of windings in a largecapacity, high-speed induction motor, *Applied Thermal Engineering*, 100 (2016) 658-667.
- [62] A.S. Fawzal, R.M. Cirstea, K.N. Gyftakis, T.J. Woolmer, M. Dickison, M. Blundell, Fan performance analysis for rotor cooling of axial flux permanent magnet machines, *IEEE Trans. Ind. Appl.*, 53(4) (2017) 3295-3304.
- [63] J. Wen, J. Zheng, Numerical analysis of the external wind path for medium-size high-voltage asynchronous motors, *Applied Thermal Engineering*, 90 (2015) 869-878.
- [64] P. Asef, R.B. Perpina, M.R. Barzegaran, An innovative natural air-cooling system technique for temperature-rise suppression on the permanent magnet synchronous machines, *Electr. Pow. Syst. Res.*, 154 (2018) 174-181.
- [65] A.S. Fawzal, R.M. Cirstea, T.J. Woolmer, M. Dickison, M. Blundell, K.N. Gyftakis, Air inlet/outlet arrangement for rotor cooling application of axial flux PM machines, *Applied Thermal Engineering*, 130 (2018) 1520-1529.
- [66] A. Saleem, M.H. Park, T. Ambreen, S.C. Kim, Optimization of oil flow distribution inside the in-wheel motor assembly of electric vehicles for improved thermal performance, *Applied Thermal Engineering*, 201(A) (2022) 117753.
- [67] C. Guo, L. Long, Y. Wu, K. Xu, H. Ye, Electromagnetic-thermal coupling analysis of a permanent-magnet in-wheel motor with cooling channels in the deepened stator slots, *Case Studies in Thermal Engineering*, 35 (2022) 102158.
- [68] D.H. Lim, S.C. Kim, Thermal performance of oil spray cooling system for in-wheel motor in electric vehicles, *Applied Thermal Engineering*, 63 (2014) 577-587.
- [69] Z. Rehman, K. Seong, Three-D numerical thermal analysis of electric motor with cooling jacket, *Energies*, 11(1) (2018) 92.
- [70] J. Li, Y. Lu, Y-H. Cho, R. Qu, Design, analysis, and prototyping of a water-cooled axial-flux permanent-magnet machine for large-power direct-driven applications, *IEEE Trans. Ind. Appl.*, 55(4) (2019) 3555-3565.
- [71] M. Satrústegui, M. Martínez-Iturralde, J.C. Ramos, P. Gonzalez, G. Astarbe, I. Elosegui, Design criteria for water cooled systems of induction machines, *Applied Thermal Engineering*, 114 (2017) 1018-1028.
- [72] P. Wu, M. Hsieh, W.L. Cai, J. Liu, Y. Huang, J.F. Caceres, S.W. Chang, Heat transfer and thermal management of interior permanent magnet synchronous electric motor, *Inventions*, 4(4) (2019) 69.
- [73] A. Deriszadeh, F. de Monte, M. Villani, L. Di Leonardo, hydrothermal performance of ethylene glycol and water mixture in a spiral channel for electric motor cooling, *EPE Association*, (2019) 1-10.
- [74] C. Yang, H. Wang, X. Niu, J. Zhang, Y. Yan, Design and analysis of cycling oil cooling in driving motors for electric vehicle application, *IEEE*, (2016) 1-06.
- [75] C. Liu, Z. Xu, D. Gerada, J. Li, C. Gerada, Y.C. Chong, M. Popescu, J. Goss, D. Staton, H. Zhang, Experimental Investigation on Oil Spray Cooling With Hairpin Windings, *IEEE TRANSACTIONS ON INDUSTRIAL ELECTRONICS*, 67(9) (2020).
- [76] F. Zhang, D. Gerada, Z. Xu, C. Liu, H. Zhang, T. Zou, Y.C. Chong, C. Gerada, A Thermal Modeling Approach and Experimental Validation for an Oil Spray-Cooled Hairpin Winding Machine, *IEEE TRANSACTIONS ON TRANSPORTATION ELECTRIFICATION*, 7(4) (2021).

REFERENCES

- [77] J. Montonen, J. Nerg, M. Polikarpova, J. Pyrhonen, Integration principles and thermal analysis of an oil-cooled and -lubricated permanent magnet motor planetary gearbox drive system, *IEEE Access*, 7 (2019) 69108-69118.
- [78] A. Acquaviva, O. Wallmark, E.A. Grunditz, S.T. Lundmark, T. Thiringer, Computationally efficient modeling of electrical machines with cooling jacket, *IEEE Trans, Transp. Electron.*, 5(3) (2019) 618*629.
- [79] Y. Alexandrova, R.S. Semken, J. Pyrhonen, Permanent magnet synchronous generator design solution for large direct-drive wind turbines: Thermal behavior of the LC DD-PMSG, *Applied Thermal Engineering*, 65(1-2) (2014) 554-563.
- [80] M.C. Kulan, N.J. Baker, A thermal equivalent circuit to quantify the effect of thermal paste on heat flow through a pm machine, *IEEE International Electric Machines and Drives Conference (IEMDC)*, Miami,USA, (2017).
- [81] R. Wrobel, A. Hussein, A feasibility study of additively manufactured heat guides for enhanced heat transfer in electrical machines, *IEEE Trans. Ind. Appl.*, 56(1) (2020) 205-215.
- [82] J. Bellettre, V. Sartre, F. Biaist, A. Lallemand, Transient state study of electric motor heating and phase change solid-liquid cooling, *Applied Thermal Engineering*, 17 (1997) 17-31.
- [83] J.X. Wang, Y.Z. Li, S.N. Wang, H.S. Zhang, X. Ning, W. Guo, Experimental investigation of the thermal control effects of phase change material based packaging strategy for on-board permanent magnet synchronous motors, *Energy Convers. Manage.*, 123 (2016) 232-242.
- [84] S. Wang, Y. Li, Y-Z. Li, J. Wang, X. Xiao, W. Guo, Transient cooling effect analyses for a permanent-magnet synchronous motor with phase-change-material packaging, *Applied Thermal Engineering*, 109 (2016) 251-260.
- [85] S. Ayat, C. Serghine, T. Klonowski, S. Yon, A. Mutabazi, The use of phase change material for the cooling of electric machine windings formed with hollow conductors, *IEEE International Electric Machines & Drives Conference (IEMDC)*. San Diego, USA, (2019).
- [86] J. Park, J. An, K. Han, H. Choi, I.S. Park, Enhancement of cooling performance in traction motor of electric vehicle using direct slot cooling method, *Applied Thermal Engineering*, 217 (2022) 119082.
- [87] Y. Sun, S. Zhang, G. Chen, Y. Tang, F. Liang, Experimental and numerical investigation on a novel heat pipe based cooling strategy for permanent magnet synchronous motors, *Applied Thermal Engineering*, 170 (2020) 114970.
- [88] N. Putra, B. Ariantara, Electric motor thermal management system using L-shaped flat heat pipes, *Applied Thermal Engineering*, 126 (2017) 1156-1163.
- [89] G. Fang, W. Yuan, Z. Yan, Y. Sun, Y. Tang, Thermal management integrated with three-dimensional heat pipes for air-cooled permanent magnet synchronous motor, *Applied Thermal Engineering*, 152 (2019) 594-604.
- [90] A. Boglietti, A. Cavagnino, D. Staton, M. Shanel, M. Mueller, C. Mejuto, Evolution and modern approaches for thermal analysis of electrical machines, *IEEE Trans. Ind. Electron*, 56 (2009) 871-882.
- [91] E. Galloni, P. Parisi, F. Marignetti, G. Volpe, CFD analyses of a radial fan for electric motor cooling, *Therm. Sci. Eng. Prog.*, 8 (2018) 470-476.
- [92] T. Nakahama, D. Biswas, K. Kawano, F. Ishibashi, Improved cooling performance of large motors using fans, *IEEE Trans. Energy Convers.*, 21(2) (2006) 324-331.
- [93] S.T. Lundmark, A. Bergqvist, S.D. Chakarova-Kaeck, Coupled 3-D thermal and electromagnetic modelling of a liquid-cooled IPM traction motor. *IEEE Vehicle Power and Propulsion Conference (VPPC)*. Belfort, France, (2017).
- [94] A. Tikadar, N. Kumar, Y. Joshi, S. Kumar, Coupled Electro-Thermal Analysis of Permanent Magnet Synchronous Motor for Electric Vehicles, *IEEE ITherm Conference*, (2020) 249-256.

REFERENCES

- [95] T. Zou, D. Gerada, A.L. Rocca, M. Moslemin, A. Cairns, M. Cui, A. Bardalai, F. Zhang, C. Gerada, A Comprehensive Design Guideline of Hairpin Windings for High Power Density Electric Vehicle Traction Motors, *IEEE TRANSACTIONS ON TRANSPORTATION ELECTRIFICATION*, 8(3) (2022).
- [96] J. Li, T. Abdallah, C.R. Sullivan, Improved Calculation of Core Loss with Nonsinusoidal Waveforms, *IEEE*, (2001) 2203.
- [97] S. Shittu, G. Li, X. Zhao, Y.G. Akhlaghi, X. Ma, M. Yu, Comparative study of a concentrated photovoltaic-thermoelectric system with and without flat plate heat pipe, *Energy Conversion and Management*, 193 (2019) 1-14.
- [98] COMSOL, https://doc.comsol.com/5.3/doc/com.comsol.help.comsol/COMSOL_PhysicsBuilderManual.pdf.